Comparative Analysis of Vaccinia Virus Encoded Markers Reflecting Actual Viral Titres in Oncolytic Virotherapy

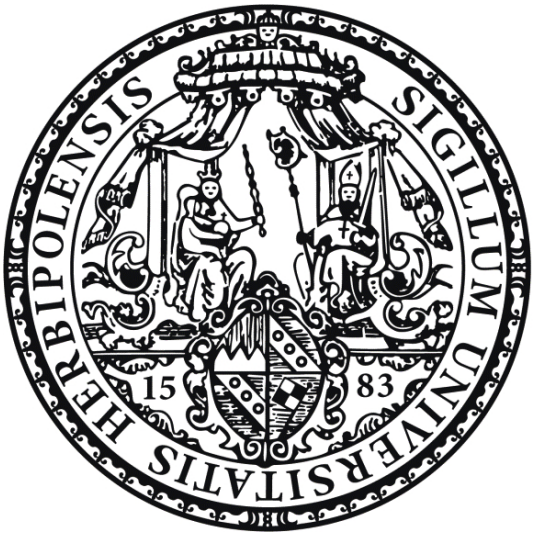

Dissertation

zur Erlangung des naturwissenschaftlichen Doktorgrades der

Julius-Maximilians-Universität Würzburg

vorgelegt von

Jacqueline Sui Lin Nube

aus Singapur

Würzburg, April 2013

Eingereicht am:

Mitglieder der Prüfungskommission:

Vorsitzender:	Prof. Dr. W. Rössler
Erstgutachter:	Prof. Dr. A. A. Szalay
Zweitgutacher:	Prof. Dr. T. Dandekar

Tag des Promotionskolloquiums:

Doktorurkunde ausgehändigt am:

Contents

Summary

Using viruses to treat cancer is a novel approach to an age-old disease. Oncolytic viruses are native or recombinant viruses that have the innate or enhanced capability to infect tumour cells, replicate within the tumour microenvironment and subsequently lyse those cells. One representative, the vaccinia virus (VACV), belongs to the orthopoxvirus genus of the *Poxviridae* family. GLV-1h68, a recombinant and attenuated vaccinia virus developed by the Genelux Corporation, is a member of this family currently being tested in various phase I/II clinical trials under the name GL-ONC1. It has been shown to specifically replicate in tumour cells while sparing healthy tissue and to metabolise prodrug at or transport immunological payloads to the site of affliction.

Since imaging modalities offer little insight into viral replication deep within the body, and because oncolytic virotherapy is dependent on replication within the target tissue, the need for a monitoring system is evident. Pharmacokinetic analysis of this oncolytic agent was to give insight into the dynamics present in tumours during treatment. This, in turn, would give clinicians the opportunity to monitor the efficacy as early as possible after the onset of treatment, to observe treatment progression and possibly to gauge prognosis, without resorting to invasive procedures, e.g. biopsies.

A criteria for viable biomarkers was that it had to be directly dependent on viral replication. Ideally, a marker for treatment efficacy would be specific to the treatment modality, not necessarily the treatment type. Such a marker would be highly detectable (high sensitivity), specific for the treatment (high specificity), and present in an easily obtained specimen (blood). Taking this into consideration, the biomarkers were chosen for their potential to be indicators of viral replication. Thus, the biomarkers analysed in this thesis are: the native proteins expressed by the viral genes A27L and B5R, the virally encoded recombinant proteins β-galactosidase, β-glucuronidase, green fluorescent protein (GFP), carboxypeptidase G2 (CPG2) and carcinoembryonic antigen (CEA). Each marker is under the control of one of five different promoters present. All recombinant viruses used in this thesis express A27L, B5R, GFP and β-glucuronidase and all are derived from the parental virus GLV-1h68. In addition to these markers, GLV-1h68 expresses β-galactosidase; GLV-1h181 expresses CPG2. GLV-1h415 has a full-length CEA gene

inserted; GLV-1h416, 1h417 and 1h418 all express a short-length version of CEA (sCEA) under different promoter strengths.

These seven proteins were first tested in cell culture by analysing the production of protein during viral infection and replication. After positive results were attained, the viruses and the detection of these markers were tested *in vivo* in athymic nude mice carrying human GI-101A tumour xenografts. Each group in the study was treated with a dose of virus and the organs and blood harvested at discrete time points. GFP images were taken of all treated mice every seven days post treatment to confirm the presence of virus in the tumour. Serum samples, along with tumour lysates, were analysed for biomarker concentration and correlated, among others, with the viral titre present in the tumour.

Cytotoxicity assays showed that at similar replication rates the viruses GLV-1h416 and 1h417 showed a higher toxicity than the control virus GLV-1h68. In the xenograft mouse model however, the regression of all the tumour treated groups was comparable. These tumours were extracted for further analysis. Histological tumour slides showed inhomogeneous viral infiltration of the tumour. Slides from tumours taken later in the study also suggest an outward pushing border of actively replicating virus, which left dormant virus and necrotic tissue in its wake. This border was most prominent in tumours excised at 63 days post viral injection. Analysing the viral titre present in the tumour, it was shown that the titre concentration stayed relatively constant throughout the study. However, tumour measurements show the tumours had undergone regression towards the end of the study. This means that in order to for a constant virus concentration to be sustained over time, in spite of a shrinking tumour volume, the absolute amount of virus in the whole tumour had to increase. Since the biomarker data indicated that concentrations of both β-glucuronidase and sCEA decreased with tumour size, it was concluded that the amount of actively replicating virus in the tumour was less than the amount determined by viral plaque assay.

Five of the seven markers initially analysed, β-galactosidase, the A27L and B5R expressed proteins, CPG2 and GFP, as well as the viruses GLV-1h415 and 1h418 were disregarded for various reasons, e.g. incompatible assay requirements, high detection limits and interference through blood-related components. In comparison, β-glucuronidase and sCEA showed promising results after initial experiments and were selected for further analysis.

The enzyme β-glucuronidase, whose expression is controlled by the native late promoter p^{11K}, is a cytoplasmic protein which is released into the blood circulation upon cell lysis.

The β-glucuronidase encoding gene *gusA* is found in the genome of many recombinant viruses, most importantly GLV-1h68, 1h416 and 1h417. First, these viruses were assayed in cell culture pertaining to their expression efficacy of β-glucuronidase. Results showed that the amount of β-glucuronidase expressed by the different viruses was comparable, as the *gusA* gene of these viruses was controlled by the same viral promoter. In the GI-101A xenograft mouse model, β-glucuronidase could be detected in both tumour homogenates, as well as serum samples. The total amount of enzyme measured in serum was two hundred times smaller than the amount determined to be in the tumour. Furthermore, the trend depicted by the chronological development of the total enzyme amount in the tumour was reflected in the progress of the viral titre in tumour over time, showing that a direct correlation exists between the viral replication and biomarker production.

Carcinoembryonic antigen in its secreted form (sCEA) was the second biomarker to be analysed in detail. It is already found in clinics today as a diagnostic tool for certain cancer types, predominantly colorectal cancer. This protein was analysed in combination with two different synthetic viral promoters, the early p^{sE} promoter in GLV-1h416 and the early/late p^{sEL} promoter in GLV-1h417. The expression strength of these promoters was first tested in cell culture. It was found that at similar viral titres, a ten-fold difference in sCEA expression was found between the two different viruses. This difference in sCEA expression was also seen when assaying biological samples from the *in vivo* study. GLV-1h416 treated tumour-bearing mice showed an eight-fold higher sCEA concentration in the tumour compared to the serum. In comparison, tumour-bearing mice that had been treated with a dose of GLV-1h417 showed a four-fold higher concentration of sCEA in the tumour than in the serum. Both groups showed comparably high viral titres were present in the tumour. The difference in expression levels of sCEA were thus seen as a direct result of the difference in promoter strength.

This study analysed the use of biomarker quantification in order to gauge viral replication taking place in the tumour. In summary, the enzyme β-glucuronidase and the secreted carcinoembryonic antigen CEA were shown to be the most promising candidates for this application. Both showed a direct viral replication-dependent expression of the respective marker and were both detectable in tumour as well as in serum. However, sCEA was shown to have a distinct advantage over β-glucuronidase, as the ratio of sCEA assayed in serum, in comparison to the amount measured in the tumour, was higher than that of β-glucuronidase. This is an important aspect, as the release of marker from the tumour into the blood stream results in a loss of that marker due to physiological effects. A

smaller difference between marker concentration in tumour and marker concentration in serum translates to a smaller loss of biomarker upon release and a more direct relationship between that same marker and the viral titre in the tumour.

Basing future virus designs on the information gained in this thesis is instrumental in acquiring more insight into the pharmacokinetics of the VACV-based oncolytic virotherapy. Even though no biomarker diagnostic test is completely definitive, the information it provides by itself, or in combination with other tests, could prove essential to guide the physicians decision-making process in the treatment of cancer patients. This in turn may one day result in the concrete clinical application of the monitoring methods mentioned here, as this cancer treatment progresses from bench-side to bed-side.

Zusammenfassung

Onkolytische Viren sind natürliche oder rekombinante Viren, die die angeborene oder erworbene Fähigkeit besitzen, Tumorzellen zu infizieren, sich in ihnen zu replizieren und anschließend diese Zellen zu lysieren. Ein Vertreter dieser Viren, das Vaccinia-Virus (VACV) gehört zu der Gattung der Orthopoxviren der Familie der Poxviridae. GLV-1h68 ist ein von der Fa. Genelux entwickelter, rekombinant attenuierter Vaccinia-Virus Stamm (rVACV). Er hat die nachgewiesene Fähigkeit, ausschließlich in Tumorzellen zu replizieren und dabei gesundes Gewebe zu verschonen. Viren dieses Stamms können auch sogenannte Prodrugs lokal am Tumor metabolisieren und/oder immunologische Payloads in die Tumorzellen einschleusen. Die Effizienz von GLV-1h68 (auch bezeichnet als GL-ONC1) wird zurzeit in mehreren klinischen Studien der Phase I/II getestet.

Da die derzeitigen bildgebenden Verfahren wenig Aufschluss über die virale Replikation und damit den therapeutischen Effekt des Virus geben, ist es dringend notwendig, eine Methode zu entwickeln, die Virusreplikation anhand von Blutproben und nicht-invasiver Untersuchungsmethoden nachzuweisen. Eine pharmakokinetische Analyse des Virus sollte Informationen über die Dynamik geben, die sich während der Therapie im Tumorinneren manifestiert. Dies gibt wiederum den behandelnden Ärzten die Möglichkeit, sowohl den Fortschritt also auch den Erfolg der Therapie im Patienten zu verfolgen. Daher wurden in dieser Arbeit verschiedene biologische Merkmale des Virus auf ihr Potenzial als Indikator für die Virusreplikation getestet.

Ein biologisches Merkmal kann als ein sogenannter Biomarker der Virustherapie angesehen werden, wenn dessen Expression in direkter Abhängigkeit zur viralen Replikation steht. Zusammen mit der Voraussetzung, im Blut einfach und spezifisch nachweisbar zu sein, kommen folglich bei der onkolytischen Virotherapie nur Proteine in Frage, die viral kodiert sind. Die Biomarker, die im Rahmen der oben genannten Problematik in dieser Arbeit diskutiert wurden, sind das exprimierte Protein des A27L-Gens, das B5R-exprimierte Glykoprotein, β-Galaktosidase (β-Gal), β-Glukuronidase (β-Glc), das grün-fluoreszierende Protein (GFP), Carboxypeptidase G2 (CPG2) und das carcinoembryonale Antigen (CEA). Zur Untersuchung der einzelnen Marker fanden neben GLV-1h68 weitere Viren Anwendung, die sich vom Parentalvirus ableiten und neben GFP, β-Glukuronidase

und den viralen Proteinen A27L und B5R weitere Proteine exprimieren können. GLV-1h68 exprimiert β-Galaktosidase, während GLV-1h181 das Gen für CPG2 trägt. GLV-1h415 exprimiert CEA in seiner vollen Länge, wahrend GLV-1h416, 1h417 und 1h418 jeweils eine verkürzte Version des CEA-Gens unter verschiedenen Promotorstärken exprimiert.

Die sieben Proteine wurden zunächst in Zellkultur durch Infektion mit den jeweiligen Viren auf ihre Expression bzw. Aktivität getestet und nach positiven Resultaten auch in vivo im GI-101A-Xenograft-Modell analysiert. Alle sieben Tage wurden Blut- und Gewebeproben entnommen und auf die Gegenwart von Biomarkern untersucht. Dabei wurde auch der Virustiter bestimmt, um diesen anschließend mit der Biomarker-Konzentration korrelieren zu können. Zytotoxizitätsstudien zeigten, dass bei ähnlicher Replikationsrate GLV-1h416 und 1h417 eine höhere Zytotoxizität als der Kontrollvirus GLV-1h68 besaßen. Im GI-101A-Xenograft-Mausmodell war hingegen die Regression der behandelten Tumoren in allen Virusgruppen vergleichbar. Diese Tumore wurden extrahiert, um die Virusverteilung im Tumor genauer zu analysieren. Histologische Untersuchungen zeigten anfänglich eine inhomogene Virusinfiltration des Tumors. Ein, vom Infiltrationspunkt aus wandernder Ring an aktiv replizierendem Virus hinterließ im Laufe der Untersuchung im Tumorinneren einen Bereich an nekrotischem Gewebe und inaktivem Virus. Dieser sogenannte Virusring war zu späten Zeitpunkten (63 Tage nach Virusbehandlung) am stärksten sichtbar. Trotz der Tumorregression blieb die Viruskonzentration im Verlauf der Therapie konstant. Um diese über die Zeit aufrecht zu erhalten, müsste sich die absolute Virusmenge im Gesamttumor erhöhen. Da sich aber die Biomarkerkonzentration sowohl von β-Glukuronidase als auch sCEA zusammen mit der Tumorgröße reduzierte, deuten diese Ergebnisse auf eine kleiner werdende Menge an replizierendem Virus hin.

Fünf der sieben Merkmale, β-Galaktosidase, die Proteine der Gene A27L und B5R, CPG2 und GFP, wurden zusammen mit den Viren GLV-1h415 und 1h418 nach eingehender Analyse aufgrund von hohen Detektionsgrenzen, nicht erfüllbarer Methodenvorraussetzungen und Blut abhängigen Störsignalen nicht weiter berücksichtigt. β-Glukuronidase und sCEA dagegen wurden nach positiven Resultaten eingehender auf ihr Potenzial als Biomarker untersucht. Das Enzym β-Glukuronidase steht unter der Kontrolle des nativen, späten p^{11K} Promoters, ist ein zytoplasmatisches Protein und wird erst bei der Zelllyse ins Blut sezerniert. Das β-Glukuronidase kodierende Gen *gusA* ist im Genom vieler rekombinanter Viren vorhanden, unter anderem auch in GLV-1h68, 1h416 und 1h417. Zunächst wurden die verschiedenen Viren in Zellkultur auf ihre Expressionsef-

fizienz von β-Glukuronidase untersucht. Die Menge an exprimierter β-Glukuronidase war in den untersuchten Virusstämmen vergleichbar, da das *gusA* Gen in allen Viren dem gleichen Promoter unterliegt. Im GI-101A-Xenograft-Mausmodell konnte β-Glukuronidase sowohl im Tumorhomogenat als auch im Serum nachgewiesen werden. Die Gesamtmenge an Enzym, welches im Serum nachgewiesen werden konnte, war ein um mehr als zweihundertfaches kleiner als im Tumor. Des Weiteren konnte gezeigt werden, dass der Virustiter im Tumor tendenziell mit der Gesamtenzymmenge im Tumour übereinstimmte. Dies weist auf eine direkte Korrelation zwischen Virusreplikation und Biomarkerproduktion hin.

Als zweiter Marker wurde die sezernierte Form des carcinoembryonalen Antigens CEA (sCEA) eingehender untersucht. Dieses Protein findet bereits in der Klinik bei der Diagnostik von beispielsweise Darmkrebs Anwendung. Es wurde in Kombination mit zwei viralen Promotoren untersucht, dem frühen synthetischen p^{sE}-Promotor in GLV-1h416 und dem früh/späten synthetischen p^{sEL}-Promotor in GLV-1h417. Die Expressionsstärke wurde zunächst in Zellkultur getestet, wobei bei gleicher Virusmenge ein zehnfacher Unterschied zwischen den beiden Viren in Bezug auf die produzierte sCEA-Menge festgestellt wurde. Diese unterschiedlichen Expressionsstärken von sCEA waren auch im Xenograft-Modell ersichtlich. In GLV-1h416 infizierten, tumortragenden Mäusen zeigte sich im Tumor eine achtfach höhere Menge an sCEA als im Serum. Im Gegensatz dazu wiesen Mäuse, die mit GLV-1h417 behandelt wurden, eine vierfach höhere sCEA Konzentration im Tumor im Vergleich zur sCEA Menge im Serum auf, obwohl die im Tumor vorhandene Virusmenge in beiden Gruppen vergleichbar war. Dieser Expressionsunterschied von sCEA zwischen den Viren ließ sich auf die verschieden starken Promotoren zurückführen.

In dieser Arbeit wurde untersucht, ob über die Quantifizierung bestimmter Markerproteine eine Aussage über die virale Replikation im Tumor getroffen werden kann. Zusammenfassend lässt sich sagen, dass zwei virale Markerproteine, das Enzym β-Glukuronidase und das carcinoembryonale Antigen CEA sich als die vielversprechendsten Kandidaten erwiesen haben. Beide zeigen eine virale replikationsabhängige Produktion des Markers und sind sowohl im Tumor als auch im Serum detektierbar. Jedoch hat CEA gegenüber β-Glukuronidase den Vorteil, dass die sezernierte Proteinmenge im Serum im Vergleich zu der im Tumor vorhandenen Konzentration größer ist. Da es wichtig ist, dass bei der Freisetzung des Markers aus dem Tumor in die Blutzirkulation der Verlust möglichst gering ist, kann dieser Marker besser die Virusreplikation im Tumor widergeben.

Die Ergebnisse dieser Dissertation, vor allem die Daten zur CEA-Sekretion, sollten bei der Konstruktion zukünftiger Viren berücksichtigt werden, um weitere Informationen über die

Pharmakokinetik der VACV-abhängigen Virotherapie zu erhalten. Die hier dargestellten Methoden könnten dann als zusätzliche Diagnostik in der Klinik Anwendung finden.

1 Introduction

1.1 Cancer and present cancer therapies

Cancer, the "Emperor of all Maladies" [1], has long eluded clinicians as to the exact cause and cure of this disease. In 2008 alone, cancer accounted for 13% of deaths worldwide [2], with lung cancer being the number one cancer-dependent cause of death for both sexes, followed by prostate and liver cancer in men; and breast and colorectal cancer in women. In spite of the analysis by Jemal *et al.* [3] of cancer statistics, stating that there had been an average decrease of cancer death rates by 14.45% in 2004 compared to 1994, there still has been no breakthrough as far as an absolute cure for cancer goes.

In order to rise to the challenge of curing a disease, it is essential to know the strengths and weaknesses of one's adversary. Today, cancer is known as a disease where many genomic changes have to occur, resulting in an oncogene gaining function, or, tumour suppressor genes losing function. [4] It has been implied that tumourigenesis in humans is a multi-step process, with each step reflecting alterations driving normal cells towards becoming malignant counterparts of their former selves. Hanahan and Weinberg give a detailed overview of the way points in this process, showing that there are many ways for a cell to become tumourous, and also that the order in which these characteristics are gained plays no role. [5] According to this summary, the main "hallmarks", or signature characteristics, of cancer are six properties that cells have to acquire on their way to becoming cancerous (Fig. 1.1) . These are sustaining proliferative signalling, evading growth suppressors, enabling replicative immortality, activating invasion and metastasis, inducing angiogenesis, and resisting cell death. It is possible to attain each attribute through different methods. The loss of function in the *p53* tumour suppressor gene, for instance, infers the ability to evade apoptosis [6], and so does an upregulation of Bcl-2 and c-Myc [7]. Ancillary to these six hallmarks are each two emerging hallmarks and various enabling characteristics. Avoiding immune destruction and deregulating cellular energetics belong to the former, as their exact role has yet to be fully scientifically validated. Tumour promoting inflammation, along with genomic instability & mutation, belong to the latter category, as they are enabling characteristics that support and promote the acquisition of malignant cellular attributes.

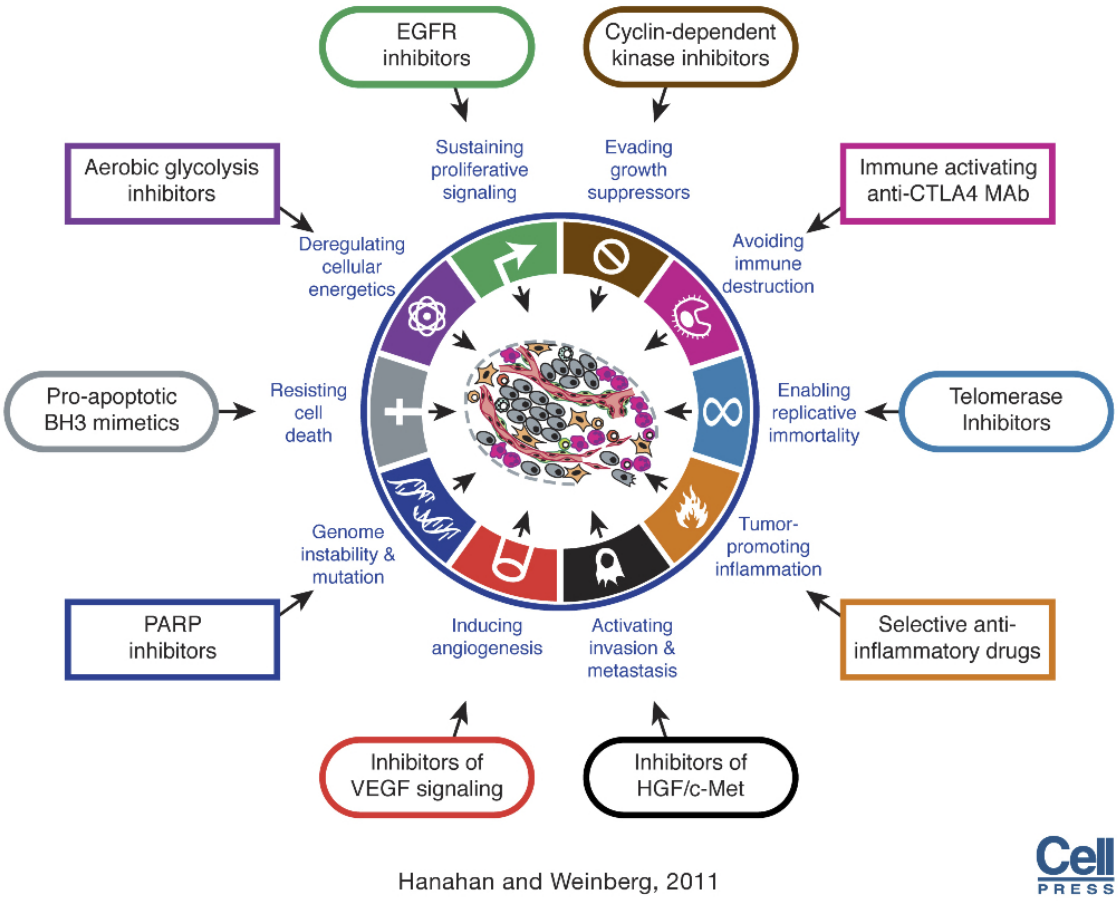

Figure 1.1: Hallmarks of cancer and its therapeutic targets. This overview depicts the hallmarks of cancer, as elucidated by Hanahan *et al.*[5]. The therapeutic targets are framed, pointing to the hallmark that they target. The square frames depict emerging hallmarks, that have yet to be scientifically generalised or fully validated, or enabling characteristics that support or have tumour promoting consequences.

Current therapies for cancer range from chemotherapy to surgical resection of the afflicted site and radiation therapy, with combination therapies becoming the standard of care today. Most common combinations are those including radiotherapy, since a combination herewith has been shown to have the most synergistically beneficial effect for the patient. Targeted therapy and diverse small molecule therapies have been in development since the late 1990s, with approaches covering monoclonal antibodies, targeted prodrug delivery and cancer immunotherapies, just to name a few. Hormonal therapies modulating the endocrine system by targeting oestrogen/testosterone have also shown to be therapeutically beneficial and represents one of the main modalities in cancer therapy. Steroid hormones elicit a strong cellular response, especially pertaining to gene expression in certain cancer types, possibly going so far as to cause cancer cells to undergo apoptosis.[8] An example

for targeted therapies (also known as biotherapeutics) is to target the angiogenesis component that plays an important role in the process of cancer establishment. Therapies using α-VEGF antibody to engage this system have shown some promise in patients, but as with most current therapies have either reduced efficacy or marked side-effects.

No matter how effective a treatment, the currently available methods only prolong survival or transform cancer into a stable, manageable disease. They are by no means a definitive cure, with chances of recurrence and survival varying greatly among patients, hereby making the need for progression in this field sorely felt. As there has been limited progress in the field of conventional cancer therapies, some researchers have turned towards more exotic methods. Using viruses is just one such method.

1.2 Viruses in cancer therapy

Oncolytic viruses are native or recombinant, attenuated viruses that have the innate or enhanced capability to infect tumour cells, replicate within the tumour microenvironment and subsequently lyse those cells. Most of the viruses being researched today have been chosen or engineered for their ability to specifically replicate in certain tumour cells while disregarding healthy tissue, their tropism towards cancer cells or their ability to transport prodrug or immunological payloads to the site of affliction. Some representatives of these viruses are currently being tested at differing stages in clinical trials.

1.2.1 Oncolytic virotherapy

Oncolytic virotherapy was studied intensively in the 1950s and 1960s. Southam *et al.* first described the use of viruses as "antineoplastic agents" in 1952.[9] After that, research in virotherapy declined due to safety concerns. As of the 1990s, new genetic engineering techniques and technological advances enabled viruses to be used as a vector for gene therapy and an oncolytic tool. Oncolytic activity of viruses is considered to be a two-pronged approach, in which tumour cells are lysed by direct viral replication on the one hand, and tumour cells further become targets for the immune system on the other hand.[10]

There are a number of alternative viruses available, that exploit a distinct, characteristic trait or tropism within the tumour microenvironment. Reoviruses are known to require an activated Ras pathway in order to infect cells, thus have been suggested for treating cancers with upregulated Ras pathways, as in human pancreatic, colon, ovarian and breast cancers.[11] Some adenoviruses, i.e. ONYX-015, were engineered to have an *E1B* gene deletion, resulting in greater targeting of *p53* deficiencies common to cancer cells. *E1B*-55kDa protein normally binds to *p53*, resulting in the degradation of its binding partner and preventing early cell death and enabling viral replication. A deletion of the gene results in the virus replicating specifically in cells that have defective *p53* pathways, as the infection of normal cells would conclude in the cell initiating apoptosis or similar immune responses.[12] [13]

Another commonly employed virus is the herpes simplex virus (HSV)[14], of which many mutants have been constructed. The one of the first mutants, *hr3*, was created by an in-frame insertion of the *E. coli* gene lacZ into the ICP6 gene that codes for the large subunit of the viral ribonucleotide reductase (RR) found in the HSV genome. Since mammalian ribonucleotide reductase and nucleotide levels are low in normal cell, but high in cancer and metastatic cells, this microenvironment enables *hr3* to replicate specifically. Importantly, *hr3* and other mutants are hypersensitive to acyclovir due to their attenuation, hence a fail-safe is in place able to prevent systemic toxicity arising from unchecked and unplanned HSV replication. As with VACV, HSV does not insert itself into the host genome and is capable of accepting large foreign gene fragments for replication.

Paramyxoviruses, to which the modified measles viruses[15] and the mumps virus[16] belong, is another virus used in oncolytic virotherapy. Newcastle disease virus (NDV), a further representative of this family, as an antitumour treatment, was first reported in 1965 by Cassel *et al.*[17] as having been administered as a regiment against human adenocarcinomas. The virus had been passaged repeatedly through Ehrlich ascites carcinoma cells *in vivo* and *in vitro*, resulting in an attenuated version of the virus.[18] A derivative of this NDV was used by Csatary *et al.* in a 1996 clinical study, reporting the successful intravenous treatment of grade IV glioblastoma multiforme in fourteen patients[19], of which four were still alive in 2004. The main mechanism of NDV as an effective oncolytic agent is believed to lie within the mitochondrial/intrinsic pathway. Moreover, the ability of NDV to fuse with tumour cells results in syncytia, a heightened immune response and ultimately apoptosis, contribute further to its killing capabilities.[20] However, there is a

downside to treating cancer with NDV. As with many virus based treatments, the risk of one day developing an immunity to the treatment agent itself is ever-present.

1.2.2 Poxviruses

An important oncolytic virotherapeutic agent belongs to the *poxviridae* family, know since the 19th century. Edward Jenner, an English physician of the time, introduced and developed a method of inoculation using the cowpox virus, belonging to the *Poxviridae* subfamily *chordopoxviridae*, which confers immunity to other members of the orthopoxvirus genus, including smallpox (variola major/minor). The vaccinia virus (VACV) belongs to this genus, although genetic testing shows that vaccinia is not closely related to the other members[21], thus its exact origins remain unknown.

Typically, a smallpox infection results in a macropapular rash on the body with the highest density of papules/pustules being on the face and the distal extremities of the body. Mortality due to a smallpox infection is generally dependent on the infecting virus type, with variola major having a fatality rate of 30-35% and variola minor a fatality rate of about 1%. Since smallpox was declared eradicated by the WHO in 1980, in most part due to rigorous ring vaccination and similarly developed vaccination and quarantine strategies, the vaccinia virus has found its use as a viral expression system[22] and, as in our case, in oncolytic virotherapy.[23] [24] [25]

VACV is chosen due to its ease of genetic manipulation. Using modern genetic engineering and molecular biological methodologies, manipulating the VACV genome can be done efficiently, generating clones with newly inserted genetic material within a matter of weeks. On top of that, VACV is a virus that replicates in the cytoplasm, leading many to believe that it is a safer alternative to, e.g. retroviruses, whose genome is integrated into the host genome. Another safety aspect that supports the use of VACV in human clinical research is its long history of used as a vaccine. Extensive knowledge of adverse side-effects and tolerability within the human population has been well documented, even leading up to the eradication of smallpox, with the resulting data analysed being further used to aid other vaccination regimens.

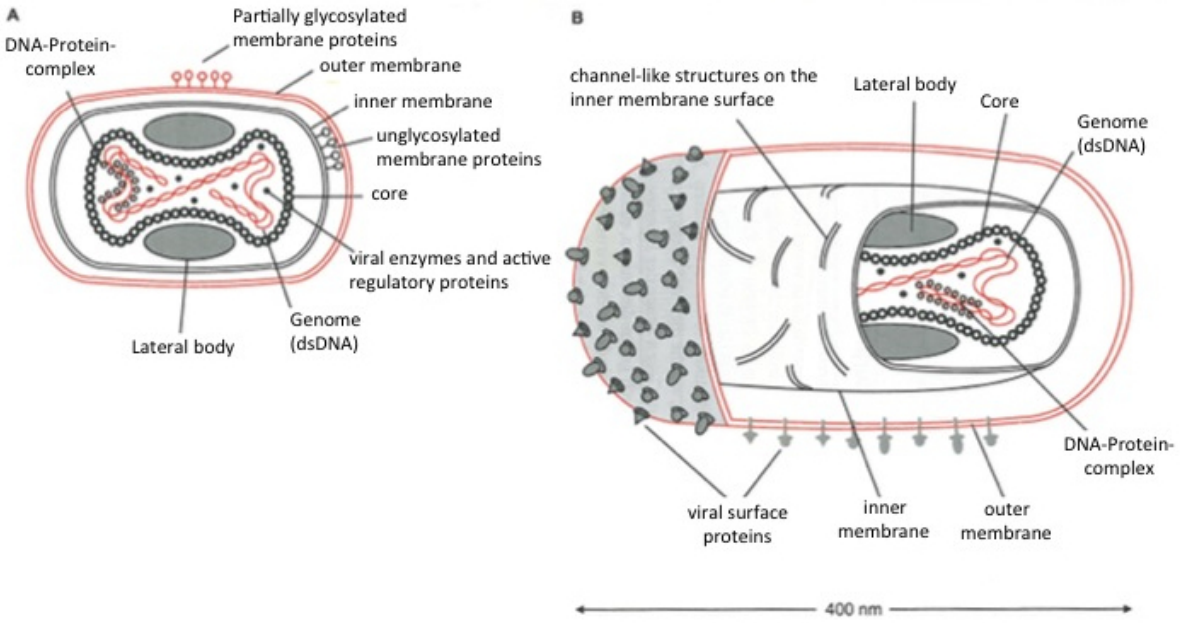

Figure 1.2: Structure of a *Poxviridae* particle. A: The extracellular form of a *Poxviridae* particle in lateral cross-section. The function and composition of the lateral bodies is unknown. It is possible that these bodies are artefacts from the preparation method used for the electron microscopy of the particles. This form of the poxvirus is infectious. B: Horizontal cross-section of an EEV particle. On the surface of the inner membrane, channel-like structures formed from viral membrane proteins can be seen. Taken and modified from "Molekulare Virologie", 3rd Edition.[21]

Vaccinia

Vaccinia virus is a double stranded DNA virus that replicates solely in the cytoplasm of its host cell. In the course of a vaccinia virus infection, four different types of virions can be found within and without the cells: intracellular mature virus (IMV), intracellular enveloped virus (IEV), cell-associated enveloped virus (CEV) and extracellular enveloped virus (EEV).[26] [21]

During the viral replication cycle, different genes are expressed under different promoters, enabling the differential expression of genes in a time-dependent manner. Fig. 1.4 shows a schematic, showing the replication cycle and location of VACV virions within the host cell. At first, virus particles are taken up into the host cell, thus losing their outer membrane. Only the virus core enters the cytoplasm (1). It binds to microtubuli filaments and is transported deeper into the cell (2). There, the transcription and translation of early viral mRNAs takes place, resulting in the formation of early viral proteins. These early viral

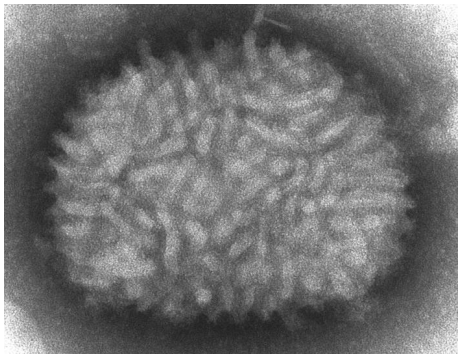

Figure 1.3: Electron microscope image of a vaccinia virus particle. The image was taken from the Centre for Disease Control's Public Health Image Library, ID# 2143.[27]

proteins initiate the release of the viral genome from the core structure and its replication, which takes place within discreet areas of the cytoplasm known as virosomes (3). Following this, the synthesis of late mRNA and proteins occurs (4). Structure proteins assemble, along with membrane fragments and and the virus genome, to form unfinished, immature virus particles, which later form the IMVs (5; Fig. 1.2). These unfinished particles are transported to the membrane compartments within the *trans*-Golgi network, where they are encased in two further membranes, thus creating IEV particles (6). The IEVs bind to microtubuli and are transported to the membrane of the cytoplasm (7). Here, the outer IEV membrane fuses with the cytoplasm membrane. Some particles form into CEVs, that adhere to the cell surface and that are released into neighbouring cells via actin filaments (8). The other portion of these particles detach from the cytoplasm surface and become EEVs (9).

1.2.3 The development of GLV-1h68 as an anti-cancer drug

GLV-1h68, also known as GL-ONC1, is an oncolytic, triple-mutated therapeutic virus. It was engineered by Zhang *et al.* in 2007 and shown to eradicate solid human breast tumours (GI-101A) in nude mice.[28] It is most closely related to the Lister strain and has foreign gene inserts in three loci, namely *J2R*, *A56R* and *F14.5*, the first two disrupting the expression of thymidine kinase and hemagglutinine HA, respectively, significantly attenuating the virus. The inactivation of the *F14.5* locus, which encodes an unknown protein, further contributes to a reduced virulence when compared to the unaltered virus, making it a prime candidate for use as a therapeutic agent. Furthermore, the insertion of GFP into that particular locus allows non-invasive monitoring of viral spread in the

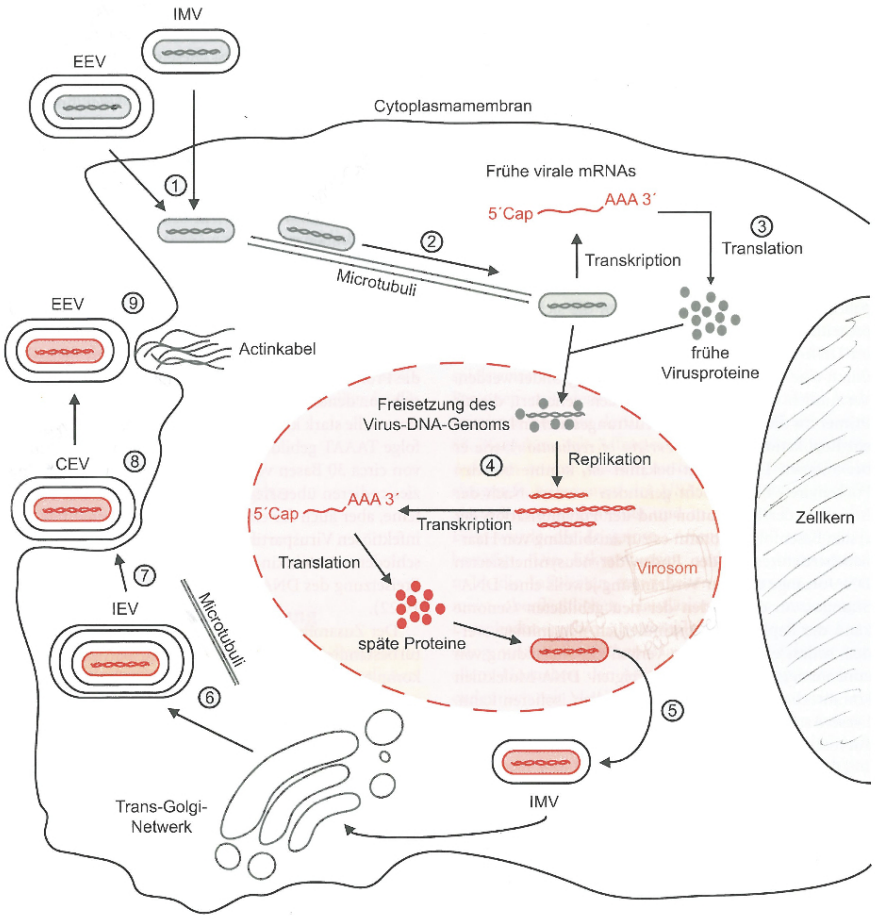

Figure 1.4: Schematic representation of the replication cycle of VACV within a host cell. All the steps noted are explained in section 1.2.2 Taken and modified from "Molekulare Virologie", 3rd Edition.[21]

tumour through GFP fluorescent imaging.[29] Studies showed, that viral replication of the recombinant VACV was specific to tumour cells, based on GFP imaging. When compared to the Western Reserve (WR), Lister and Copenhagen (COP) strain, GLV-1h68 was found to have additional mutations outside of the three modified loci, that might account for its attenuated virulence. For instance, GLV-1h68 lacks *crmE*, a cytokine response modulator present in the Lister strain genome.

Three different promoters were used when inserting the foreign genes into the VACV genome. The renilla luciferase-GFP fusion cDNA was inserted under the control of the synthetic early/late promoter p^{sEL}. The human transferrin receptor-β-galactosidase (TFR-*lacZ*) construct was inserted under the control of the $p^{sEL}/p^{7.5}$ promoter, with $p^{7.5}$ being the native early/late promoter found in VACV. *gusA* was inserted under the native VACV late promoter p^{11K}. The relative promoter strengths between the native and

synthetic representatives are discussed by Chakrabarti *et el.*[30], and are as followed: p^{sEL} >p^{11K} >$p^{7.5}$(EL), with p^{sEL} being as strong or stronger than p^{sL} (s: synthetic; E: early; L: late; EL: early/late; promoters without a "s" denotes native promoters). It is also relevant to know that p^{sEL} in the *F14.5* locus was twice as strong as the same p^{sEL} in the *J2R* locus.[31] The aforementioned relationships are important later when comparing and analysing the resulting protein expression as promoter strength and temporal initiation have great influence on those parameters.

Limitations & Concerns

So far, data from previous clinical trials tell an indecisive, albeit promising, story. Concerns have been expressed that using a virus, where there is a possibility of viral genome integration into a host genome despite genetic augmentation and engineering, is a risk. Neutralizing antibodies could also subdue the effectiveness of intravenously administered virotherapy by binding to budding virus particles, muting or even actively preventing viral replication and oncolysis. The human body develops immune responses to all viral agents, only giving the virus itself a very small window of opportunity to achieve oncolytic activity. Thus, the efficacy of certain therapies has been questioned because some only work in combination with immunosuppressants, increasing the risk of opportunistic infections.[32] [33] The methods for targeting tumour cells has often been a cause for debate, with different methods emerging, e.g. translational and transcriptional targeting[34], and having varying success in practice (For more information on targets, see Fig. 1.1). Most histological analyses of tumours treated in animal models show that viral replication within the tumour is highly heterogeneous, even when the virus is administered intratumourally. It has been shown that the extracellular matrix (ECM) surrounding the tissue plays an important role in preventing uniform virus spreading within the tumour, as it represents a physical barrier.[35] Tumour vasculature, tumour size and proximity of the cells to the vasculature play an important role in assisting viral infiltration of the tumour, as many therapies are administered intravenously.[36] High interstitial pressure within the tumour also prevents the virus from disseminating in a favourable manner.[37] Natural variance between the immune responses of different patients, with the variance and heterogeneity of tumours in general, make it even more problematic to predict patient outcome prior to treatment.[38] [39]

While oncolytic virotherapy is effective by itself, it is most effective in combination with other therapy methods, i.e. radiation therapy[40] or chemotherapy.[41] This synergy makes

it difficult to pinpoint exactly which therapy is providing the decisive component of a successful treatment. Additionally, oncolytic virotherapy has shown much promise in treating metastatic tumours, as virus particles travelling in the blood stream are able to "seek and destroy" tumour cells. Animal models used to gauge effectiveness, toxicity and other important characteristics of any viral treatment, most commonly immune-compromised athymic nude or severe combined immunodeficient (SCID) mice. The difference in host physiology, varied pathways of complement activation of the immune system and viral tropism towards different cell species are all circumstances that have to be taken into consideration when determining the therapeutic efficacy of any tested therapy for humans.[42] This imposes uncertainty of the translation between models and humans. Research is under way to improve experimental models by attempting to account for interspecies differences.[43] [44]

1.3 Biomarkers

In general usage, a (bio-)marker is any molecule (disease- or drug-related) or physical parameter (as in body temperature) that can be used to track and identify changes in an organism, either in a quantitative or qualitative manner. It could be used to deduce metabolism, pharmacodynamic and pharmacokinetic responses to a drug treatment, and/or denote cellular processes.[45] [46] A suitable biomarker can also be used to identify a certain type of cell, e.g. Oct-4 for embryonic stem cells, or it can be used to quantify the state of any given process. For instance, the accumulation of antibodies in blood signifies an immune response, or a raised body temperature may indicate the presence of an infection. In molecular biology, expression (bio-) markers are used to follow and denote certain stages in cellular mechanisms, whereby a foreign gene insert is only expressed/visible under controlled circumstances.

The hallmarks of good biomarkers in medicine are that they are accessible through readily obtained bodily fluids, the most common being blood and urine. Ease of detection, quantification and low general cross-reactivity are important characteristics of suitable biomarkers. An ideal biomarker is stable in solution, or degrades in a consistent and predictable manner, providing a large detection window, in which the sample can and should be obtained. Ease of detection is important as a complicated quantification assay would impede its practicality. Generally, quantification of a biomarker in itself is preferable, as opposed to a qualitative measure, yielding a positive/negative answer.

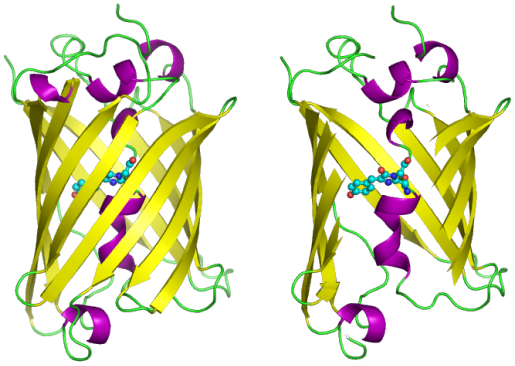

Figure 1.5: Ball and stick representation of a green fluorescent protein (GFP). In the right image, a part of the β-sheets (yellow) that make up the cylinder wall have been removed, providing insight into the chromophore.[49]

1.3.1 Green Fluorescent Protein (GFP)

Green fluorescent protein (abbrev. GFP) was first isolated from the Pacific jellyfish, *Aequorea victoria*, and is the most commonly used visual gene expression reporter in cellular and molecular biology today. By inserting the cDNA sequence required for its expression, GFP can be incorporated into almost any organism[47] and is mainly detected by measuring its emission wavelength after excitation with ultraviolet (UV) light. GFP isolated from *A. victoria* has a major excitation peak at 395 nm and a minor one at 495 nm. The corresponding emission peak is measured at 503 nm. This method of detection can be used *in vivo*, as well as *in vitro*, and thus can be used to image any cell expressing GFP. In cell culture, GFP released from lysed cells can be detected using a range of assays, from photometric detection to antibody-dependent assays (as in ELISA). With the further development of a palette of fluorophores by Tsien *et al.*[48], GFP has a wide variety of applications, making it one of the most prominently used biomarkers of our time. In the GLV-1h68 construct, GFP is contained as a fusion gene with renilla luciferase, located within the *F14.5* locus under the p^{sEL} promoter.

1.3.2 Bacterial β-galactosidase (lacZ)

β-Galactosidase, also known as β-gal or beta-gal, is a hydrolase, specifically an exoglycosidase. It catalyses the cleavage of the β-glycosidic bond between a glucose and its organic neighbour. In *Escherichia coli*, the gene lacZ encodes β-galactosidase and is part

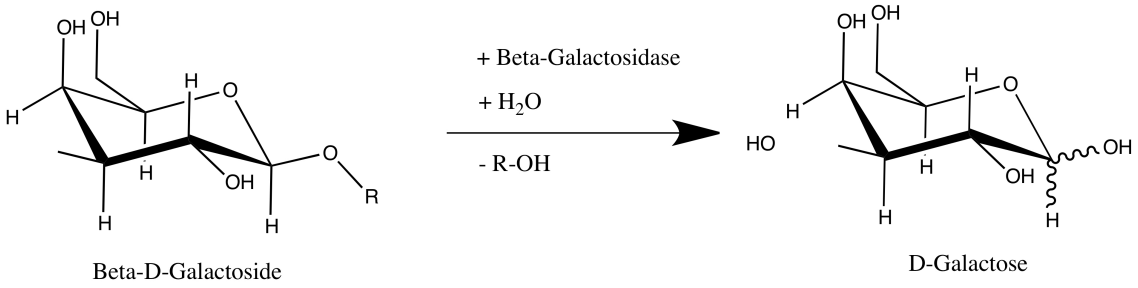

Figure 1.6: Schematic representation of the mechanism of a hydrolysis of β-galactoside into monosaccharides. The reaction is catalysed by the enzyme β-galactosidase.

of the so-called lacZ operon, an inducible system, able to be activated by lactose when glucose is depleted.

In GLV-1h68, β-galactosidase from *E. coli* is inserted in the *J2R* locus and is expressed during viral replication. It accumulates in the cytoplasm, but is only released into surrounding tissue and the blood stream upon cell lysis, thus it is defined as a cytoplasmic protein. Human β-galactosidase (UniProt no. P16278) and *E. coli* β-galactosidase (Uniprot no. P00722) are distinctive enough to allow specific antibody detection of one, but not the other. BLAST analysis of both protein sequences results in four alignment regions, with each having less than twelve common amino acids and with E values ranging from 0.85 to 9.7 for all four regions (data not shown).

1.3.3 β-Glucuronidase from *E. coli*

β-Glucuronidase, expressed by the gene gusA, is member of the glycosidase family and, more specifically, is an enzyme that hydrolyses β-D-glucuronic acid residues from mucopolysaccharides.[50] Isolated most commonly from *E. coli*, it is a reporter system that has been used since the 1980s, for monitoring gene expression in plants, as well as in animals.[51] [52] This enzyme is active as a tetramer and different substrates can be used for its activity-dependent detection, with 4-methylumbelliferyl-β-D-glucuronide (4-MUG) being the substrate most commonly used for fluorimetric assays. The activity can be read as relative fluorescent units (RFUs) using a spectrophotometer, using an excitation of 365 nm and an emissions of 455 nm.

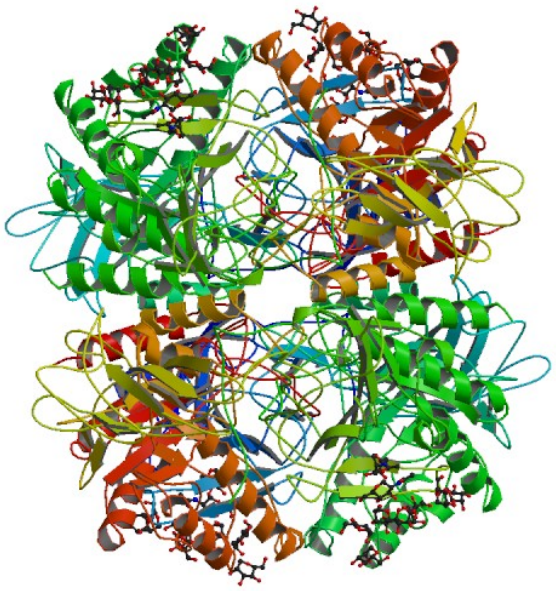

Figure 1.7: β-Glucuronidase homotetramer. The X-ray structure of the homotetrameric human beta-glucuronidase as determined at 2.6 Å resolution.[53]

1.3.4 Carboxypeptidase G2 (CPG2) from *Pseudomonas* sp.

Carboxypeptidase G2 (CPG2), also known under commercial names such as Voraxaze or glucarpidase, is a folate-metabolising enzyme that was first isolated by Goldman *et al.* in 1965[54] from the organism *Pseudomonas* sp. Carboxypeptidases in general are enzymes that hydrolyse the peptide bond found at the carboxy (C-) terminal end of peptides and proteins, and play different roles from protein maturation to metabolism.[55] It is a dimeric protein, totalling 92 kDa depending on the expression system and post-translational modifications acquired. For its enzymatic activity, CPG2 requires four zinc ions (Zn^{2+}) per enzyme molecule. The enzymatic reaction catalysed is the hydrolysis of folic acid and derivatives to pteroic acid and glutamic acid (Fig.1.8).[56]

Methotrexate (abbrev. MTX), formerly known as amethopterin, is a competitive dihyrdrofolate reductase (DHFR) inhibitor. It is an antimetabolite drug commonly used in chemotherapy, for ectopic pregnancies[57] and for the treatment of certain autoimmune diseases.[58] MTX mimics the function of folic acid, binding to DHFR and disrupting its role in the tetrahydrofolic acid pathway.[59] Tetrahydrofolic acid is an important coenzyme in many reactions pertaining to the metabolism of amino and nucleic acids, notably thymidine and purines, a shortage of which ultimately leads to diseases like megaloblastic anaemia. Since MTX ultimately prevents DNA synthesis, it has a cytotoxic effect on cells

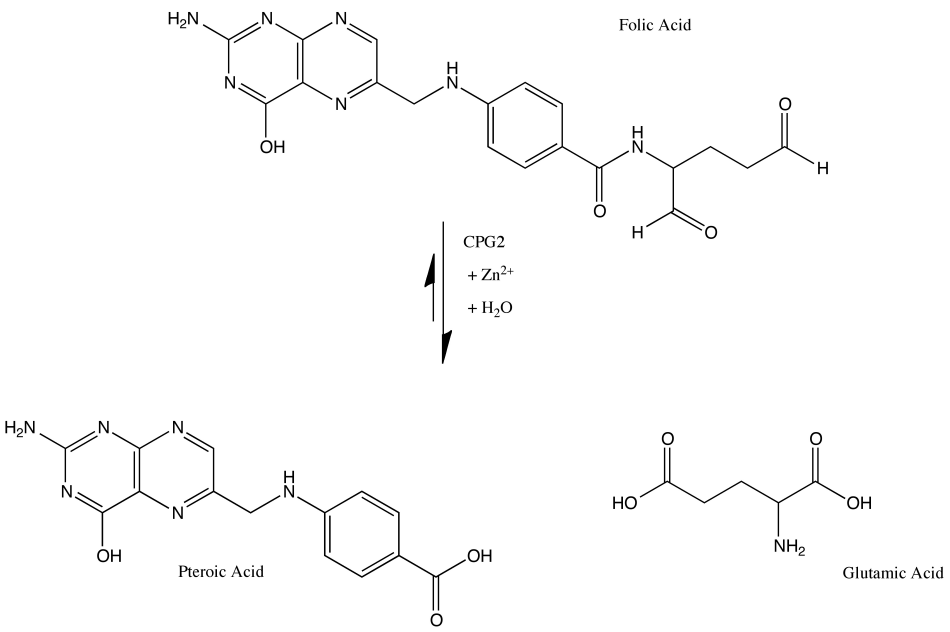

Figure 1.8: Schematic representation of the mechanism of hydrolysis of folic acid into pteroic acid and glutamic acid catalysed by CPG2.

in the S-phase of cellular replication. Because of this, MTX has a greater toxic effect in rapidly dividing cells, due to a faster DNA/RNA metabolisms. The higher demand for thymidine in those cells, which, unable to cope with the lack of thymidine, eventually results die a thymidine less death. This mechanism is the reason for MTX's use as a chemotherapeutic drug, as it has a thousand-fold higher affinity to DHFR than folic acid, shifting the weight of the reaction markedly towards the MTX-DHFR product.[60]

Due to CPG2's ability to metabolise MTX, it is used today as a methotrexate intervention drug, clearing the chemotherapeutic from the patient's system before it can cause any serious metabolic damage.[61]

1.3.5 Human carcinoembryonic Antigen (CEA)

Carcinoembryonic antigen (CEA) was first discovered in 1965 by Gold and Freedman to correlate with the presence of carcinomas, most predominantly with human colon carcinomas.[62] Antigens are defined as any substances that can be bound by an antibody. It is not required to be immunogenic and does not always have to elicit an immune response.[63] CEA is a 180 kDa[64] large glycosyl phosphatidyl inositol (GPI) cell surface anchored glycoprotein involved in cell adhesion, signal transduction and innate immunity.[65] It is

deemed to be closely related to the human pregnancy-specific β1 glycoprotein (PSG).[66] This antigen is most commonly expressed in the fetal stages of human development and is restricted to specific organs. Its expression decreases markedly before birth and may or may not persist throughout life, with the exception of certain organs (mostly containing epithelial cells) displaying minute concentrations.[65] It is usually not readily detectable in healthy individuals, with heavy smokers being an exception in displaying raised levels of CEA. Typically, a healthy patient can have up to 2.5-3 ng/ml, a heavy smoker up to 5 ng/ml CEA in serum.[67]

In 1969, Thomson *et al.* established the first method for detecting CEA in human serum[68] using a radioimmunoassay, and the principle of using CEA in pre-clinical testing for the detection of myriad types of adenocarcinomas (e.g. colorectal, lung, breast etc.) is still being applied.[65] [69] However, as with many preclinical tests, the detection of CEA is not a fail-safe method for early cancer detection or cancer diagnosis and warrants further investigation when a positive result occurs. The half-life of CEA is being used as a postoperative prognostic value after surgical resection, indicative of resection success and if the patient might require follow-up treatment due to metastasis formation.[70] Thus, using CEA as a tumour biomarker has long been established in the clinic. The recombinant CEA used in this thesis was modified in part according to a protocol published by Terskikh *et al.*[71] Using this method, the deletion of a 3′ cDNA region, which translated into loss of the C-terminal 26 aa long hydrophobic domain, was achieved, consequently rendering the resulting CEA soluble (sCEA), as opposed to the normally membrane-bound, full-length version (fCEA). The binding of CEA to the cell membrane is mediated by the GPI anchor, which is generally assumed to be added post-translationally by substituting the hydrophobic C-terminus with said anchor. The lack of this anchor renders CEA soluble, making it detectable in bodily fluids, most notably blood serum.

1.3.6 Indigenous vaccinia virus proteins

In addition to foreign, recombinant genes inserted into the VACV genome, native viral proteins also represent another group of viral replication-dependent markers.

A27L

A27L is a gene under a native late promoter (p^L) that expresses a 14 kDa viral envelope/surface protein, embedded in the membrane of IMV particles.[72] It is a type I

membrane protein, with a trimeric coiled-coil structure characteristic of cell fusion proteins.[73] Experiments using antibodies binding specifically to the 14 kDa protein inhibit syncytium formation of VACV infected cells, showing that it plays an essential role in viral cell fusion. The A27L encoded protein also mediates initial cell binding[74], and the exit of VACV from the host cell.[75] A27L$^-$ mutants are unable to be released into the host, thus the formation of EEV molecules is suppressed[76][77] On IMV particles, which represent 70 to 90% of all virions[78], the A27L protein is abundant and can be detected, whereas EEV particles lack detectable A27L protein.

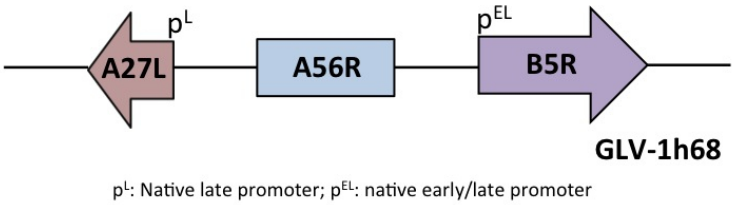

Figure 1.9: A schematic representation of the vaccinia loci A27L and B5R. p^{EL} and p^{L} represent the native early/late and late promoters respectively. The distances shown are for representation purposes only and do not reflect the actual distances between loci.

B5R

B5R is a gene within the vaccinia virus genome, whose expression under its native early/late promoter (p^{EL}) results in the production of a specific EEV type-I membrane glycoprotein. This protein is required for the trans-Golgi/endosomal membrane-wrapping of IMV virions. It has a total molecular mass of 35 kDa and has also been implicated to play a role in plaque size determination and host range.[79]

1.4 Aims

As shown by Zhang *et al.*[29], monitoring viral replication within the tumour, albeit not quantitatively, can be achieved using GFP for fluorescent imaging of infected tumours. However, this method only works on tumours within the subcutaneous and cutaneous regions of the skin. Tumours located deeper inside the human body would not be visible, as the excitation wavelength required for visualising GFP would not be able to penetrate far enough, at least not without surgical assistance. Viral titres within the body are also difficult to ascertain, as the viral DNA in the blood is present in concentrations so minute that quantifying it is a difficult task and at present can only be interpreted in a semi-qualitative manner.

The most straightforward method of gathering information about any pathway or bodily process is utilising bodily fluids for biomarker detection specific to that process. This allows repeated sample retrieval at little or no risk to the patient, and, once analysed, gives physicians and researchers information on the progress of the treatment and possible patient prognosis. So, there is a need for a non-invasive manner of monitoring patient progression and viral replication. Monitoring the viral titres present in the body not only give an indication if the treatment is working, but also enables supervision of the viral replication in order to ensure the safety of the patient.

The aim of this thesis was to identify biomarkers that would lend themselves to a non-invasive method for monitoring and quantifying viral replication, and judging patient response to oncolytic vaccinia virus treatments, i.e. using GLV-1h68 or its derivatives. For that purpose, an array of potential biomarkers was chosen; some which had already been present in the GLV-1h68 viral genome, and others which were cloned into the virus specifically for this purpose. It was expected that the monitoring of these biomakers would give rise to pharmacokinetic, and possibly pharmacodynamic insight to treatments and infections using oncolytic viruses, enabling clinicians to predict treatment prognosis on the basis of serum testing.

2 Materials & Methods

For materials, please see Appendix B and following. All solutions mentioned here are listed in Appendix I.

2.1 Cell culture

2.1.1 African Green Monkey Kidney Cells (CV-1)

African Green Monkey Kidney cells (CV-1) are cells commonly used for vaccinia virus generation and production.

For CV-1 sub-cultivation of established CV-1 cell lines, medium was removed from confluent T225 tissue culture flasks and cell monolayers washed with 10 ml PBS. 2 ml trypsin/EDTA was added to disperse the monolayer and incubated for 2 minutes at 37 °C. Cells were removed by gently tapping the flask and adding 10 ml Dubelcco's Modified Eagles Medium containing 10% FBS (DMEM 10%). Cells were gently resuspended by pipetting and counted according to the method mentioned in section 2.2.2

For virus infection and replication assay, 24-well culture plates were seeded with $2x10^5$ cells per ml in 1 ml of DMEM 10% and were incubated at 37 °C and 5% CO_2 for 24 hours. Virus titration experiments are carried out on the next day on monolayers of 95-100% confluency.

2.1.2 Human cancer cells in culture

The human cancer cell lines utilised in this thesis were A549 (lung carcinoma), HT29 (colorectal adenocarcinoma), DU145 (prostate cancer), GI-101A (breast cancer) and OV-CAR3 (ovarian epithelial carcinoma). The media and cell culture conditions were selected according to ATCC recommendations.

2.1.3 Cell count

Medium was aspirated from cell culture plates and each well was washed with 1 ml of PBS. PBS was aspirated and the cells were trypsinised by adding 0.5 ml trypsin/EDTA solution per well and incubating for 8 minutes at 37 °C. 0.5 ml DMEM 10% were added to each well well and the cells were pooled in a 15 ml conical tube. An aliquot of 100 μl cells were stained with 400 μl of a trypan blue solution (1:5 ratio) and 10μl loaded into each chamber of a Neubauer hemocytometer. All viable, unstained cells were counted in all quadrants of the upper and lower chambers. This procedure required a minimum of 2 wells from any culture plate containing cells, to allow for statistical variances. The final

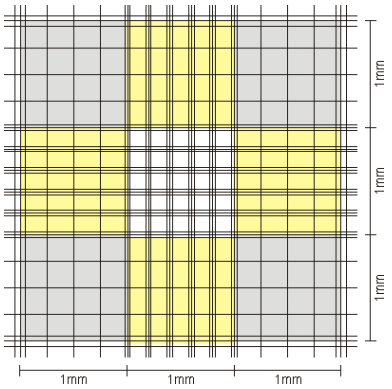

Figure 2.1: A Neubauer improved hemocytometer: the scheme represents one counting chamber. There are two counting chambers per Neubauer slide. The quadrants of interest are coloured in gray.

concentration was calculated using the following formula:

$$\text{cell count in } \left[\frac{cells}{ml}\right] = \frac{\sum \text{cells in all quandrants} \times d}{\text{number of quandrants} \times F} \tag{2.1}$$

with $d = 5$ being the dilution factor of the trypsinised cells with trypan blue; and $F = 0.0001$, a compensation factor for the volume between the coverslip and the hemocytometer.

2.1.4 Harvesting of cells for further analyses

Cells were harvested from various cell culture containers by adding 1 ml of the cell line appropriate growth media and scraping with a cell scraper. These cells were then dispersed by pipetting repeatedly and then transferred to a reaction tube. Three freeze-thaw

cycles were performed in order to prepare cells for viral plaque assay, or another other quantification method required.

Spiked samples

If required, cell culture samples were diluted in a ratio of 1:1 with human plasma, resulting in spiked samples. When using these samples, a dilution factor of 2 was used in calculations, or double the volume was used in the experiment itself, e.g. for Western blots. The human plasma used in these experiments was spun down from commercially acquired human whole blood, using ACD as an anti-coagulant.

2.1.5 Cytotoxicity assay

An MTT assay is an assay which is performed in order to gain insight into cell viability, proliferation or cytotoxicity before, during or after a defined treatment. Surviving cells reduce the tetrazolium salt, used to formazan, a purple insoluble dye.[80] This dye is then solubilised by adding an acid, in this case acidified ethanol. The resulting solution is transferred and read in a photometer.

24-well cell culture plates containing cells of 80-90% confluency were infected in duplicate with the required virus at an MOI of 0.1 or 0.01 in DMEM 2%. One plate was planned for each time point. The infection media was removed after one hour and replaced with DMEM 10%. In the case of the 1 hpi plate, 0.5 ml dimethyl thiazolyl diphenyl tetrazolium salt (MTT; Invitrogen) solution per well was added. This was incubated for 2 hours at 37 °C, after which the MTT solution was aspirated and the plates frozen down. The same was repeated at 24, 48, 72 and 96 hours post infection, with the media being removed and the plate being frozen down after each staining. Negative control well were included on each plate. After the last plate hat been frozen down, the plates were thawed at room temperature by adding 1 N HCl in isopropanol and placed on a shaker for 20 minutes. 0.2 ml of each well was loaded onto a well in a clear-bottomed 96-well plate and read at 570 nm on an SpectraMax M5 plate reader.

2.2 Virological Methods

2.2.1 Generation & purification of recombinant vaccinia virus

Cloning of plasmids for virus generation

The cDNA for human CEA was isolated from a human cDNA mix (Clontech) using primers designed specifically to amplify the complete cDNA sequence for CEA. A restriction site was added to each primer end, SalI to the forward primer and PacI to the full-length CEA reverse primer. The CEA fragment was amplified in a modified PCR reaction (annealing temperature 56 °C, elongation for 2.5 minutes) and after 30 rounds of amplification, separated by 1% agarose gel electrophoresis and isolated using agarose gel extraction kit from Zymo Research (section 2.7). The resulting PCR fragment was cloned into Invitrogen's ZeroBlunt TOPO Cloning vector, pCR-Blunt II-TOPO. Successfully grown clones were picked and mini-preps preformed on the resulting Luria Bertani-cultures using the PureLink Quick Plasmid Miniprep kit (Invitrogen). The resulting plasmids were then sent for DNA sequencing to Retrogen. When the sequence proved to be correct, the short-length CEA version was amplified from this construct using the sCEA-SalI forward primer and the sCEA-PacI reverse primer. Following the same procedure as above but replacing the reverse primer with the fCEA-PacI reverse primer, the full-length CEA plasmid was constructed. These plasmids containing the desired insert (fCEA or sCEA) was then sequentially digested using SalI and PacI. The insert was then subcloned into the pre-digested vectors TK-SE, TK-SEL and TK-SL using the Quick Ligation kit (NEB), thus placing CEA under the control of synthetic early, early/late or late promoter respectively. The resulting constructs were then used for virus generation.

Recombinant VACV (rVACV) generation with GLV-1h68 as a parental virus

The strategy used to generate the recombinant VACV is a method called transient dominant selection (TDS).[81] Prerequisite for applying this method is the presence of the *E. coli* guanidine phosphoribosyltransferase (*gpt*) expressing gene within the TK shuttle vector containing the gene of interest. First the transfer vector was used to transfect CV-1 cells infected with the parental virus GLV-1h68. The resulting cells were lysed and used for virus purification. The resulting single crossover was facilitated by the TK regions flanking the insert of interest, enabling the integration of this foreign gene into the TK-locus of the vaccinia virus. This intermediate is unstable due to the presence of

direct repeats and resulted in a second crossover event, which formed either the wild type virus or the recombinant vaccina virus (rVACV) containing the foreign gene. Plaque isolation was first performed in the presence of mycophenolic acid, xanthine and hypoxantine, allowing only the growth of viruses expressing *E. coli gpt*, i.e. the aforementioned "unstable" intermediates. The next round of plaque selection was performed without the use of the previously listed selection agents, since successfully recombined viruses, having undergone two recombinations, did not contain the *gpt* gene any more. Screening for marker gene expression was performed to ensure that the isolates picked were not the reformed parental virus GLV-1h68. In the case of the viruses containing CEA, isolates were shown to be *gpt*$^-$ and lacZ$^-$ after multiple selection rounds. *Gpt*$^-$ denoted successful recombination and lacZ$^-$ confirmed the presence of the CEA gene insert within the rVACV, as CEA was inserted into the *J2R* locus, replacing the human transferrin receptor (TFR) and lacZ insert. DNA was extracted from cells infected with these isolates and screened via sequence confirmation to ensure the correct insertion of the foreign gene. After sequence confirmation of the foreign gene insert the new recombinant virus was used to infect CV-1 cells. The harvest of the virus from these cells was accomplished using trypsin to release the virus from the cells. Multiple equilibrium sucrose gradients were applied to purify the amplified virus from cell debris and other cytoplasmic fractions. The purified virus was stored at -80 °C in 1 mM Tris-HCl (pH 9.0) until use to ensure stability.

2.2.2 Replication assay

The aim of a replication assay is to determine the infectability and proliferation of a virus in a certain cell line. This assay is divided up into four parts: cell counting, infection, titre confirmation and a plaque assay of the infected samples. CV-1 cells are used as the positive controls to confirm viral infection and replication.

For cells in cell culture, where the exact cell count is known or can be determined, the cells are infected according to the desired MOI (multiplicity of infection). An MOI of 1 means every cell is infected, an MOI of 0.5 every second cell, and so on and so forth. The infectability of a virus is given in pfu (plaque forming units), as it is unknown how many viral particles are required to form one plaque. The required pfu is calculated as a product of cell count and the desired MOI.

$$\text{required virus amount}\,[pfu] = \text{cell count} \times \text{MOI} \tag{2.2}$$

2.2.3 Infection

The required virus concentration was calculated using the above-mentioned equation 2.2. A vial of virus stock was quick-thawed in a 37 °C water bath for 5 minutes and vortexed vigorously for 10 seconds. Depending on the dilution ratio calculated, the virus was then diluted in Dubelcco's Modified Eagles Medium containing 2% FBS (DMEM 2%). Medium was aspirated from the cells and 200 μl diluted virus was added to each 12-/24-well and the cells were incubated at 37 °C in a 5% CO_2 incubator. After 1 hour, the infection media was removed and the cells washed with 1 ml PBS per well, aspirating the PBS after washing. 1 ml DMEM 10% was added to each well and the cells were returned to the incubator until time for the required time-points had lapsed.

2.2.4 Viral plaque assay/ titre confirmation

A 24-well plate was plated according to the procedure described in section 2.1.1 24 hours before the viral infection procedure. DMEM 2% media was prepared in 1.5 ml micro-centrifuge tubes (900 μl per tube). From the stock vial, the virus was serially diluted down, from 10^{-2} to 10^{-6} (1:10 step dilutions), vortexing vigorously between every dilution step. The media was aspirated from the 24-well cell culture plates and 0.2 ml of a virus dilution was added per well, in duplicate. The plate was incubated for 1 hour at 37 °C, after which 0.5 ml of CMC-overlay was added to each well. The plate was returned to the incubator for further 48 hours. Using a crystal violet staining solution, each well was stained with 250 μl and left to incubate at room temperature for a minimum of 4 hours. The staining solution was then poured off and the plate carefully washed with ddH_2O until the viral plaques became visible. Dilutions showing individual, countable (i.e. non-overlapping) plaques were counted and the viral titre calculated using the following equation:

$$\text{viral titre} \left[\frac{pfu}{ml}\right] = \frac{\text{avg plaques per well}}{\text{dilution factor} \times \text{sample volume}} \tag{2.3}$$

with the sample volume being 0.2 ml and the dilution factor being displayed as a potential factor to the base of 10, e.g. 10^{-2} for a dilution factor of 100.

For confirming a viral titre used for an infection, the calculated viral titre must be within a two-fold range of the theoretical viral titre calculated and used in the infection.
For tumour samples, the procedure was done as described above, with the tumour samples being diluted in the same fashion. Organ homogenates from animal studies were diluted

only once (1:20) in DMEM 2% and added to duplicate wells. If any further dilution was required, the experiment was repeated using a dilution range starting at 10^{-2}.

2.3 Biomarker detection methods

2.3.1 Viral ELISA (vELISA)

Determination of kit variables

This kit was developed in-house and is based on a simple, indirect ELISA. No capture antibody was developed because the target protein did not have second immunogenic site required for capture antibody development. Other parameters, such as primary and secondary antibody concentration, blocker concentration and incubation times were developed using the "Assay Development Technical Handbook" by Thermo Scientific Pierce [82], as well as "The Experimenter: Immunology" by Luttman *et al.* [83] as guidelines. The peptide sequence used for antibody generation was as followed and had been determined by antigenicity analysis performed by Genscript:

A27L: CAKKIDVQTGRRPYE (Lot: 45887-4). Genscript also provided the resulting antibody using their "Complete affinity-purified polyclonal antibody package" (rabbit polyclonal). 7 ml antibody (0.938 mg/ml) was delivered and stored in PBS (pH 7.4) with 0.02% sodium azide.

B5R: RTNEKFDPVDDGPDC (Lot: 45887-2). The corresponding rabbit polyclonal antibody was delivered as a lyophilised powder and reconstituted to a 0.327 mg.ml solution in PBS (pH 7.4) with 0.02% sodium azide.

A clear-bottomed 96-well plate was coated with 200 μl of sample per well overnight at 4 °C. The plate was then blocked using 200 μl of a 2% BSA in PBS solution and incubated at 37 °C for 1 hour. After that the plate was washed 3 times with PBS-Tween (PBS-T) using 250 μl per well. 200 μl of α-A27L (diluted in PBS-T 1:5000) was added per well and incubated at room temperature for 2 hours. After washing the plate, 200 μl of a goat α-rabbit antibody solution (diluted in PBS-T 1:5000) and incubated at room temperature for 1 hour. After washing, 100 μl of ready-to-use TMB was added to the plate and incubate for 30 minutes. 100 μl of stop solution was added and the plate read on the

SpectraMax M5 plate reader at 450 nm. For quantification, A27L antigen or deactivated pure virus was used.

2.3.2 Quantification of GFP

The GFP ELISA were performed using the commercially available ELISA kit from Cell Biolabs as per the manufacturer's instructions. The standard range here ended at 1 ng/ml and the samples used were diluted 1:100.

GFP was also quantified using a luminescence-based quantification kit from BioVision. Samples here were diluted with sample buffer in order to be within the standard range and read at 390/507 nm (ex/em), as opposed to the 488/507 nm suggested by the kit, with a standard range up to 400 ng/well. Cell culture samples were diluted 1:100, serum samples had to be used undiluted.

2.3.3 β-Glucuronidase enzymatic activity assay

β-Glucuronidase was assayed according the method developed by Hess*et al.*[84] Serum samples were pre-diluted 1:50 or 1:500 with PBS containing 2% FBS. 10 μl of diluted sample and 70 μl of 4-MUGlc substrate reagent (Sigma) were pipetted into each well of a 384-well clear bottom plate and incubated at 37 °C for 1 hour, after which the plate was read for relative fluorescent units using a SpectraMax M5 plate reader. The substrate reagent consisted of 69.8 μl PBS and 0.2 μl 4-MUG stock per well and was prepared fresh for each reading. For quantification purposes, β-glucuronidase (Sigma) was diluted with assay buffer in a serial dilution from 0.1 ng to 0.01 pg in 1:10 dilution steps. The linear regression resulting from the standard curve was used to quantify unknown samples.

2.3.4 β-Galactosidase Quantification

The ELISA for β-galactosidase was performed according to, and using, the β-Gal ELISA kit available from Roche. The standard range for this kit was from 78 to 1250 pg/ml and a dilution factor of 1:100 and 1:200 for early and late time points was used for serum samples.

Quantification via absorption was performed using the Galacto-Light Plus chemiluminescent reporter system for detection of β-galactosidase from Applied Biosystems. Samples were diluted either 1:1 or serial diluted (cell culture) or used undiluted (serum samples).

2.3.5 CEA enzyme-linked immuno sorbant assay (ELISA)

The CEA ELISA was performed using the human CEA ELISA kit from Abcam, specifically detecting human carcinoembryonic antigen. For murine serum samples, the dilution factor used was 1:100 and 1:200 for early and late time points respectively. The standard curve spanned from 0.343 to 250 ng/ml and was plotted in a log/log grid and the best fitting linear trend line was chosen. The trendline showing a "power of" relationship between variables showed the best fit.

2.3.6 Carboxypeptidase G2/MTX Activity Assay

CPG2 was quantified using an enzymatic activity assay based on publications by McCullough *et al.* and Sherwood*et al.* using methotrexate (MTX) as the assay substrate.[85] [86]. A slight modification was undertaken, substituting $ZnSO_4$ with $ZnCl_2$, with no effect to the activity of the enzyme.

In a reaction tube, 590 μl of CPG2 assay buffer were mixed with 6 μl MTX stock solution (end concentration: 0.45 mM) and heated in a 37 °C incubator for 10 minutes. In a spectrophotometer heated to an internal temperature of 37 °C, 10 μl of undiluted sample or standard enzyme was added to an Eppendorf UV cuvette and the spectrophotometer programmed to read the sample at 320 nm every 2 minutes at 37 °C for 2 hours. Prior to this, a blank sample was read for subsequent baseline subtraction. The detection limit for this assay was determined to be at 10 ng of purified enzyme. The linear regression was plotted and the enzyme activity was calculated per ml of sample, with the molar extinction coefficient (ϵ) of MTX being 8300 L mol^{-1} cm^{-1}.

2.4 Vivarium procedures for working with nude mice

The mice required for this study had been purchased from Harlan and were three to four week-old male Hsd:athymic nude *Foxn1*^{nu}. The animals were handled following the rules and guidelines set by Explora Biolabs and according to the ACUP protocol no. EB11-025.

2.4.1 Subcutaneous implants

The tumour cells to be implanted were raised in cell culture and suspended in sterile PBS. 5x10^6 cells in 0.1 ml PBS were implanted into each athymic nude mouse subcutaneously into the upper right flank, above the knee joint using a 29 G sterile needle and syringe. The mice were then monitored for swelling of the leg or any adverse reactions to the tumour implant. After the tumour had formed, it was measured and monitored accordingly.

The mouse weight was also recorded for the duration of the study. Together with the tumour volume, the net body weight of each mouse was calculated and monitored as an indicator for the general well being of the mouse. The net body weight of the mouse is defined as followed:

$$\text{net body weight}\,[g] = \text{body weight}\,[g] - \text{tumour weight}\,[g] \div 1000 \tag{2.4}$$

This body weight is later represented as the fractional body weight calculated from the net body weight at any given time over the initial body weight at the starting point of treatment, in this case day 0. The tumour weight was converted from the tumour volume using the conversion 1 mm^3 = 1 mg.

2.4.2 Tumour measurements

Each tumour was measured at least once weekly using a digital calliper. The dimensions width (w), length (l) and height (h) of the tumour were noted in millimetres (mm) and used to calculate the tumour volume using the following equation:

$$\text{tumour volume}\left[mm^3\right] = 0.5 \times w \times l \times (h - 5) \tag{2.5}$$

2.4.3 GFP imaging

An imaging modality was used here to monitor GFP expression as an indication of viral replication *in vivo*. From 7 days post viral injection onwards, the mice were imaged for 280 ms using a Lightools Research imager and an image capture program. These images were then ranked on a scale of one (1) to five (5) with half increments (0.5) allowed for accuracy. The ranking was defined as following: (0) no signal; (1) diffused, weak signal possibly showing minimal focal points; (2) one to three discrete focal points; (3) more than four focal points; (4) multiple strong focal points on a larger area; (5) multiple distinct loci and diffused signal thought the tumour. At end time points, the ranking was then correlated to the viral titre in the mouse measured that day.

2.4.4 Viral treatment of nude mice

When the tumours had reached the required size of 200-300 mm^3, the mice were inoculated retro-orbitally with $5x10^6$ pfu of virus. For this procedure, the mice were anaesthetized with isoflurane.

2.4.5 Blood and tissue sample collection and preparation

Murine serum collection

For the duration of the study, all mice were bled according to the schedule shown in Fig. 3.46. The mice were bled from the saphenous vein on the superficial posterior of the left hind leg, as the tumours were implanted on the right and interfered with blood sampling. The vein was nicked using a 29 G sterile needle with an attached syringe. The resulting blood drop was aspirated and deposited into a reaction tube on ice. After sample collection, these tubes were spun down at 14,000x g for 30 seconds and the resulting separated serum transferred to a fresh reaction tube. This method was used when small volumes of serum (up to 50 μl) were required. For serum collection at time point sacrifices, the mice were bled using the cardiac puncture method.

Organs and tissue homogenates for titration and biomarker analysis

Tumour and other relevant organs were excised and combined in a whirl bag with twice the w/v ratio of RBM lysis buffer with proteinase inhibitor. One tablet of Complete Protease Inhibitor Cocktail (Roche) was added to 25 ml of RBM lysis buffer. The bag was closed and subjected to mechanical pulverization using a mortar and pestle. The bags were then subjected to three freeze-thaw cycles. Samples could then be taken for further analysis.

For titration, the organ samples were diluted 1:20 and tested in duplicate. The tumour samples were diluted in serial dilutions starting at 10^{-2} in DMEM 2%, with further 1:10 dilution steps. Each sample was measured in duplicate. Both samples were assayed according to standard viral titration procedure.
Biomarker analysis was later performed using various kits and methods listed in section 2.3.

2.5 Histological methods

2.5.1 Preparation of biological samples for histological staining

Fixation for paraffin embedding

The tissues to be fixed and processed had been cut to a size no larger than 3 mm thick (10x10x3 mm) and allowed to fix in 10% neutral buffered formalin (Z-Fix) at room temperature for a minimum of 8 hours, but not exceeding 24 hours. Only one tumour piece was allowed per cage.

Dehydration

To dehydrate the tissue sample, the following steps were be performed at room temperature in the listed solutions on a stirrer moving at a gentle rate. The samples were incubated for one hour at each step.

1. 0.9% NaCl
2. 30% ethanol in 0.9% NaCl
3. 50% ethanol in 0.9% NaCl

4. 70% ethanol in H_2O
5. 90% ethanol in H_2O
6. 100% ethanol
7. 100% ethanol

Embedding in paraffin wax

The paraffin embedding wax was melted ahead of time in a 58 °C dry oven. A mixture of wax and xylene substitute (1:1) was prepared ahead of time and left in the 58 °C oven. In a beaker, the tissue samples were subjected to the following steps for 1 hour each, stirring slowly.

1. 100% Ethanol at room temperature
2. 1:1 mixture of ethanol and xylene substitute at room temperature
3. 100% xylene at room temperature
4. 1:1 mixture of xylene and wax at 58 °C (no stirring needed)
5. 3 changes of embedding wax at 58 °C

After this procedure, during which the tissue had been completely infiltrated with wax, the tissue was placed in an embedding mould and set in embedding wax to form a block. These blocks were allowed to cool at least overnight at room temperature.

Sectioning

The cutting (sectioning) of the tumours was done using a microtome cutter. A water bath consisting of autoclaved water was nearby and had been set to around 50 °C. A slide warmer was used to dry the sections at 38 °C. The blade in the microtome was set to cut at an angle of 10 ° at a thickness of 5 μm. Using brushes, the cut wax slices were lifted off the microtome plate and lain into warm water to facilitate the relaxation of the wax, thus removing any wrinkles that might have occurred. The slices were mounted onto treated glass Superfrost plus microscope slides, avoiding any bubbles or tears, and left on the slide warmer to dry overnight. It was imperative that as many adjacent slices as possible were accumulated. After drying, the slides could be left at 4 °C to 20 °C.

Deparaffinization and re-hydration of tissue slide

Before deparaffinization, the slides were placed into a 58 °C oven for 10 minutes in order to melt the paraffin wax. The slides were then placed into a slide holder and subjected to the following steps:

1. Xylene substitute, 3 minutes (3x). Excess was blotted before continuing
2. 100% ethanol, 3 minutes (3x)
3. 95% ethanol in H_2O, 3 minutes
4. 80% ethanol in H_2O, 3 minutes
5. dd H_2O, 5 minutes

After these steps, the slides were subjected to either H&E staining or immuno-histochemistry staining for VACV.

2.5.2 Hematoxylin & Eosin (H&E) staining

The following steps were performed for staining paraffin embedded tumour slides.

1. Incubation in hematoxalin (Gills Formula, undiluted), 3 minutes
2. Rinse in dd H_2O
3. Tap water for 5 minutes, allowing stain to develop
4. Quickly dip 8 to 12 times in acid ethanol[1]
5. Rinse for 1 minute each in tap water (2x)
6. Rinse in dd H_2O for 2 minutes. Blot excess water before immersing into eosin
7. Undiluted eosin, 30 seconds
8. 95% ethanol, for 5 minutes each (3x)
9. 100% ethanol for 5 minutes each (3x)
10. Xylene substitute for 15 minutes each (3x)

[1]Acid ethanol was made up of 1 ml concentrated HCl in 400 ml of 70% ethanol

After this procedures, coverslips were mounted onto the microscope slide atop a drop of cytomount xylene based mounting solution, taking care not to move the fixed tissue samples. The slides were then left to dry overnight under the fume hood

2.5.3 Histological staining with α-vaccinia antibody

The VACV staining procedure stated here was used to detect VACV on tumour sections that had been embedded and deparaffinized according to the procedure mentioned previously. A counterstaining with hematoxylin was performed in order to visualise the cell nuclei. The kits used here were from VECTASTAIN Elite ABC Kit (HRP) and ImmPACT DAB Peroxidase Substrate, both from Vector Laboratories.

1. Deparaffinization and hydration of tissue sections according to the aforementioned protocol
2. Sections incubated in pre-steamed citrate buffer (10 mM, pH 6.0) for 20 minutes
3. Cooling for 20 minutes at room temperature
4. Rinse for 5 minutes in tap water
5. Incubate sections in 3% H_2O_2 for 5 minutes
6. Rinse in dd H_2O for 2-3 minutes
7. Wash in PBS for 5 minutes
8. Incubate sections for 20 minutes with diluted normal blocking serum[1]
9. Blot excess serum from sections
10. Incubate sections for 30 minutes with 1:1 000 dilution of primary antibody[2]
11. Wash slides for 5 minutes in PBS
12. Incubate sections for 30 minutes with diluted biotinylated secondary antibody solution[3]
13. Wash slides for 5 minutes in PBS
14. Incubate sections for 30 minutes with pre-prepared VECTASTAIN Elite ABC Reagent[4]
15. Wash slides for 5 minutes in PBS
16. Incubate sections in ImmPACT DAB Peroxidase Substrate[5] for 2.5 minutes
17. Wash for 5 minutes in water
18. Counterstain with Vector Hematoxylin QS for 45 seconds
19. Rinse sections with running tap water until rinse water is colourless
20. Dehydrate sections with 100% ethanol for 1 minute each (3x)
21. Incubate in xylene substitute for 3 minutes each (3x)
22. Mount coverslips using xylene based mounting solution

[1] Diluted normal blocking solution: 3 drops of serum stock to 10 ml of PBS.
[2] Genelux custom made rabbit polyclonal antibodies against vaccinia A27L, diluted in blocking serum.
[3] Diluted biotinylated secondary antibody: add 1 drop of biotinylated antibody stock into 10 ml diluted normal blocking serum.
[4] VECTASTAIN Elite ABC Reagent: 2 drops of Reagent A to 5 ml of PBS. Add 2 drops of Reagent B to the same mixing bottle, and mix immediately. Allow to stand for about 30 minutes before use.
[5] ImmPACT DAB Peroxidase Substrate: 1 drop of ImmPACT DAB Chromogen concentrate to 1 ml ImmPACT Diluent, mix well before use.

After either the H& E staining or IHC for VACV, the slides were analysed under a either stereo microscope (low magnification) or a normal microscope (magnification range of 4x to 20x). Digital images were taken for further analysis and comparison.

2.6 SDS-polyacrylamide gel electrophoresis

A gel electrophoresis is normally used to separate proteins, which run depending on the density of the gel used. In SDS-polyacrylamide gel electrophoresis (SDS-PAGE), the native charge is masked by sodium dodecyl sulfate (SDS), a negatively charged detergent that attaches itself to the proteins, denaturing them in the process. Depending on the density of the gel, proteins of up to 5 kDa in size can be accurately separated.

Loading and running gels

In our lab we use the Invitrogen Novex Mini gel system. The gels used are 10-12 % Bis-Tris gels and 16 % Tricine gels for proteins that have a very low molecular mass. The samples are mixed with LDS sample buffer (4x) and denaturing solution (10x) and cooked at 95 °C before being loaded onto the SDS gel. The required marker is loaded, 10 μl for a Coomassie gel and 5 μl for a transfer. The gel is then run for about 1 hour at 120 V, depending on the progression of the bromphenol blue front.

Transfer

The following procedure was used to transfer the proteins from the SDS or tricine gel to a nitrocellulose membrane. Using an electrical current, negatively charged proteins were pulled from the gel onto the membrane, towards the anode('+' pole). The scheme below depicts how the semi-dry blotting apparatus was assembled. The nitrocellulose membrane was chosen for its protein binding abilities, which is caused by hydrophobic interactions between membrane and protein. The SDS gel was placed on top of the membrane between two double layers of Whatman paper (Fig. 2.2). Each layer was first soaked in blotting buffer, then laid on the blotting apparatus and rolled over with a sterile cylindrical object (e.g. a glass pipette) to eliminate air pockets. The apparatus was assembled and the membrane blotted for 1 h at 30 V.

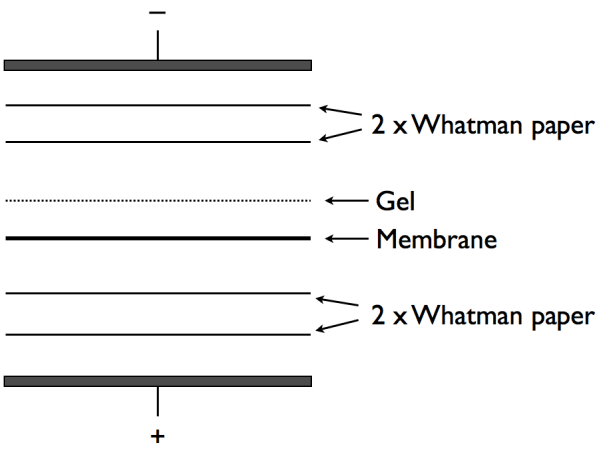

Figure 2.2: A schematic of a semi-dry blotting apparatus assembly. Each layer was soaked in blotting buffer and rolled over with a pipette to remove air pockets.

2.6.1 Western blotting

Also known as a protein immunoblot, a Western blot is an analytic method for the detection of specified proteins via their interaction with an antibody and a secondary antibody conjugated with horseradish peroxidase (HRP).

Antibody binding

The blotted membrane was incubated with the first antibody (diluted in PBS-T) overnight at 4 °C. It was then washed three times with PBS-T, in order to remove any unbound antibody. The second antibody (diluted in PBS-T) was added and incubated for 4 hours at room temperature. The second antibody binds specifically to the first and is conjugated with horseradish peroxidase (HRP). The following table lists first the primary antibodies, then their secondary antibodies and dilutions used:

A27L detection	Rabbit α-A27L (1:5,000)
	Donkey α-rabbit-HRP (1:50,000)
B5R detection	Rabbit α-B5R (1:5,000)
	Goat α-rabbit-HRP (1:5,000)
CEA detection	Mouse α-CEA (1:50)
	Rabbit α-mouse-HRP (1:5,000)
CPG2 detection	Rabbit α-CPG2 (1:5,000)
	Goat α-rabbit-HRP (1:5,000)

ECL detection

After the second incubation, the membrane was washed again as described above and the chemiluminescence was performed using the ECL Plus Reagent Kit from Amersham. The ECL solution was made according to the supplied protocol. The membrane was incubated for 1 minute. It was exposed to X-ray film for 30 seconds in a film cassette. Depending on the strength of the bands, further films were made with differing exposure times. The films were developed using a Kodak developing machine.

Colorimetric staining of nitrocellulose membranes

After detecting the bands via ECl, it was also possible to stain the nitrocellulose membrane itself using the Opti-4CN colorimetric kit from Biorad. The reagents were prepared according to the protocol mention on page 10 of the manual. The membranes were incubated at room temperature for 15 minutes with the substrate and subsequently scanned using a HP Photosmart scanner.

2.7 General cloning methods

2.7.1 Agarose Gels

Depending on the size (kB) of the sample in question, between 0.8 % and 1.2 % low melt, low electroendosmosis (EEO) agarose was used in the gel. 50 ml 0.5x TBE buffer was added and heated until the solution was clear and free of streaks. After letting the solution cool, 5 μl ethidium bromide was added (end concentration: 0.5 μg/ml), the gel poured into a gel slide and left to set at room temperature. A sample of 20 μl was mixed with 4 μl of 5x loading dye and loaded onto the gel. 5 μl of DNA marker was used in each marker lane. The gel was placed in an electrophoresis chamber and run at 80 V for roughly 45 minutes or longer, depending on the marker front position. The bands were detected using a UV lamp and an image capture program. If needed, the relevant bands were excised from the gel using a scalpel and purified using a gel extraction kit, i.e. from Zymo Research or similar.

2.7.2 Primer Design

The required primers were designed using an online program provided by IDT (Integrated DNA Technologies). Depending on what kind of primer was required, the task settings and parameters were changed accordingly. Primer pairs were designed to have similar melting and annealing temperatures. The exact primer sequences can be found in Appendix D.

For the cloning of CPG2 constructs, one primer pair was designed for the isolation and amplification of CPG2 from the viral DNA template. The forward primer was designed to integrate a BamHI restriction site at the end of the insert, while the reverse primer was designed to add a HindIII restriction site to the auxiliary end of the insert.

The CEA constructs required two different pairs of primers. For cloning, it was required to design a forward primer attaching a SalI restriction site to the insert, and two reverse primers, one for the full-length insert and one for the short-length, truncated version of CEA, each containing a PacI restriction site. For sequence confirmation of the cloning plasmids, a CEA mid-sequence forward primer was also devised. For sequence confirmation of the viral DNA, two further mid-sequence forward primers were designed for the repetitive domains within the viral isolate. One primer was made for domain 1 and one

for domain 2 of the CEA sequence. Depending on the target sequence, all forward primers were combined with either the full-length or the short-length CEA reverse primer.

2.7.3 Polymerase Chain Reaction

In a PCR reaction tube the following solutions were added:

Template DNA (50 ng)	2 μl
AccuPrime Pfx Mastermix	22.5 μl
Forward primer (20 pmol/μl)	0.5 μl
Reverse primer (20 pmol/μl)	0.5 μl

The reaction tube was placed into a thermocycler and treated using the following protocol:

1. 3 minutes	95 °C	Initial denaturation
2. 30 seconds	95 °C	Denaturation
3. 30 seconds	55 °C	Primer annealing*
4. 1 minute per 1 kbp	68 °C	Elongation**
5. 6 minutes	68 °C	Final elongation
Hold	4 °C	

*Primer dependent; for CEA primers 58 °C was used; for CPG2 primers: 57 °C
** Fragment size dependent: for CEA: 2.5 minutes; for CPG2: 1.5 minutes

Steps 2 to 4 (denaturation to elongation) were repeated for 30 cycles. The heating lid was set to 103 °C. The PCR product was purified either using an agarose gel or a purification kit.

2.7.4 DNA sequencing

All samples where sequencing was required were sent to Retrogen for sequencing. Primers were either provided or one could chose in-house primers.

2.7.5 TOPO cloning reaction

The blunt end PCR products were cloned into the pCRII-Blunt-TOPO vector using Invitrogen's ZeroBlunt TOPO PCR Cloning kit. The following was pipetted into a reaction tube:

gel purified PCR product	0.5 to 4 μl
Salt solution	1 μl
pCRII-Blunt-Topo	1 μl
DNase/RNase free H_2O	final volume 6 μl

The tube was incubated at room temperature for 30 minutes. After that the cells were immediately transformed using the One Shot chemical transformation protocol below.

2.7.6 Transformation

The transformation was performed using the protocol provided for One Shot Chemically Competent TOP10 E. Coli Cells from Invitrogen.
2 μl of a finished ligation mix was pipetted onto one vial containing of 50 μl TOP10 cells and gently mixed (no vortexing/pipetting). This mix was incubated on ice for 5 minutes, followed by a heat-shock treatment at 42 °C for 30 seconds without shaking. The tube was immediately transferred onto ice and 250 μl of super optimal broth with catabolite repression (SOC) medium added. The cells were incubated at 37 °C and 200 rpm for one hour, after which 50 μl of transformation solution was distributed onto a pre-warmed selection plate containing an antibiotic as a selection agent. The plates were incubated overnight at 37 °C in a bacteria incubator and screened the next day for colony formation. For pCRII-Blunt and pET-28a vectors, kanamycin was used as a selection agent. For the TK-vectors, either kanamycin or ampicillin was used. CPG2-bearing plasmids were transformed into B21(DE3) *E. coli* strains ideal for protein overexpression.

2.7.7 Enzymatic restriction digest

Generally, for digesting 1 μg of plasmid, 1 U of restriction enzyme and 2.5 μl of restriction buffer were added to the reaction tube. H_2O was added to 25 μl and the complete solution incubated at 37 °C for 1.5 hours or longer. The digest product was loaded onto an agarose

gel for electrophoretic analysis or purified for use in a ligation.
The CEA insert was enzymatically digested using SalI and PacI enzymes in a double digest reaction, meaning that both enzymes were added to the digest mix. All target viral transfer (TK) vectors for CEA were also digested using SalI and PacI. CPG2 was cleaved from its plasmid by performing a sequential digest with HindIII followed by BamHI, as these enzymes exhibit reduced efficacy in restriction buffers other than their own. Since CPG2 was to be ligated into the pET-28a vector, this vector was also digested using the same sequential digest as the CPG2 insert.

For a 25 μl reaction	
Plasmid DNA	10 μl
Restriction buffer (10x)	2.5 μl
Restriction enzyme	1 U
DNase/RNase free H_2O	ad 25 μl

2.7.8 QuickLigation

This ligation was performed according to New England Biolabs Quick Ligation kit. The following components were mixed in a reaction tube:

Insert	3x molar excess compared to vector
Vector	50 ng
dH_2O	Adjust to 10 μl
2x QuickLigase buffer	10 μl
Quick T4 DNA ligase	1 μl

This reaction mixture was incubated room temperature for 5 minutes, then transferred onto ice.

2.7.9 Measurement of DNA concentration

The concentration of the DNA in water was determined using a photometer by measuring the extinction at 260 nm. A sample was diluted 1:20 with water and measured. The concentration was determined by applying the following equation:

$$concentration\left[\frac{\mu g}{\mu l}\right] = OD(260\text{ nm}) \times D \times F(\text{DNA}) \div 1000 \tag{2.6}$$

with D being the dilution factor and F the multiplication factor for DNA, in this case F = 50.

2.7.10 Miniprep

For plasmid minipreps, PureLink Quick Plasmid Miniprep kits from Invitrogen were used according to the manufacturer's specifications.

2.8 Cloning and overexpression of CPG2 in BL21(DE3) *E. coli*

The gene encoding for CPG2 was first isolated from the TK-SE-CPG2 construct, which had previously been used to construct the virus, and subsequently cloned into the pET-28a vector for over-expression in the BL21DE strain of *E. coli* (Novagen). The resulting protein was isolated from inclusion bodies under denaturing conditions and then refolded, according to the paper published by Goda *et al.*[87], prior to a His-tag-dependent purification. In conclusion the protein was dialysed into storage buffer and stored at -20 °C.

Isolation of CPG2 from TK-SE-CPG2 viral construct and sub-cloning to pet-28a(+)

The gene for CPG2 was amplified using the CPG2 BamHI for and CPG2 HindIII rev primers, using the viral TK-SE-CPG2 DNA as the template. The PCR product was the inserted into the pCRII-Blunt-TOPO vector, then sequence verified before being sub-cloned into the pET-28a(+) vector, which had been pre-digested sequentially with BamHI/HindIII and dephosphorylated. The transfer of the insert into the pET-28a(+) also added a His-tag to the N-terminus of the protein, enabling it to be purified using Ni-NTA or any other His-tag-specific purification downstream.

Over-expression of pET-28a-CPG2 in a BL21DE strain

BL21DE cells transformed using the pET28a-CPG2 plasmid were grown overnight in a 37 °C shaker in 10 ml of LB-media containing kanamycin as a starter culture. This starter culture was added to two 1 l Erlenmeyer flasks containing 300 ml-LB/kanamycin media each. These flasks were shaken for 4 hours, after which the optical density (OD) was

measured at 600 nm every 30 minutes. Once an OD between 0.5 and 0.6 was reached, IPGT was added to an end concentration of 1 mM. The flasks were incubated at room temperature (25 °C) for 3-4 hours. Using a cold centrifuge, 50 and 100 ml aliquots of cells were pelleted, the supernatant discarded and frozen at -20 °C until the purification step.

Denaturing

Pellets from the previous step were thawed and resuspended every 1 l culture pellet in 30 ml of Tris lysis buffer. Lysozyme was added to an end concentration of 0.25 μg/ml and incubate at room temperature for 30 minutes. The suspension was then sonicated for four 2 minute cycles (1 minute sonication, 1 minute rest on ice). The resulting suspension was then centrifuged at 4 °C, 10,000x g for 15 minutes and the supernatant discarded. Resuspension of the pellet was done in 2 M urea and centrifuged again according to the above specifications. This wash step was repeated 3 times. The accrued pellet was then left to dissolve in 6 M guanidinium chloride at room temperature for 16 hours with continual stirring.

Refolding & His-tag purification

In order to regain the proteins enzymatic function, CPG2 had to be refolded into a more suitable storage buffer. The protein acquired from the previous denaturing step was rapidly diluted into refolding buffer, with a minimum 25-fold dilution, and let to incubate overnight at room temperature without further agitation, after which followed a centrifugation step at 4 °C, 10 000x g for 20 minutes. The samples were then dialysed against the dialysis buffer for 48 hours, stirring constantly, with a buffer change at 4, 12 and 24 hours. This was performed using Slide-a-lyser dialysis cassettes (molecular cut-off at 20 kDa) from Thermo Scientific, according to the manufacturers specifications. Subsequently, Amicon spin columns with a molecular cut off of 30 kDa were utilised to reduce the sample volume to 0.5 ml, following the suppliers instructions (3700x g, 4 °C, 25 minutes). Using the attached His-tagged domain, CPG2 was purified with the help of Promega's MagneHis Bead System. This system used tagged paramagnetic beads to bind the protein in order to facilitate washing and elution. This step was done according to the manufacturers specifications and the purified protein eluted twice into a total of 0.2 ml of elution buffer. The elution buffer was then exchanged by spin column purification using the aforementioned Amicon tubes and dialysis buffer (pH 7.3). The sample was

repeatedly spun down to 0.5 ml and re-diluted into 15 ml dialysis buffer, spun down again and repeated a total of three times. A Bradford assay was performed in order to determine the protein concentration.

Bradford Assay

The concentration of protein in the eluted sample was determined using a Bradford Coomassie Protein Kit from Thermo Scientific. 5 μl of undiluted sample were added to 250 μl of Coomassie solution in a 96-well plate, with each sample being measured in duplicate. The plate was then read at 595 nm. The readings were compared to a standard dilution range of BSA, measured concurrently. A linear regression of the standard average was plotted and the concentration of the unknown sample calculated.

3 Results

A word on the samples used in this thesis

In order to be able to compare biomarkers and quantification methods comprehensively, the cell culture samples harvested and used in the following experiments were all similar samples, unless otherwise stated. This comparison basis was made from infected CV-1 cells, which had been inoculated with the required virus (GLV-1h68, GLV-1h416, GLV-1h417 or GLV-1h181) at an MOI of 0.1. The cells and supernatant had then been harvested at the following time points: 0, 4, 8, 12, 16, 20, 24, 30, 36, 48 and 54 hours post infection, unless otherwise stated. All samples were then exposed to three freeze-thaw cycles, aliquoted and frozen down to prevent protein degradation attributed to repeated freezing and thawing. Spiked samples were samples that had been diluted with human plasma in a ratio of 1:1. This dilution factor was then calculated back into the concentration upon quantification.

3.1 Vaccinia virus specific A27L & B5R expressed proteins

As described above (section 1.3.6), A27L and B5R are loci within the viral genome that encode for virally expressed proteins that are produced in various stages of viral replication-dependent on their promoter. A27L is under the p^{L} promoter, B5R is under the $p^{E/L}$ promoter. Here, we attempted to assay and quantify these proteins in cell culture, murine serum and tumour samples.

3.1.1 Western blot analysis of A27L/B5R proteins

Firstly, A27L/B5R proteins were analysed using SDS-PAGE and Western blot analysis. The samples used were CV-1 cell culture samples, infected with GLV-1h68 and harvested at different time points, human blood plasma (both spiked and unspiked) and pure, inactivated virus. The spiked samples were done by diluting a volume of cell lysate in a ratio of 1:1 with human plasma. This cell lysate had a titre of $2.38\text{x}10^{6}$ pfu/ml. The volumes loaded onto the gel were 15 μl for all unspiked samples. For samples containing

plasma, the double volume was loaded in order to compensate for the dilution factor. A27L proteins run at 12.6 kDa, whereas B5R proteins are found at 35.1 kDa. Visible bands indicated the detection of the same using custom-made primary antibodies and a HRP-conjugated secondary antibody. Fig. 3.1 shows the results of this experiment. Both A27L and B5R proteins were detectable with this method, but reliably only in virus samples. All other samples show an extremely weak signal, in spite of compensating for the dilution in spiked and unspiked samples. The figure following, Fig. 3.2 shows the

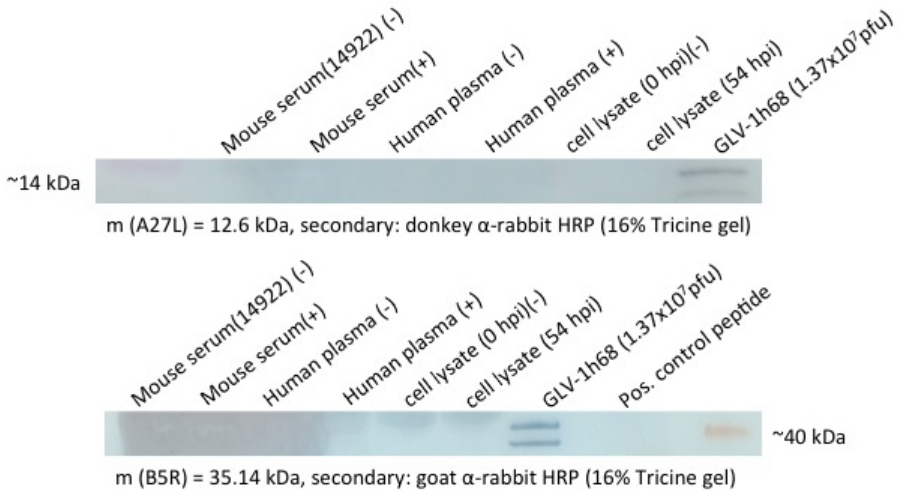

Figure 3.1: Western blot detection of A27L and B5R after denaturing SDS-PAGE. (+) indicates plasma samples that were spiked 1:1 with cell lysate, (-) indicates negative control samples. The volume loaded onto each lane was 15 μl for unspiked and 30 μl for spiked samples. A27L is found at 12.6 kDa, B5R at 35.1 kDa. The pure virus (top band, lane 8; lower band, lane 7) served as a positive control and was inactivated under denaturing conditions, along with all other samples.

detectable amount of both viral proteins in pure, denatured and inactivated virus samples. These samples showed that A27L and B5R are still visibly detectable in samples containing 2.5x10^6 pfu, with A27L displaying a stronger signal. The titres shown above each lane are the actual viral titres present on those samples, accounting for dilution factor and sample size.

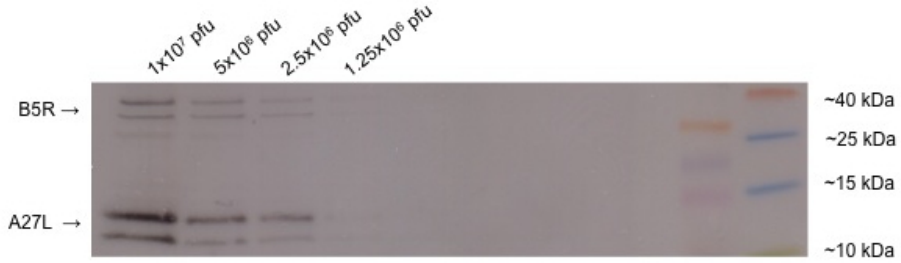

Figure 3.2: Simultaneous detection of A27L and B5R in samples containing pure GLV-1h68 virus. In Western blots, the viral proteins were detectable up to $1.25x10^6$ pfu. B5R is found at 35.1 kDa, A27L at 12.5 kDa. The double bands shown were attributed to degradation of the protein due to handling.The sample volume loaded was 10 μl per lane. The titres shown reflect the samples volumes.

3.1.2 A27L/B5R protein detection using ELISA: Assay development

Since there are no commercially available kits for quantifying protein encoded for by either A27L or B5R, an ELISA was developed to quantify these two proteins in samples (section 2.3.1). Firstly, peptides were used to gauge the range for the standard to be used in ELISA experiments. Fig. 3.3 shows an example of the peptide standard being tested. The peptides used were primarily antigens that had been used to generate the A27L antibody. Later, this standard, together with the virus standard, would be utilised in an attempt to quantify and correlate A27L in GLV-1h68-infected cell culture samples, spiked blood plasma, as well as pure virus. Fig. 3.4 shows just one such viral standard. Inactivated virus was coated onto the plate and then detected using the in-house ELISA method. The chart shows that while a linear correlation could be made for the A27L data, no discernible reading could be made for B5R, as the readings are not in the positive numeric range. This next graphs in Fig. 3.5 shows the data from a comparison of samples with plasma and samples without, as it is imperative to ascertain if human plasma has any effect on the detection of viral proteins. Fig. 3.5a shows the standard as it was without any human plasma. A linear range is visible, with a R^2 of 0.97. Fig. 3.5b depicts the same experiment with human plasma added to the samples. The data points do not indicate a correlation between the optical density reading and the concentration of B5R present in the sample.

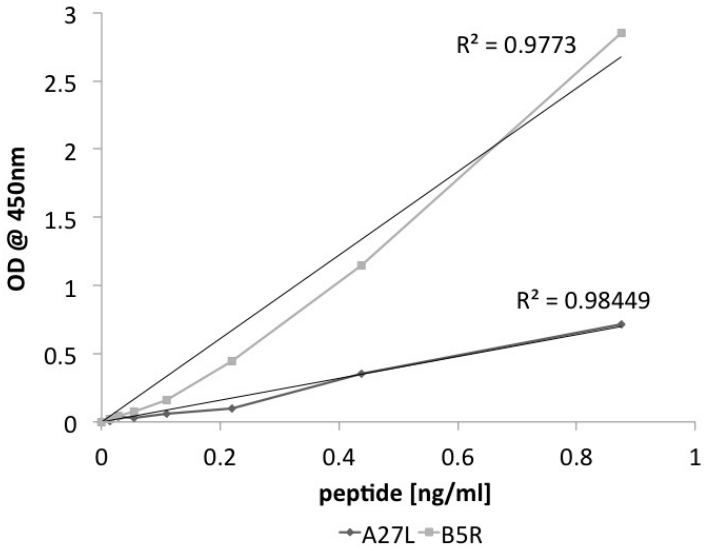

Figure 3.3: A27L & B5R peptide ELISA standards. Shown here is the correlation between OD readings at 450 nm and the level of A27L and B5R in their respective serial dilutions. The peptides used in this standard were the same ones that were used for antibody generation. A serial dilution of the samples was done to give rise to the linear standard range seen here, the detection method used was ELISA.

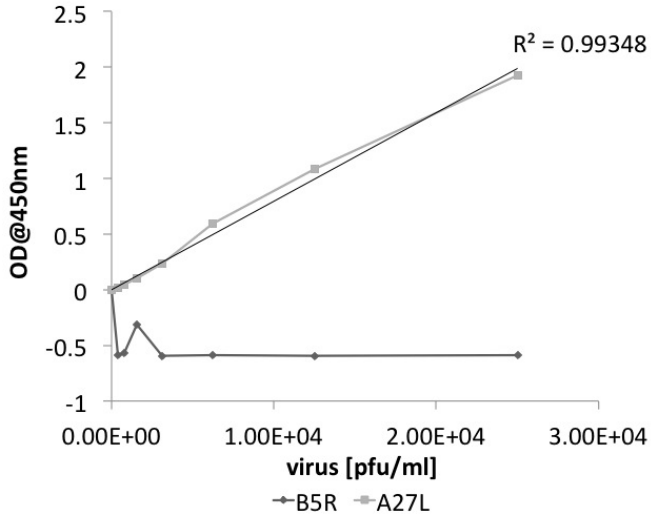

Figure 3.4: A27L & B5R viral ELISA standards.This graph shows the correlation between OD readings at 450 nm and the level of A27L and B5R in their respective samples. The total virus used in this standard was heat-inactivated GLV-1h68. A serial dilution of the samples was done to give rise to the linear standard range seen here.

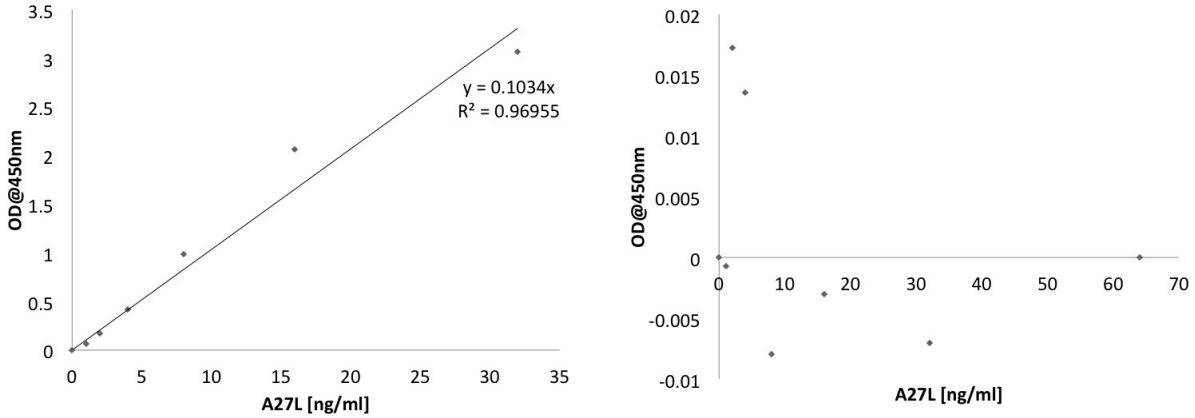

(a) Serial dilution of A27L peptide

(b) Standard curve of A27L peptide diluted in human plasma

Figure 3.5: Influence of human plasma on standard curves. Graph (a) shows a serial dilution of the A27L peptide for use as a standard curve in quantifying A27L in unknown samples. Graph (b) shows the same dilution range and peptide concentration, with the diluent being human blood plasma. The change in trend is due to the addition of plasma to the sample.

3.1.3 Quantification of the A27L-encoded protein in murine serum samples

An important aspect was ascertaining if the A27L-encoded viral envelope protein . This data was obtained by utilising serum samples from an animal study where mice had been implanted with GI-101A cells and consequently infected with one of the following viruses: GLV-1h68, GLV-1h22, GLV-1h70 to GLV1h74. Serum from an uninfected, tumour bearing nude mouse was used as a negative control. All samples were analysed using the vELISA against A27L, developed in-house. As shown by in Fig. 3.6, the level of A27L is comparable in all viruses, regardless of payload as the concentrations of all constructs appear to be around the 11 ng/ml mark. On average, for a marker, these concentrations seem to be low, in spite of A27L having a native late promoter. The last two viruses, GLV-1h73 and 1h74 are both attenuated viruses without payload and should thus show higher A27L protein levels compared to the other viral constructs, since constructs without payloads are known to display a higher viral replication rate (data not shown). Also noted is the fact that the negative control (last column) displays a very high background compared to other infected samples. Based on this data, resulting in a very low detection

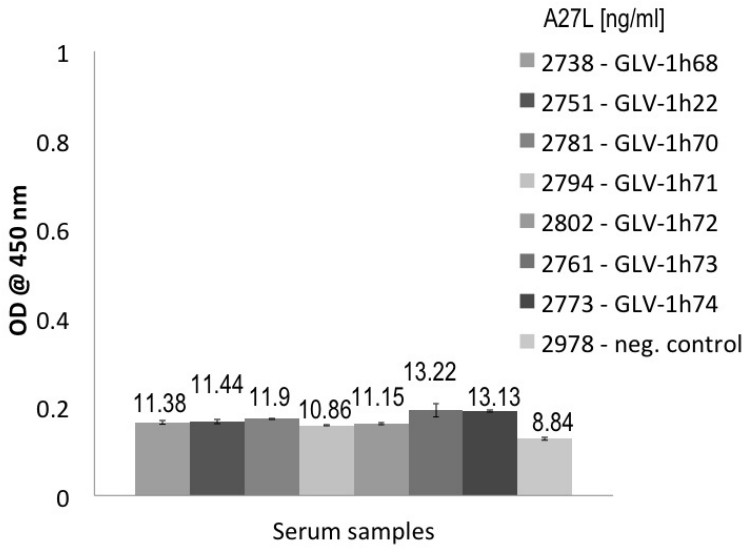

Figure 3.6: A27L-dependent protein expression in different viruses. These samples were assayed for serum samples from tumour-bearing, infected nude mice. Samples were diluted 1:50 prior to measurements. The data is shown as OD readings measured at 450 nm. The corresponding protein concentration is represented by numbers on top of each column in ng per ml.

limit, and the interference caused by the serum itself, no further tests were performed on *in vivo* samples.

3.2 GFP as a biomarker

GFP has long been used in molecular biology as a visual aid for localising gene expression through imaging. The ease of use and the stability of the protein has made it a routine imaging tool. Presented here are the results of attempts to quantify this fluorescent protein with the help of various methods. These various methods are visual analysis, fluorescence based assay kit and ELISA.

3.2.1 GFP as a biomarker for optical imaging

During the animal study, in which nude mice were implanted with $5x10^6$ cells GI-101A cells each and infected with a i.v. dose of $5x10^6$ pfu/ml of their respective virus. The mice were imaged for GFP once a week for the entirety of the study. The images were then ranked using a numeric scale from one (1) to five (5), with half increments (.5) allowed for accuracy. An example of these GFP images is given in Fig. 3.8 and 3.9a. In this particular case, this representative mouse was a part of a group of mice which had been infected with GLV-1h68, co-expressing GFP under the control of the synthetic early/late (p^{sEL}) promoter. All images were taken for 290 ms using a Lighttools Research imager with a 470 nm filter for the light source. These numbers were then plotted against the

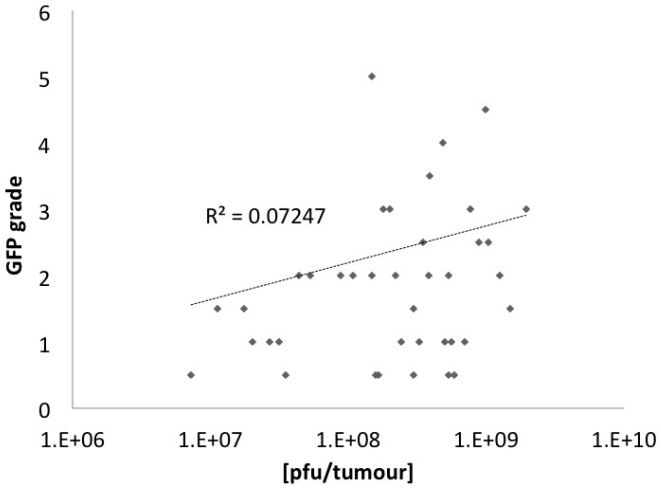

Figure 3.7: Mathematical correlation between total plaque forming units (pfu) and visible GFP signal in a whole tumour. Each GFP image was assigned a subjective score by the experimenter. The graph was plotted (n=39), a linear regression drawn and R^2 calculated using Excel and projected on the graph.

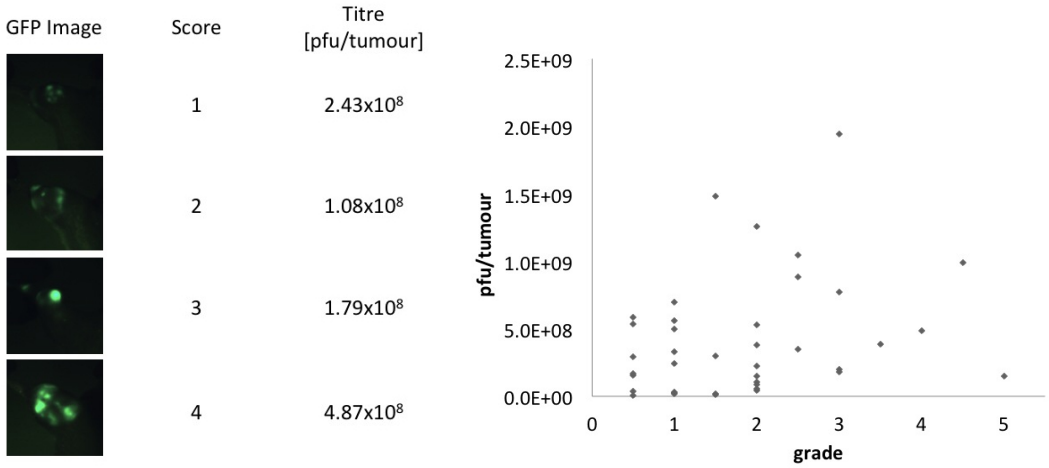

(a) **(b)**

Figure 3.8: Viral titres with corresponding GFP scores. (a) Representative images for each GFP grade, accompanied by the viral titre measured for that tumour using viral plaque assay. (b) All the GFP scores made, plotted according to their viral titres

respective viral titre and a regression curve was plotted to ascertain, if any correlation existed between the visible GFP signal and the titred viral load (Fig 3.7). The coefficient of determination, R^2, is given in the upper right hand corner of the chart and is a numerical representation of the prediction of future outcome, based on the fit of the regression curve to the data. The closer R^2 is to 1.0, the better the mathematical fit of the regression curve to the data points, thus enabling a more statistically reliable interpretation of the data trend when extending beyond the points shown. In this case, R^2 was calculated to be 0.0724. Furthermore, the tumour size was measured for each mouse in the study, starting at five days prior to infection (-5 dpi) and ending at the day of sacrifice. Fig. 3.9 shows images with visible in the tumour of mouse 19400, and (b) shows the tumour volume development during the life of this same mouse. The same data set was gathered for all mice in the study, mouse 19400 again begin shown as a representative example. As can be seen in the tumour development chart (b), the tumour increases slightly in the beginning, from the start of the treatment up to 28 dpi, showing regression of the tumour size until 49 dpi.

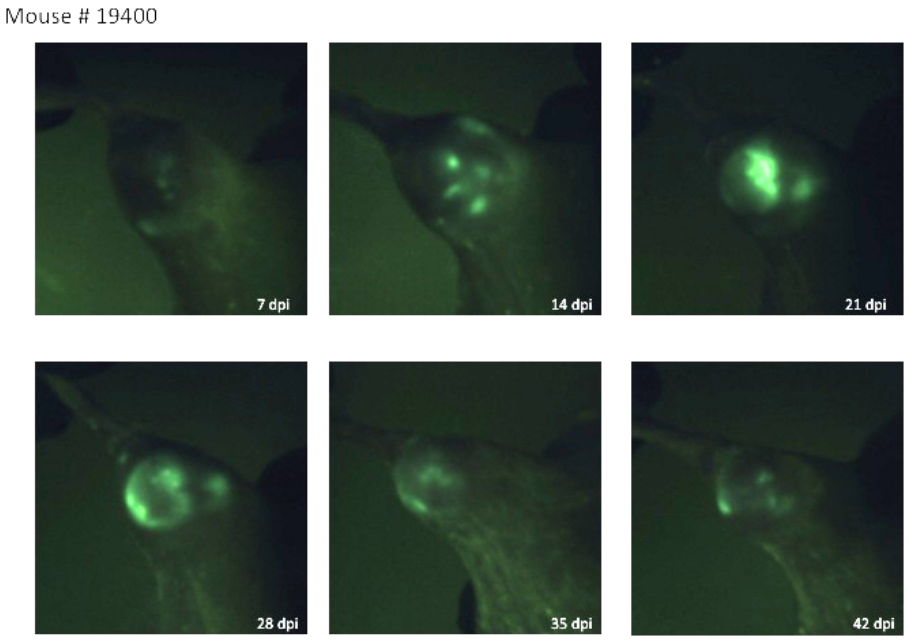

(a) Time-lapsed GFP images of mouse 19400 (290 ms)

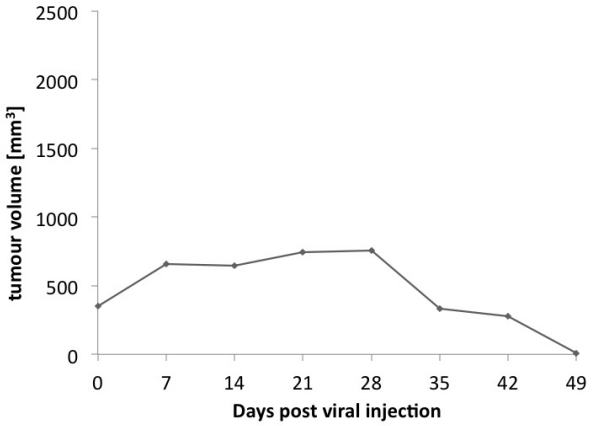

(b) Tumour development for mouse 19400 for the study duration (49 dpi)

Figure 3.9: Data from one subject in a 120 mouse animal study. Mouse 19400 had been treated with GLV-1h68 and monitored throughout the study via tumour size measurements, GFP image capture, weight and serum collection. (a) A time-lapsed collection of GFP images associated with this mouse and sorted chronologically from day 7 to 49 dpi (top left to bottom right). The increase in signal is due to viral replication. (b) Development of tumour size during the study, beginning at day of treatment (0) till 42 days post viral injection.

3.2.2 Quantification of GFP fluorescence in serum and tumour samples

For the fluorescence analysis of GFP as quantifiable biomarker, a commercial kit was acquired. The graph acquired from this data set can be found in Fig. 3.10, which shows a linear trend line through the standard curve, resulting in R^2=0.999. As proof of concept, the kit was repeatedly tested using the standard provided, as well as with human plasma spiked with protein, since our future samples were of a biological nature. Fig. 3.11,(a)

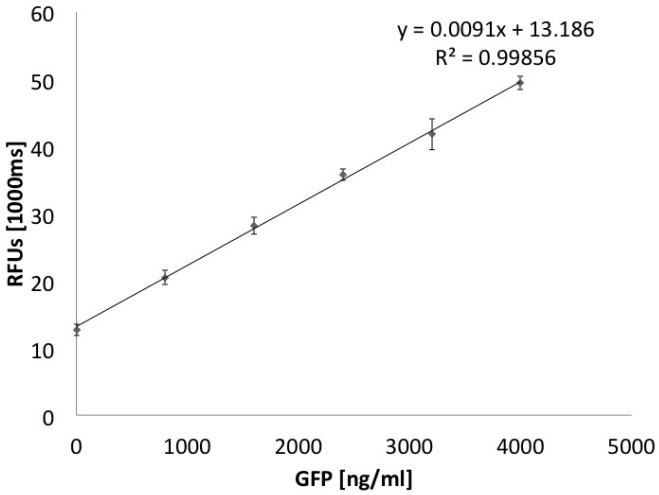

Figure 3.10: Accuracy of standards according to kit specifications. Sample size was n=3, with a resulting R^2=0.998. Diluted peptide was used as the standard and shown to be have low standard error.

shows the normal standard as dictated by the fluorescent kit with a sample size of one. In comparison, (b) shows the same kit, using human blood plasma spiked with the provided GFP peptide as sample standard.

In order to correlate between the GFP signal shown and the virus present in the samples, all cell culture samples were harvested and titred to determine the actual viral titre. Fig. 3.12 shows the result of the titration of cell culture samples and the associated GFP signal. Graph (a) shows the chronological change in GFP levels as measured using the fluorescent kit. In order to evaluate the influence of phenol red on the fluorescent reading, both samples treated with cell culture media with (w/-) and without (w/o) phenol red. The cell line used was CV-1, which had been infected with an MOI of 0.1. Fig. 3.12 (b) shows the change in viral titre, which steadily increases over the course of infection. In graph (a), however, no change in GFP reading can be seen, with the exception of

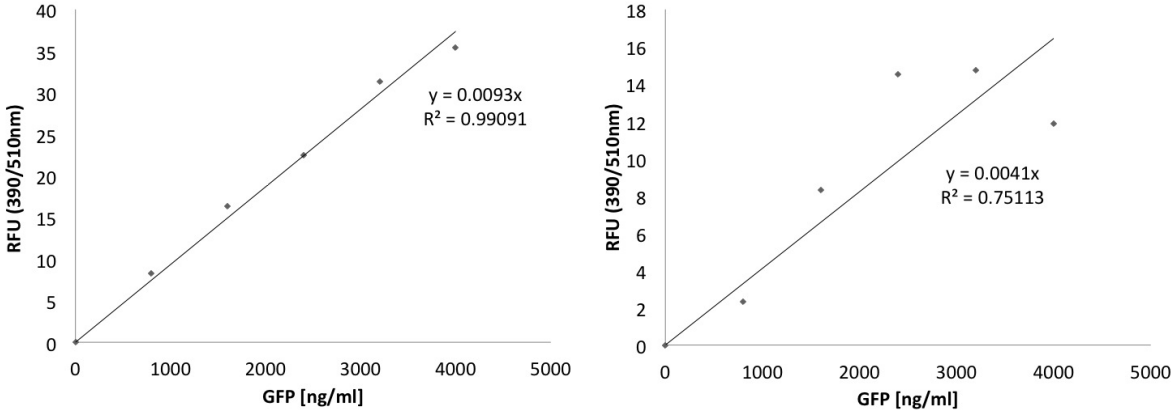

(a) GFP fluorescence - normal standard

(b) GFP fluorescence - spiked plasma standard

Figure 3.11: GFP fluorescent standard measurements according to kit specifications: (a) Fluorescent standard measured at ex/em 390/510 nm. (b) Fluorescent standard prepared with pre-spun human plasma, with unspiked plasma being used as a blank. The change in correlation is due to the plasma interfering with measurements.

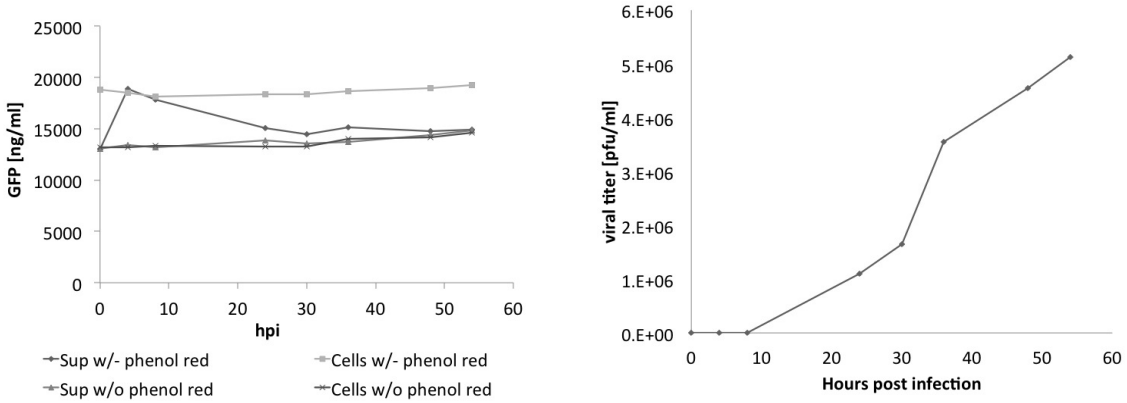

(a) GFP fluorescent readings of infected cell culture samples

(b) Viral titre time course of the cell culture samples in (a)

Figure 3.12: (a) GFP fluorescent readings of cell culture samples infected with GLV-1h68. When harvesting these cell samples, cells and supernatant were collected separately. In order to test the effect of phenol red on fluorescent readings, duplicate cell samples were seeded and infected at the same MOI with phenol red-free media. (b) Samples were titred to give the concentration of virus [pfu/ml] for each individual sample. Shown here are the titres for samples from 0 to 54 hours post infection. The increase in viral titre was expected to be reflected in the GFP concentration present.

the supernatant samples from cells treated without phenol red. Due to the interference stemming from the plasma, this method was not used in *in vivo* testing.

3.2.3 GFP as an ELISA target

Another method tested for the quantification of GFP was the ELISA method, which relies on antibody - antigen binding in order to capture and quantify an analyte.
As a proof of principle, the standard in the kit was repeated multiple times in order to confirm reproducibility and reliability of the predictions being made from this kit (R^2). The R^2 resulting from samples size n=5 was 0.999, indicating a 99.9% reliability in the prediction made based on the data presented. The next step was to test this kit in a

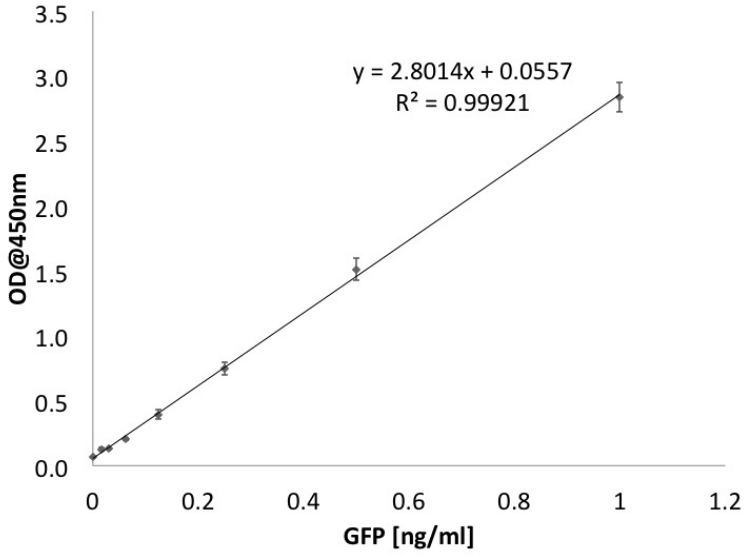

Figure 3.13: Accuracy of the standards done according to kit specifications. Sample size: n=5, with R^2=0.999 and standard errors within acceptable ranges.

time course experiment. Using infected cell culture samples, infected with GLV-1h68 and harvested at different time points, the data resulting is shown in Fig. 3.14. The GFP concentration increases the more time the virus had been given to replicate and lyse cells in the petri dish. Also represented here is the difference between GFP concentrations in cell and supernatant samples respectively. There is a visible trend showing a higher GFP level in cells at any given time, with the concentration in supernatant lagging behind by a minimum of 36 hours. After confirming the time course trend in cell culture as seen in the viral titres, a similar experiment was preformed with human blood plasma, in order to determine the influence of plasma on GFP quantification, as this method was ultimately

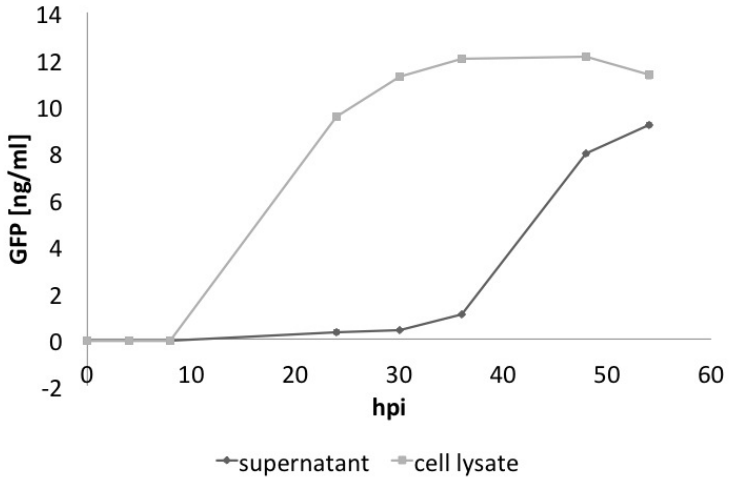

Figure 3.14: GFP quantification in cell culture samples. A GFP ELISA was performed on harvested, infected CV-1 cells, with separate measurements for supernatant and cell culture. These cells had been harvested at specific time points, in order to form a coherent, chronological representation of GFP formation and lytic release from the cell. This graph was then used as a basis for comparison between plasma and cell culture samples.

to lead to a monitoring modality in human serum. Cell lysates obtained from culture were diluted in a ratio of 1:1 with human plasma and measured as per the kits specifications. The resulting concentrations were calculated, including the dilution factor in order to ease the comparison of data represented in the charts.

The graph shown in Fig. 3.15 shows the result of an experiment with spiked human blood sample. Human blood was spiked with GLV-1h68-infected cell culture samples harvested at different time points and assayed according to kit specifications. As a result, the data points were plotted against the relevant time points. When this graph is compared to Fig. 3.12b, a similar trend is discernible, with the GFP concentrations in the plasma changing along with the viral titre that was present. The separation of cell lysate to supernatant was done to depict any differences that could appear in an *in vivo* setting, with the cells representing the tumour and the supernatant representing the excreted biomarker concentrations in serum. Represented in Fig. 3.16 is the data acquired by plotting the GFP concentration determined by ELISA against the correlating viral titres from those same samples. The resulting linear regression analysis determines $R^2 = 0.898$. On a scale of zero (0) to one (1), an R^2 of 0.898 is deemed to result in predictions based on this data set to be 89.9% accurate. In the interest of seeing if blood plasma itself might in some way influence the quantification of GFP, both readings for GFP in cell culture and blood

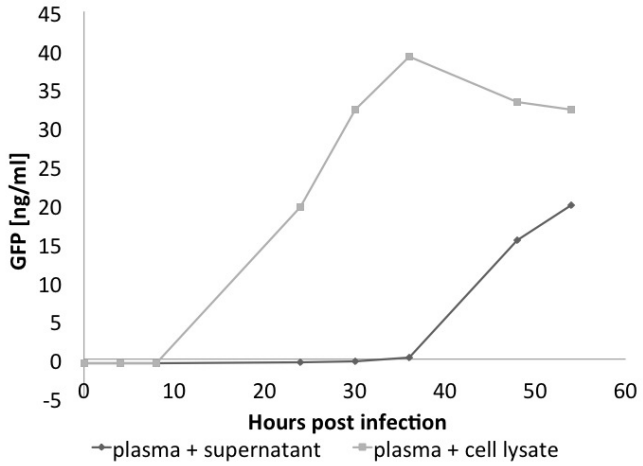

Figure 3.15: GFP quantification in plasma-spiked cell culture samples. Data shown here is from an experiment where blood plasma was spiked (1:1) with cell lysate samples containing GFP, in order to ascertain the effect of blood plasma on GFP quantification. The dilution factor was included in the calculations pertaining to the data points. The trend here is a similar the trend in Fig. 3.14, showing that the plasma had a limited effect on the measurements.

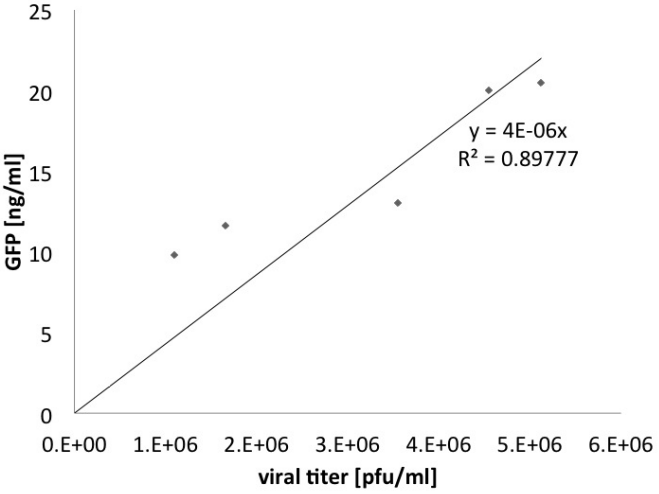

Figure 3.16: Correlation analysis between GFP (ELISA) and viral titre. Linear correlation between data points representing GFP ELISA measurements and the corresponding viral titres for the cell culture time course samples.

plasma were shown in Fig. 3.17. As depicted, a discrepancy in GFP quantity between blood and cell culture samples is visible, with the biomarker concentration being higher in the spiked blood samples than the samples containing the same cell lysate used to spike the blood plasma.

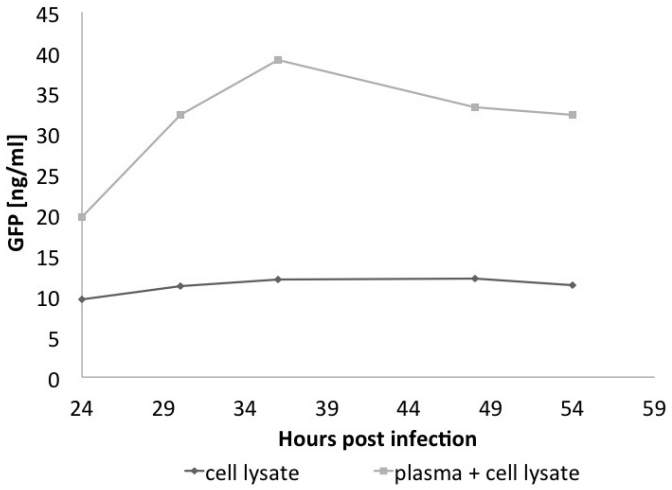

Figure 3.17: GFP in spiked and unspiked cell lysate samples. Human plasma was spiked with cell lysate (1:1) and the effect on GFP quantification assayed using a GFP ELISA. Differences are directly resultant of the interference of human plasma with GFP present.

When taken together and analysed using linear regression analysis, the resulting graph (fig. 3.16) shows an R^2 of 0.898, representing a significant increase in predictive ability of GFP as a biomarker when the method used is an ELISA, compared to the visual (R^2=0.072) or the fluorescence-based system.

3.3 β-Galactosidase as a biomarker

β-Galactosidase is a standard biomarker currently used in most of our viral constructs. It is generally inserted into the *J2R* locus, which falls under the $p^{7.5E/L}$ promoter. For more information refer to Fig. 3.30 and chapter 1.3.2.

3.3.1 Kit reliability and measurement of β-galactosidase luminescence in cell culture samples

As before, the so-called accumulative standards were run, illustrating the reliability of the kit acquired. The graph in Fig. 3.18 shows the data points, and the R^2 determined for this graph, which was 0.999. This shows that any predictions made from according to this coefficient of determination would be 99.97% accurate.

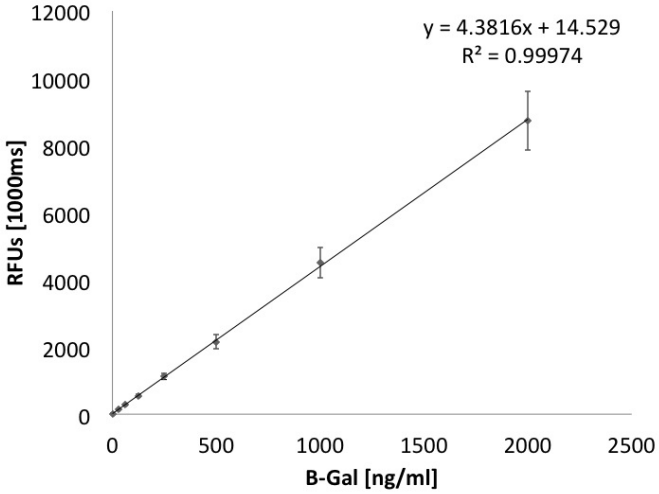

Figure 3.18: Accumulative standards for β-galactosidase chemiluminescence kit. The samples size was six (n=6), with a resulting R^2 of 0.999 and low standard errors.

Cell culture samples were then used to simulate viral replication in a tumour and the release of biomarkers into the supernatant and in the cells showing viral replication. As can be seen in Fig. 3.19, the trend of this concentration development increases over time, almost plateauing out at the last time point. The supernatant samples lag behind the cell lysate samples and never reach the levels attained in cell lysate samples. The slight dip at the end of the time course could indicate a decay of β-galactosidase within the sample. The next data set, shown in Fig. 3.20 is the comparison between cell lysate samples and the same cell lysate containing human blood plasma, depicting the differences between

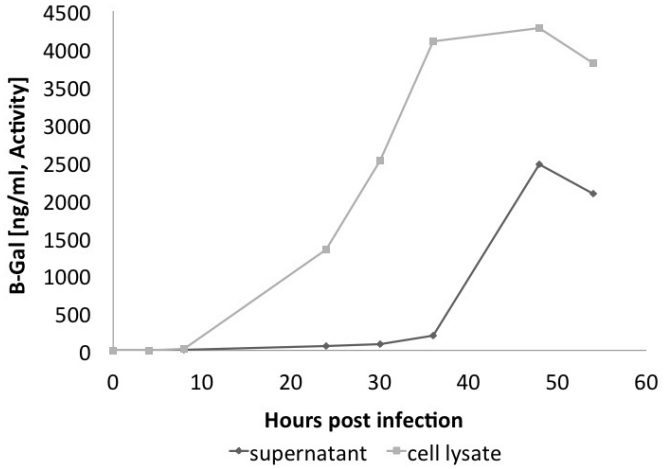

Figure 3.19: Time-dependent increase of virally expressed β-galactosidase in CV-1 cell culture samples. Cells had been infected with GLV-1h68 at an MOI of 0.5. The concentration of β-galactosidase increased chronologically, with supernatant samples containing delayed and less β-galactosidase than cell lysate.

the two readings resulting from human blood plasma being added to the sample. As can be seen, the plasma added interferes markedly with the measurements for β-galactosidase. Prior to the experiment, the samples were determined to contain the same amounts of the target biomarker.

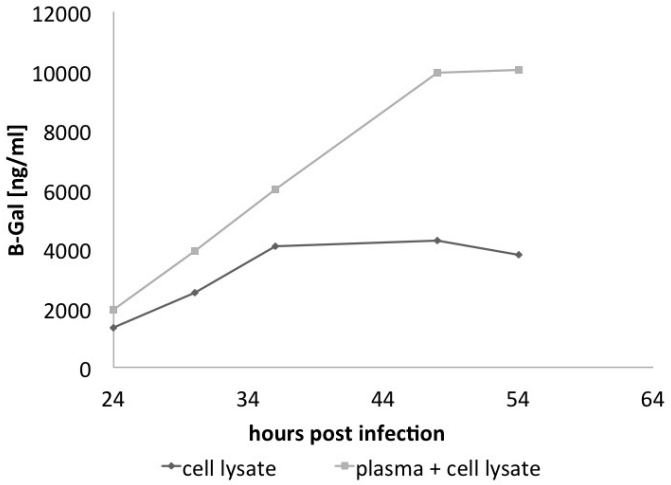

Figure 3.20: Effect of human blood plasma on quantification of β-galactosidase via chemiluminescent. The two lines represent cell lysate (darker line) and cell lysate (lighter line) spiked plasma samples (1:1) respectively. The dilution was compensated mathematically.

3.3.2 ELISA-mediated quantification of β-galactosidase

In this section, the next method of choice for quantifying biomarkers, ELISA, was used to asses the concentration of β-galactosidase in cell culture samples, as well testing for interference in readings of said biomarker in plasma. Firstly, standards from repeated experiments were accrued and collected into one graph, to show the how large the variance of measurements for this standard is. The results are shown in Fig. 3.21, whereby a sample size of 5 results in a calculated R^2 of 0.9998. Having verified little variance between the

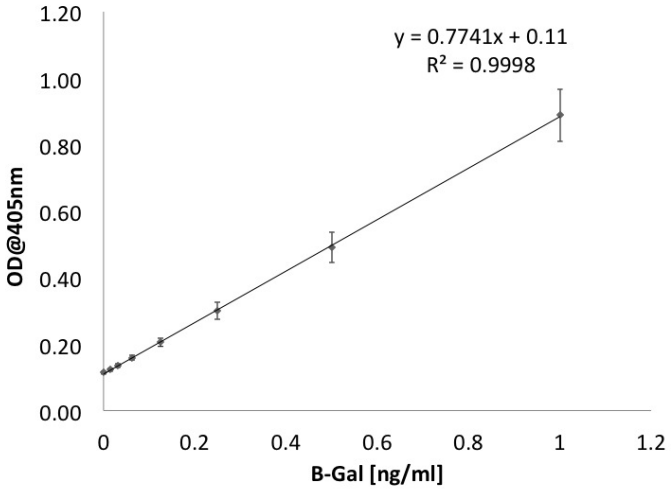

Figure 3.21: Variance of multiple standards in a β-galactosidase ELISA kit. Sample size is n=5, with $R^2 = 0.9998$

measurements for the standard curve itself, cell culture samples derived from infected CV-1 cells were used to allow testing of the biomarker in spiked plasma samples, as well as on its own. The graphs presented in Fig. 3.22 show the results of this experiment. Graph (a) depicts the measurements of the cell culture samples without any addition of plasma, whereas graph (b) shows the same cell culture samples diluted 1:1 with human blood plasma. The values shown include the dilution factor and are calculated to present the concentration of β-galactosidase in ng per ml. Both graphs reflect the same chronological change in concentration. The direct comparison of the data found in Fig. 3.22 can be found here in Fig. 3.23. It shows the divergence in concentration between lysed cell culture samples and human blood plasma samples that had been spiked with the same, stated in ng per ml, in chronological order of the time of harvest. Not only is this the divergence visible in the above mentioned case, the same can also be said for the comparison of standards under the same conditions. In Fig. 3.24 the direct comparison of a standard comprising of the kit standard is shown along side the standard modified to

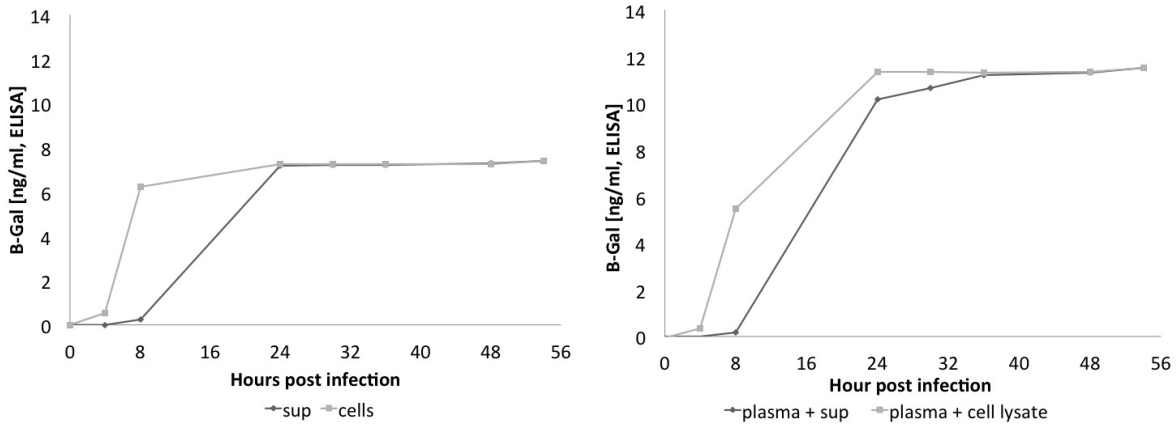

(a) β-Galactosidase in cell culture

(b) β-Galactosidase in spiked human plasma samples

Figure 3.22: Concentration of β-galactosidase in cell culture and spike human plasma samples. Chronological development. (a) Cell lysate derived from GLV-1h68 infected cells. (b) Same cell lysate samples spiked with human plasma (1:1).

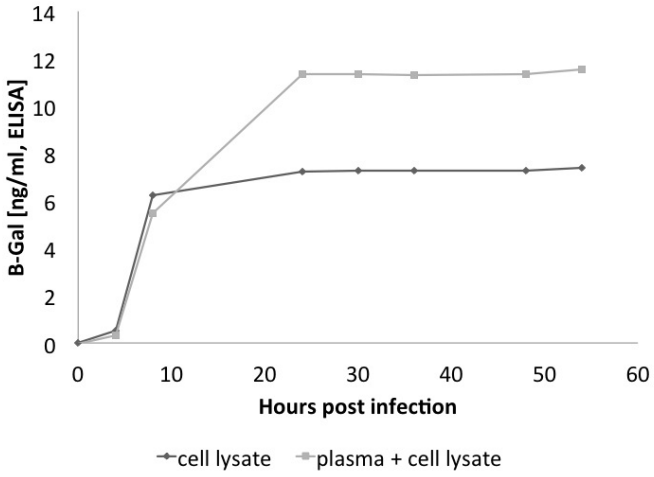

Figure 3.23: Comparison of cell lysate with and without blood plasma. The concentration in the spiked sample was calculate to compensate for the dilution factor due to spiking the sample. Quantification was done by ELISA.

include human plasma in the readings, i.e. human plasma spiked with infected cell lysate. Both standards are accurate, as their coefficient of determination were 0.994 and 0.992 respectively. However, the function shown from calculating the linear regression differs between both sample types.

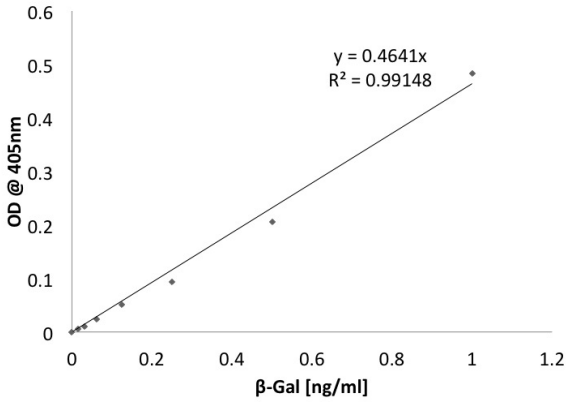

(a) ELISA standard quantifying β-galactosidase

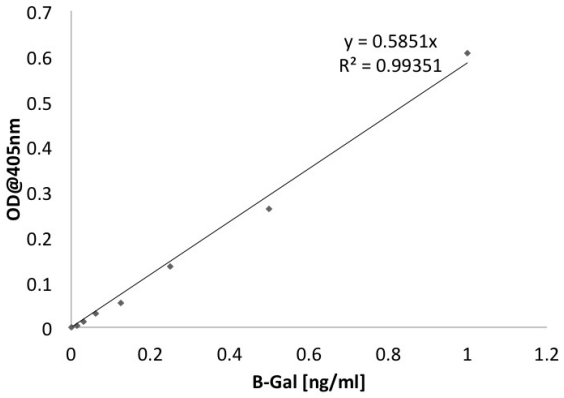

(b) ELISA standard with β-galactosidase and human plasma

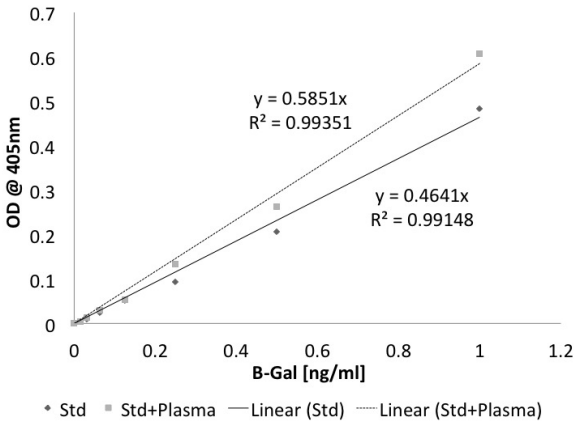

(c) Direct comparison of (a) and (b)

Figure 3.24: Comparison of β-galactosidase standards with and without plasma. Here the same analysis as done with cell lysate samples was performed using the standard peptide provided in the kit. (a) β-galactosidase standard as per kit specifications. (b) β-galactosidase standard spiked (1:1) with human plasma. (c) Result of the effect of plasma on the ELISA readings. Dilution was mathematically compensated.

3.4 β-Glucuronidase

So far, β-glucuronidase has been used as a biomarker that can be traced in small quantities due to its intrinsic enzymatic ability to metabolise the fluorgenic substrate 4-MUG-Glc. As mentioned before (section1.3.3), this enzymatic activity can be read as relative fluorescent units (RFUs) using a photometer, using an excitation of 365 nm and reading the emissions at 455 nm.
Presented following is the data gained from cell culture and *in vivo* experiments.

3.4.1 β-Glucuronidase in cell culture

β-Glucuronidase was first tested in cell culture, using CV-1 cells. The viruses used for infection were GLV-1h416 and GLV-1h417. The cells were infected using an MOI of 0.1 and the early time points, i.e. 1, 4, 8, 12, 16 and 24 hours post infection together with the respective supernatants, were harvested as stated in the methods section. The assay results are shown in Fig. 3.25.

Fig. 3.25 represents two sets of data gathered from this experiment. (a) shows a graph reporting the concentration of β-glucuronidase in relation to the early harvest. Graph (b) shows the titration data for those exact same samples, also plotted according to their harvest times. As can be seen in both cases, the more time that had passed since infection, the greater the concentration of β-glucuronidase as well as virus in the sample. A more concise picture of the relationship between viral titre and β-glucuronidase concentration is presented when the data from the previous figures is plotted in one graph, as a direct correlation between β-glucuronidase concentration (y-axis) and viral titre (x-axis). The graph and the resulting linear regression analysis of the relationship between the two variables can be seen in Fig. 3.26.

3.4.2 β-Glucuronidase in athymic nude mouse model

Having confirmed the assay method in cell culture samples, this method was then used to assay the β-glucuronidase concentration in mouse serum samples derived from tumour-bearing mice that had been treated with virus. Fig. 3.27 shows the change in β-glucuronidase in infected subjects during the course of the study. The concentrations

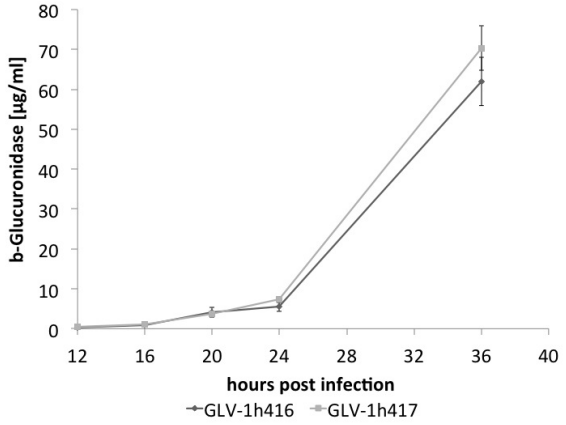

(a) β-glucuronidase in infected cell culture samples

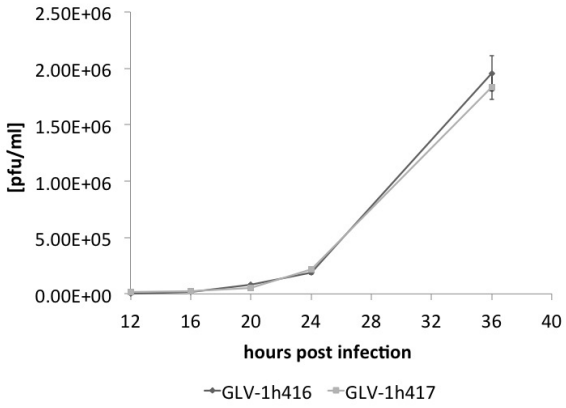

(b) Viral titration data corresponding to Fig. 3.25a

Figure 3.25: Relationship between the level of β-glucuronidase and viral titre in the same sample. (a) Time-dependent increase of β-glucuronidase in infected CV-1 samples. The viruses, GLV-1h416 and GLV-1h417 had been applied at an MOI of 0.1. The times of harvest are stated on the x-axis. (b) Corresponding viral titre in detail for samples shown in (a).

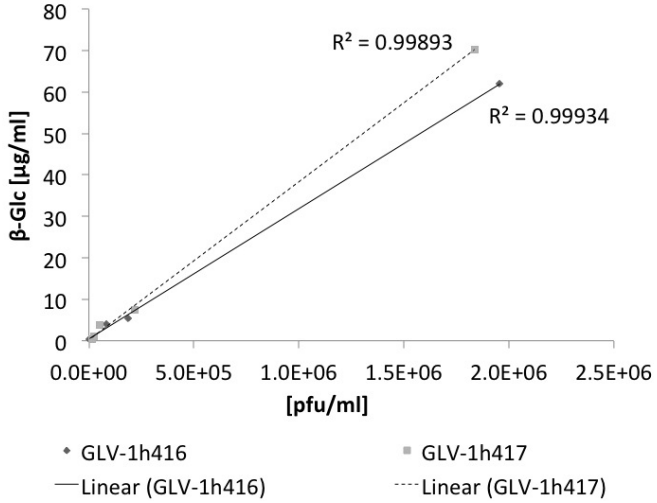

Figure 3.26: Correlation of the data shown in Fig. 3.25. The trendline shown represents a linear correlation between the two variables, concentration of β-glucuronidase and viral titre.

for β-glucuronidase on average increased for both GLV-1h416 and GLV-1h417 groups. This increases peaks between day 7 and day 14 of the study, and declined slowly from then on till the end of the study. The only group to show no change was, expectedly, the group of non-tumour bearing mice dosed with GLV-1h417.

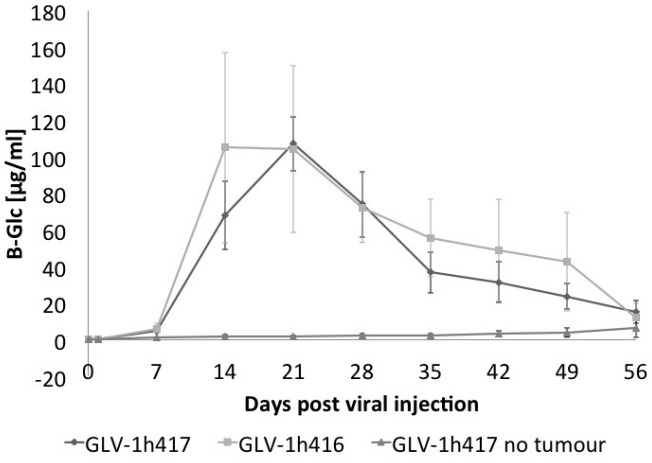

Figure 3.27: Time-dependent change in β-glucuronidase concentration. These serum samples were taken from infected athymic nude mice. The last group represented, GLV-1h417 no tumour, is the group of mice that had no tumours implanted.

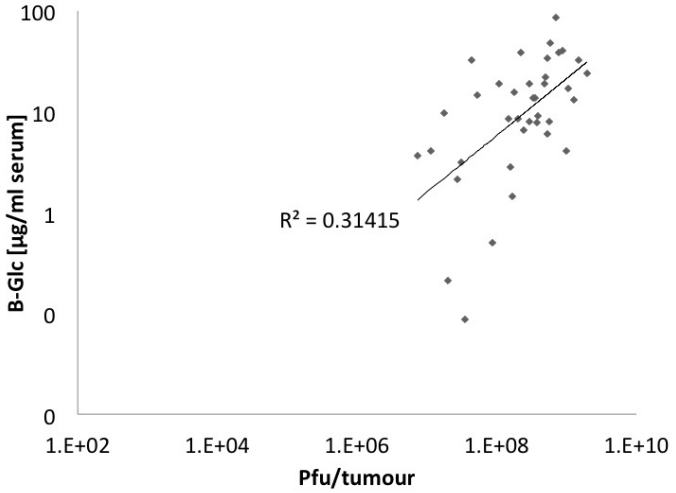

Figure 3.28: Correlation between β-glucuronidase measurements in serum. The viral titres were determined from homogenised tumour samples.

Level of β-glucuronidase in tumour and release into the blood stream

An important aspect in this study is determining the ratio between amount of biomarker produced in the tumour to concentration of marker present in the serum. For this reason, the levels of β-glucuronidase were determined in tumour homogenates and serum of the same mouse. Each time point is comprised of the data gathered from three mice, and since the mice had to be sacrificed in order to determine the tumour titre, they are different mice for each time point.These were then calculated to reflect the amount of biomarker in

the whole organ; for tumour it was μg marker per total tumour, with the tumour weight varying for each mouse ranging from 0.68 g to 0.22 g depending on the time point in question. For serum calculations, it was estimated that the average mouse has 1.5 ml of serum in circulation. The method used for quantification was the fluorigenic activity assay. Thus, the concentrations were calculated and plotted in a column graph (Fig. 3.29). This graph shows that for the GLV-1h416-treated group, both serum and tumour concentration increased in time, peaking at 42 hours post viral injection and decreasing to very low levels when measured at 63 days post viral injection. Mice which had received GLV-1h417 as a treatment showed a different trend. The maximum for both serum and tumour concentration was reached already at 14 days and declines to the last time point measured, 63 days post viral injection.

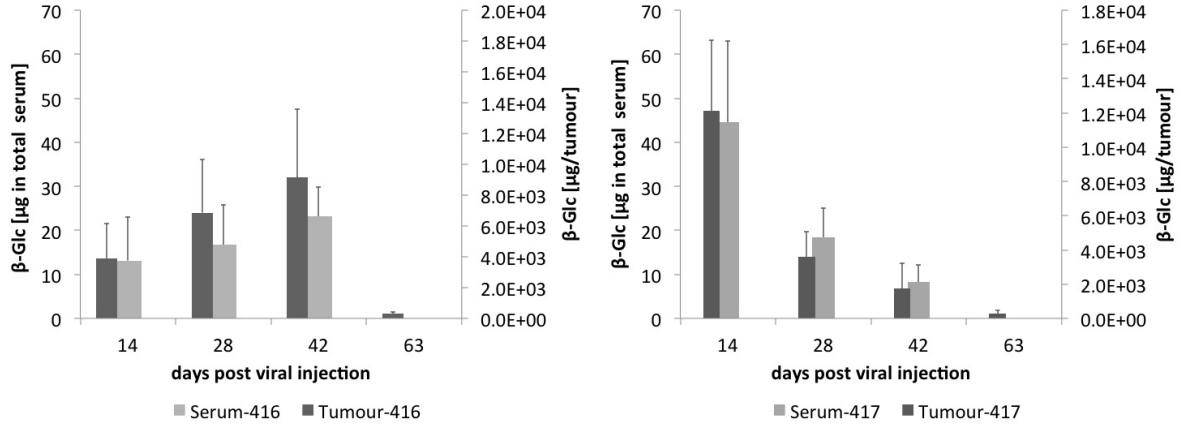

(a) GLV-1h416-treated group **(b)** GLV-1h417-treated group

Figure 3.29: Levels of β-glucuronidase in tumour and serum for GLV-1h416/GLV-1h417 treated mice. Each time point comprises of data acquired from three mice (n=3). β-Glc is presented as μg per tumour, as well as μg in serum, with the whole size/volume for serum samples being defined as 1.5 ml of serum per mouse. The tumour of all mice were weighted at time of excision and calculated into the above shown values. The average tumour weight for each time point varied between 0.68 g to 0.22 g.

3.5 CPG2 as a biomarker

CPG2 had already existed prior to these experiments as a vaccinia virus construct, but no standard for quantification was available for this enzyme. So it was first cloned into pET-28a in order to attach an N-terminal His-tag and then cloned into the over-expression vector BL21DE3. The subsequent purification was done in a His-tag-dependent manner. When referring to the CPG2 virus, the specific viral construct termed GLV-1h181 is meant, which has CPG2 in the J2R locus under the control of the synthetic early/late promoter (p^{sEL}).

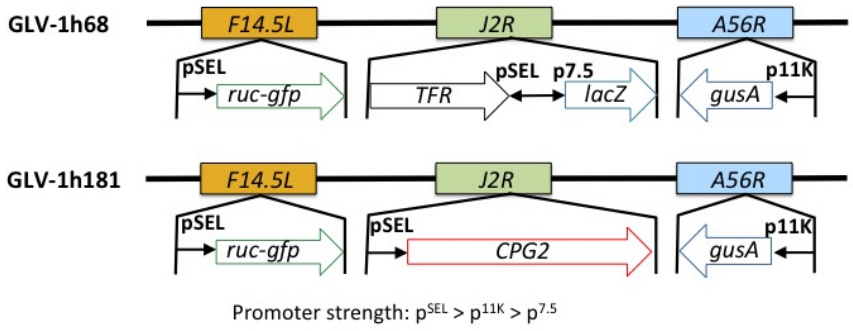

Figure 3.30: A schematic representation of the attenuated, CPG2 expressing virus GLV-1h181. Shown above that is a schematic of the parental virus GLV-1h68, adapted from Zhang *et al.*[28]

3.5.1 Confirmation of CPG2 expression and purification

CPG2 was successively digested using BamHI and HindIII, the pET-28a vector was concurrently digested using the same enzymes in a different reaction and dephosphorylated. By inserting the gene for CPG2 into the pET-28a vector, a 6x His-tag was fused with the C-terminus of CPG2. This tag was used later for purification of the overexpression product by α-His coupled magnetic bead purification. The DNA required for these cloning steps was taken from one of the intermediate cloning steps required to construct the CPG2-containing virus, GLV-1h181. The overexpression was performed in *E. coli* strain BL21DE.

In the following Fig. 3.31, cell lysates from all steps were loaded onto an SDS gel and stained with Coomassie blue. Lanes 1 to 5 consist of samples taken from the overexpressed

cell lysates BL21-DE3 show a successful His-tag-dependent purification of CPG2. Lanes 2 and 4 samples from uninduced BL21DE3 cells and uninduced, bead-purified samples, respectively. Lane 4 shows evidence of a leaky expression and/or intrinsic expression of the foreign gene inserts which was not induced by IPTG. Consequently, this was taken under consideration as background expression. A Western blot of this same gel was performed (data not shown) and showed similar patterns when detecting CPG2 in an antibody-dependent manner, thus reaching the same conclusion as shown in fig. 3.32.

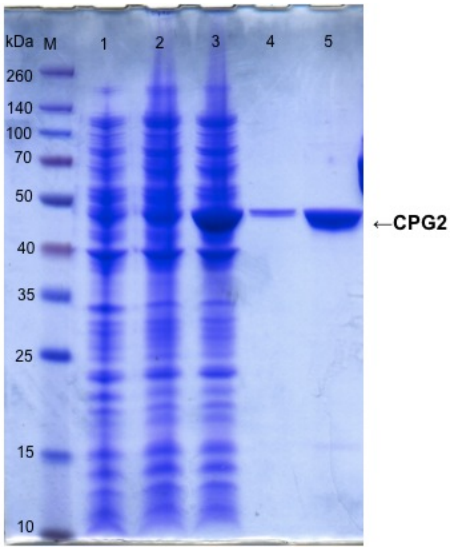

Figure 3.31: Coomassie blue stained SDS-PAGE gel. CPG2 was found at roughly 45 kDa. M: Spectra Multicolour broad range marker; 1: blank BL21DE cells; 2: BL21DE-pet28a-CPG2 cells, uninduced; 3: induced BL21DE-pet28a-CPG2 cells; 4: bead-purified, uninduced cells; 5: bead-purified, induced cells. The gel was fixed for 1 hour, incubated with a Coomassie blue staining solution overnight and destained over a period of 5 hours.

Fig. 3.32 shows aliquots taken during multiple purification steps perpetuated in order to purify overexpressed CPG2 from *E. coli* whole cell lysate. As can be seen in the image presented, the highest concentration of CPG2 is found in lanes 1, 2 and 7, representing samples accrued from crude cell lysate, flow-through after column loading and elution of the product from the column. The other lanes show that wash steps not only removed impurities, but also the target protein from the column. This could result from column overloading. The bulk product of this overexpression was shown to run at roughly 45 kDa. The protein characteristics gleaned through these experiment showed that the recombinant CPG2 had the same physical properties as stated in literature, hovering around the 42 kDa mark in both Western blot and Coomassie blue SDS-PAGE experiments. Being a dimeric enzyme, the total enzyme would come to about 94 kDa, which is consistent

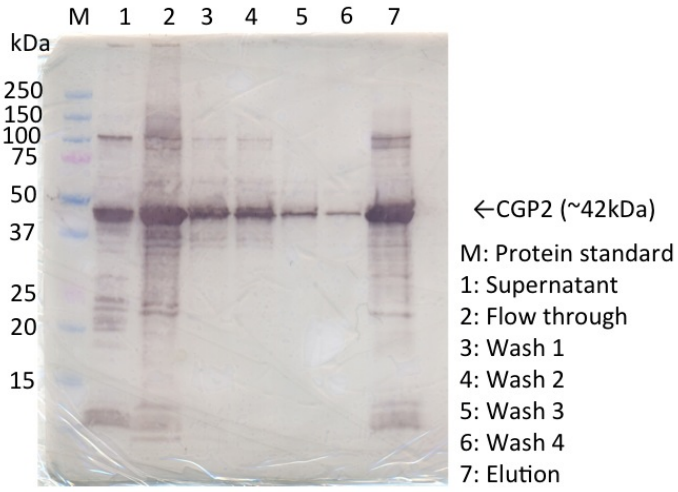

Figure 3.32: Western blot detection of CPG2 using α-CPG2. The primary antibody was diluted 1:5,000; a goat α-rabbit HRP-conjugated secondary antibody was diluted 1:5,000. The legend is found to the right of the blot. The enzyme was purified using magnetic α-His beads under denaturing conditions, in order to isolate CPG2 from inclusion bodies known to be present due to the overexpression of CPG2.[87]

with the sizes stated in literature.[87] However, the enzymes gained through this method showed little to no enzymatic activity when measured after this purification steps. Protein refolding and dialysis into a stabilising buffer were required, after which the enzymatic activity assay showed the CPG2-dependent metabolism of methotrexate.

3.5.2 Quantification of CPG2 enzymatic activity

With the overexpressed CPG2, MTX assays were performed according to Sherwood[86], substituting $ZnSO_4$ with $ZnCl_2$ (chapter 2.3.6). Various enzyme concentrations were tested, resulting in the amount of 20 ng being chosen as the standard concentration to be used at the specified substrate concentration. The measurement at 320 nm reflects a negative slope, meaning that the condition being measured that wavelength is that of MTX being metabolised. Starting at a measurement of 4 O.D., meaning that the photometer has reached its maximum reading capability, the curve reduced in readings, bottoming out at around 2.5 O.D. Fig. 3.33 shows the culmination of these experiments. The readings shown were the ones chosen for determining the CPG2 concentration to be used as a basis for its specific activity. The results of the activity analysis can be seen

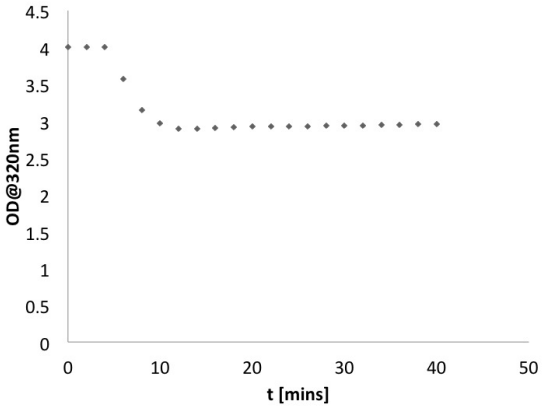

(a) MTX assay - 100 ng purified CPG2

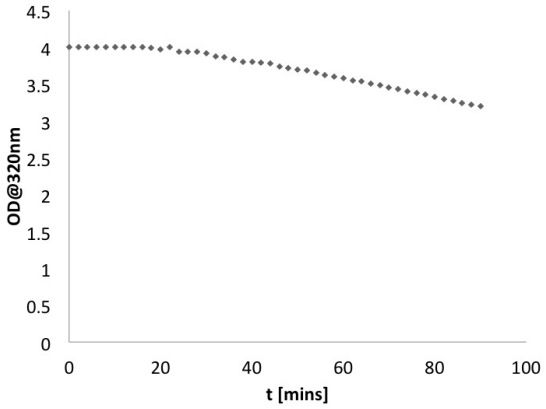

(b) MTX assay - 100 ng purified CPG2

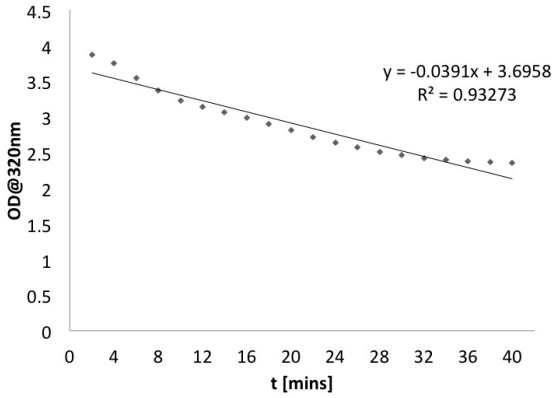

(c) MTX assay - 20 ng purified CPG2

Figure 3.33: Different enzyme concentrations for the determination of the enzymatic activity of a purified batch of CPG2. The concentration of 20 ng CPG2 was chosen for use in the calculation of its specific activity, due to the clear linear regression shown in the activity assay.

in above. These graphs show that the enzyme was within an adequate working range, which is consistent with the range stated in literature.[86] [85] From that linear regression depicted in Fig. 3.33c, with the known concentration of enzyme as determined using a Bradford Coomassie assay, the specific activity was calculated using the Lambert-Beer law, which is defined as followed:

The calculation of the actual specific enzyme activity yielded an activity of 81-94 U/mg of CPG2, which is varies from the activity stated for this enzyme in literature. One group reported an activity to 590 U/mg protein, while another group cites an activity of 7.3 U/mg CPG2.[87] [54] The difference in purification method and the protein refolding

could explain these discrepancies.

3.5.3 In vivo testing of GLV-1h181 in athymic nude mice

In order to test the efficacy and function of CPG2, and concurrently GLV-1h181, as a biomarker, an animal study involving athymic nude mice, a common xenograft model for human cancer, was done. These mice were injected with $5x10^6$ cells/mouse GI-101A cells into the right flank, subcutaneously in the lower thigh muscle. After reaching an average volume of 200-300 mm^3, each mouse was injected with $5x10^6$ pfu. Blood was taken from each mouse directly from the saphenous vein of the left flank, using sterile insulin needles, and was collected in reaction tubes without the addition of anti-coagulants. For a graphic representation of the time line, refer to Fig.3.46. Mouse weight and tumour volume were measured each week. GFP fluorescent images taken were taken every week as well.

Toxicity

The following graph shows the average body weight of mice in the different treatment groups, which were weighed once a week for the duration of the above mentioned study. The change in body weight is considered to be a general indicator of good health and well-being. The comparison of toxicity was always made in comparison to the GLV-1h68-treated group. In all, only two mice had to be sacrificed prematurely due to their drastic drop in weight loss. All other mice survived till their allotted time point or till the end of the study. In comparison, no mice had to be sacrificed early in the GLV-1h68 group. Comparing the group averages here in Fig. 3.34, there is no significant weight loss discernible due to the viral treatment. All group averages increase with time. Since the net/fractional body weight is used as reference, the tumour volume does not play any role in this analysis. The PBS group shows the highest increase in body weight, ranging from 30 g to 37 g by the end of the study. The GLV-1h68 group also starts at 30 g in the beginning, ending at around 35 g on average. The GLV-1h181 group displays the smallest increase, from beginning to end, a difference of 2 g from start to end. The difference between each group, PBS and GLV-1h68, and GLV-1h181 and GLV-1h68, does not seem to be significant.

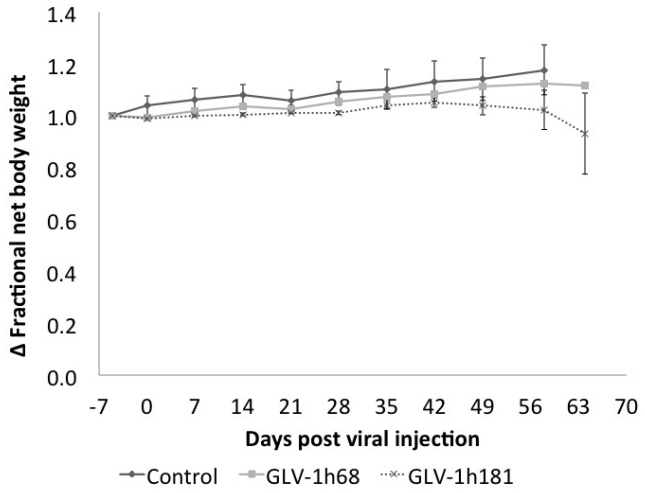

Figure 3.34: Difference in fractional body weights on average for the GLV-1h181 treatment group. Shown as well are the control groups GLV-1h68 and PBS. Fractional body weight refers to the actual body weight of the mouse, after deduction of the tumour weight.

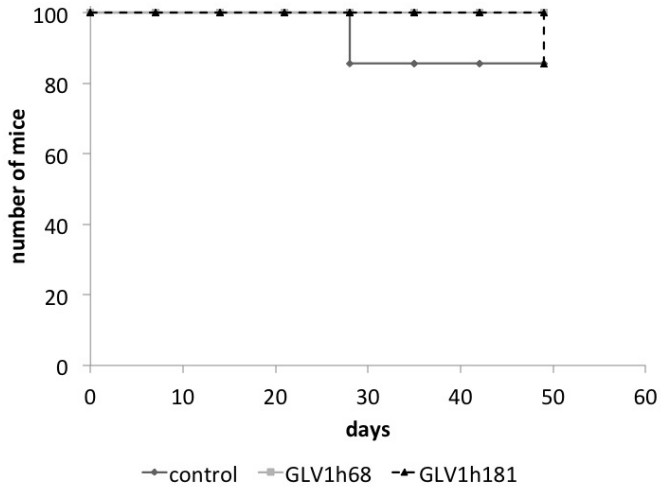

Figure 3.35: Kaplan-Meier survival plot for the control group (PBS), the GLV-1h68-infected group and the GLV-1h181-treated group. Log rank testing of the GLV-1h68 and the GLV-1h181 group showed no significant difference between the two (p=0.355).

Survival

In order to ascertain the survival of the individuals in the GLV-1h181 group and compare it to that of other groups, deaths of subjects was recorded and plotting into a Kaplan-Meier plot. This plot, depicted in Fig. 3.35, shows the survival of all group members during the course of the study. This plot only shows deaths due to natural or unnatural causes. Mice that were removed at different time points were not considered in this analysis. Thus,

the log rank testing of the GLV1h181 group against the GLV-1h68 group, considered as the standard for treatment, showed no significance between for the survivals pertaining to each group.

MTX assay in murine serum samples

MTX assays were performed with serum isolated from GLV-1h181-treated mice. However, the serum did not lend itself to be measured with the method established in cell culture, as an unknown substance in the blood was causing precipitation in the cuvette. Further modifications to the method did not ameliorate this issue and as such, the testing of CPG2 in *in vivo* samples was discontinued.

3.6 CEA as a biomarker

3.6.1 Virus construction

Firstly, the CEA-encoding virus had to be constructed. The methods used are listed in chapter 2.2. The successful cloning of various forms of CEA from a human cDNA bank into the vaccinia virus backbone was confirmed by agarose gel fragment size verification, PCR analysis and, ultimately, DNA sequence analysis. With the identity confirmed on a DNA level, the detectability of the expressed CEA protein was tested using Western blot and ELISA.

The cDNA encoding for CEA was first amplified from a human cDNA mix (Clontech) using the appropriate primers (see D for sequence), gel purified and subsequently cloned into the pCRII-Blunt TOPO vector (Invitrogen). Primers were also used to amplify the secreted CEA insert by removing a 3' section from the DNA, resulting in a deletion of 26 amino acids from C-terminus of CEA. This terminus represented the GPI anchor normally used to anchor this protein to the cell membrane. Following affirmative sequence confirmation, the pCRII-CEA construct was digested using SalI-HF and PacI and ligated into the digested viral transfer vectors TK-sE, TK-sEL and TK-sL.

After sequence confirmation in the viral transfer vector, the vaccinia viruses containing this DNA were made, using GLV-1h68 as the parental virus. Screening potential clones yielded two viable viruses per promoter construct (p^{sE}, p^{sEL} and p^{sL}), of which one each was chosen for up-scaling and amplification.

The sequence confirmation using a screening PCR is shown in Fig. 3.37. In this case, the fragment amplified using CEA sequence-specific primers shows that out of the seven viral isolates that had been tested for the presence of CEA, three viral isolates contained viral DNA with the correct insert size (lanes 5, 6 and 8). The fragment size in question is roughly 2 kbp for sCEA and 2.1 kbp for fCEA. Lane 9 shows a positive control using a transfer vector that had had CEA inserted into its genome, prior to further cloning into the target plasmid.

This construction was performed for both a full-length (fCEA) and a truncated short-length (sCEA) version of CEA.

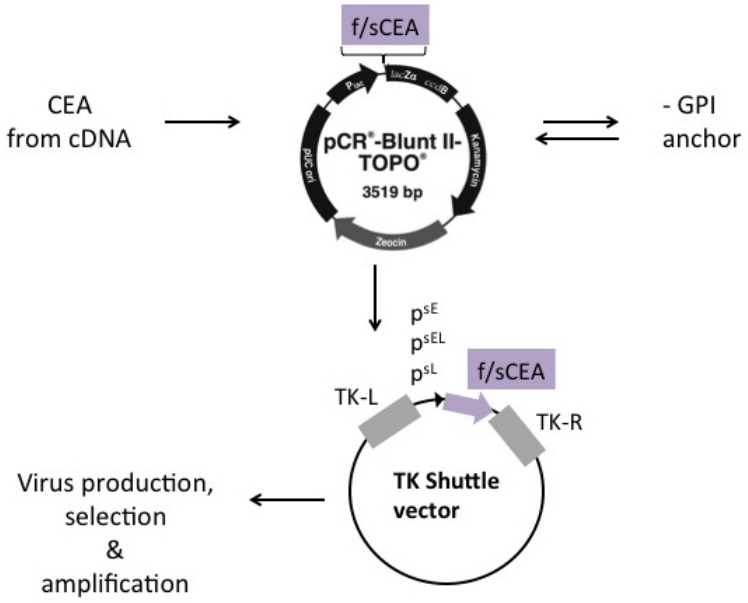

Figure 3.36: Cloning strategy for the creation of f/sCEA inserts. Cloning of the full-length CEA insert was done using a human cDNA mix template, followed by insertion into a blunt end transfer vector. Using specific primers, the GPI anchor was removed from CEA by deleting 26 amino acids from the C-terminus, resulting in a secreted version of the protein. This modified insert was then transferred into the TK-shuttle vector.

After initial experiments and judging from experimental data shown following, the available viruses were narrowed down to two viruses that were to be used in an athymic nude mouse animal study.

3.6.2 CEA expression level is dependent on the viral promoter strength and is crucial in virus choice

The viruses constructed in the previous section (3.6.1) were tested in cell culture to reconfirm that the CEA gene had indeed been inserted into loci under differing promoter strengths. CV-1 cells infected with the various primary viruses were harvested 24 and 48 hours post infection, and tested for their protein expression level. The ELISA was performed using the commercial kit mentioned in the chapter “Materials & Methods”, section 2.3.

The results of this assay (Fig.3.39) show that at a 1:50,000 dilution was sufficient for the CEA levels to fall within the range of the standard curve. It also shows the different

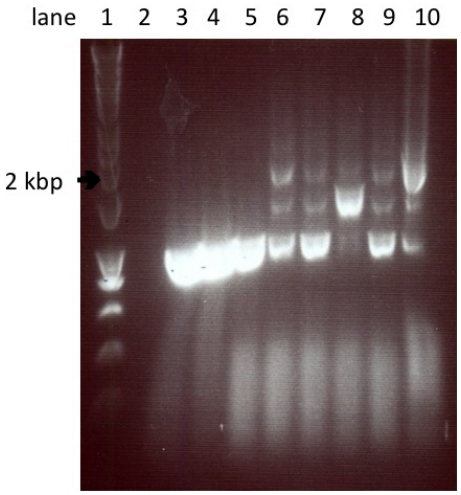

Figure 3.37: Agarose gel screening for the presence of s/fCEA inserts in viral isolates. Short and full-length CEA-specific primers were used. Lane 1: Bioline Hyperladder I; lane 2: blank; lanes 3-9: plasmids from various isolates of recombinant VACV encoding for CEA; lane 10: positive control (DNA from initial cloning used as template). The lanes containing inserts around 2 kbp were considered to contain the correct insert. These viral isolates were then further analysed in cell culture using CV-1 cells.

concentrations of target protein in accordance with the promoter strength. Virus isolate A shows no detectable CEA production at either time points and the gene inserted is under the p^{sE} promoter. Isolates B, C and D all show detectable CEA levels in lysed cells, with the 48 hours post infection samples showing a higher concentration than the 24 hours post infection samples. Isolates B and C both have CEA inserted under the control of a synthetic late promoter, whereas in isolate D, CEA is under the control of a synthetic early/late promoter. The degree of difference visible between the 24 hours post infection and the 48 hours post infection varies in correspondence to the promoter strength.

A dilution of isolate C-infected CEA sample was done, in order to more accurately ascertain the dilution range required for future measurements. The same isolate C infected CV-1 sample used in Fig. 3.39 was used in this experiment here. In order for the reading to be accurate, they have to fall within the linear section of this serial dilution range. This was determined empirically. The dilution range showed here indicates that for a reading to be viable in an ELISA assay for CEA, it had to fall within the linear range (Fig. 3.40). This showed samples had to be diluted to a dilution of 1:20,000 to 1:50,000, showing that this method has a much higher sensitivity than other ELISA assays used so far.

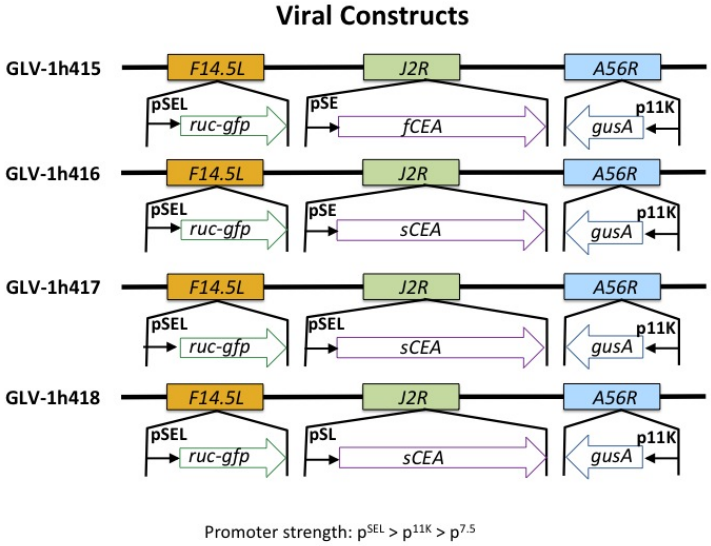

Figure 3.38: Schematic representation of the final CEA viruses chosen for experimental purposes. Both full-length (fCEA) and short-length (sCEA) versions were cloned, with each version being cloned with a synthetic early (p^{sE}), a synthetic early/late (p^{sEL}) and a synthetic late (p^{sL}) promoter respectively. Comparison to the parental GLV-1h68 virus in Fig. 3.30.

3.6.3 Preliminary testing in cell culture

Confirmation of CEA in cell culture samples

A Western blot was run to detect the ideal dilutions required for reliably detecting CEA in cell culture samples, as well as to confirm that CEA was able to be detected in cell culture samples, which is a required procedure prior to virus amplification.[88] The samples loaded on the gels were as followed: marker, cell lysate (24 hpi), cell lysate (48 hpi) and uninfected cell lysate as a negative control. The cell lysate containing CEA was from CV-1 cells infected with a CEA viral clone containing CEA under the p^{sL} promoter. The primary detection antibody used was a mouse α-CEA antibody; the secondary HRP-conjugated antibody was a goat α-mouse antibody The results of this experiment are shown in Fig. 3.41. The dilutions for the antibodies are 1:50 for the primary and 1:10 000 for the secondary antibody respectively. The detection of the secondary antibody was done using the Opti-4CN kit from BioRad. CEA runs at a height of 150 kDa, β-actin at a height of 45 kDa. Consecutive staining with α-β-actin was done as a loading control. As can be seen below, the blot shows a positive detection of CEA in both cell lysates, with the negative control being blank and showing no background resulting from cell culture. Having thus proven the presence of CEA in certain virus clones, the amplification of

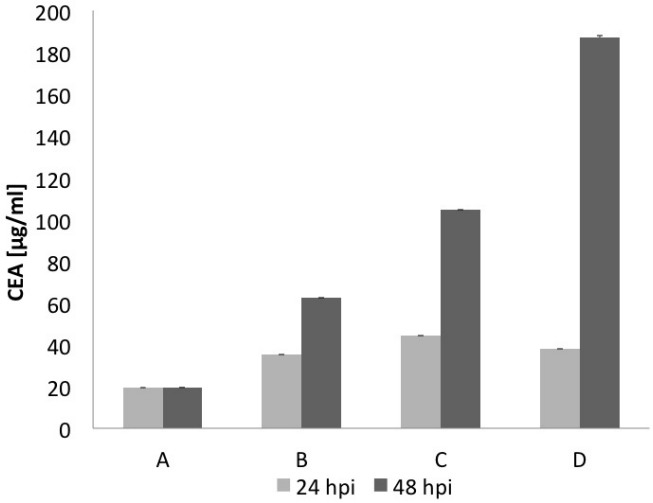

Figure 3.39: sCEA quantification via ELISA assay. Infected CV-1 cells were harvested 24 and 48 hours post infection, and diluted 1:50,000 prior to being assayed. The samples shown represent different viral isolates, within which sCEA was controlled by different promoter strengths. Viral isolate A - sE promoter; isolate B, C - sL promoter; isolate D - sEL promoter.

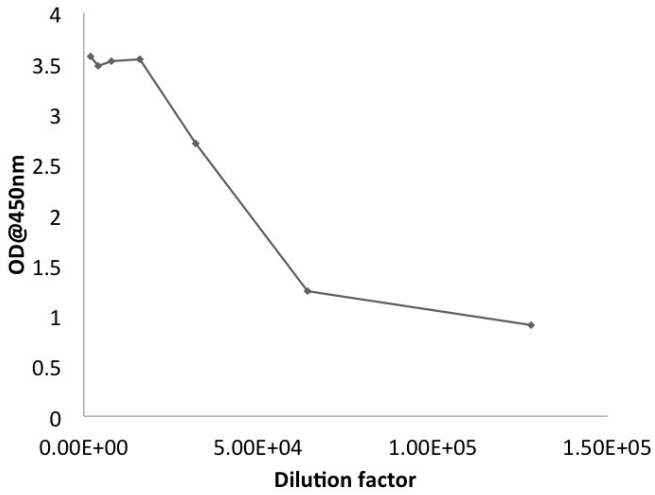

Figure 3.40: Dilution assay for CEA infected cell culture. Further dilutions performed on samples infected with virus isolate C. The measurements are absorbency readings taken at 450 nm and plotted against the dilution factor of that sample. In order for the reading to have relevancy, they had to fall within the linear range of this dilution curve.

selected clones was able to commence. The amplified constructs were as followed: GLV-1h415, GLV-1h416, GLV-1h417 and GLV-1h418. All these viruses were based on the GLV-1h68 backbone, with either the full-length (GLV-1h415) or a short-length (secreted) CEA replacing β-galactosidase in the *J2R* locus, as shown in Fig. 3.38.

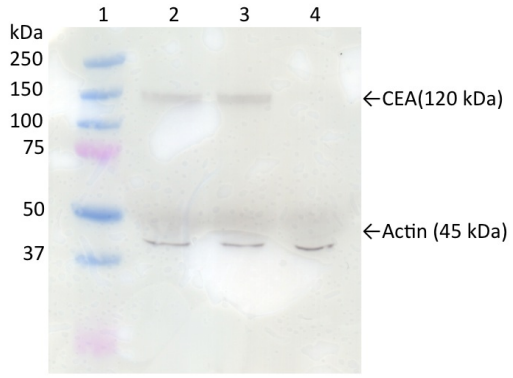

Figure 3.41: Detection of CEA in Western blots. Lane 1: marker; 2: infected cell lysate (24 hpi); 3: infected cell lysate (48 hpi); 4: uninfected CV-1 cells. The primary antibody used was a 1:50 diluted mouse α-CEA antibody. The secondary HRP-conjugated antibody was a goat α-mouse antibody, diluted 1:10,000. Actin was detected on the same blot as a loading control. The blot was incubate in each antibody overnight.

Intrinsic CEA levels in various cell lines

CEA is known to be expressed intrinsically by cancer cell lines, especially in lines deriving from colorectal cancers. In order to determine which cell line would later be used in the nude mice animal model, various uninfected cells were harvested from cell culture, treated to three freeze-thaw cycles and assayed using the same ELISA kit as used to determine CEA levels in the experiments before. These findings (Fig. 3.42) showed that the intrinsic CEA levels expressed by each cell line varied, and that GI-101A, a human breast cancer cell line, and the human colorectal cell line HT29 showed the highest intrinsic CEA expression in cell culture. Comparatively, a human lung cancer cell line A549, as well as OVCAR3, an ovarian epithelial carcinoma, showed a low to negligible concentration of CEA.

In vitro cell killing and viral replication

In order to verify the new CEA recombinant constructs lytic activity, MTT cell killing assays and replication assays were performed simultaneously with concurrently infected cells in cell culture. These experiments were performed using GI-101A cells, the cell line with which the nude mouse study had been planned. Fig. 3.43a shows an MTT assay performed using GI-101A cells and the following viruses: GLV-1h68 as a control, GLV-1h181 (CPG2) and viruses GLV-1h416 (sCEA, p^{sE}) and GLV-1h417 (sCEA, p^{sEL}). The signal shown is the reading of the MTT substrate, that was metabolised by living cells present in the well. The less viable cells available, the weaker the reading. These

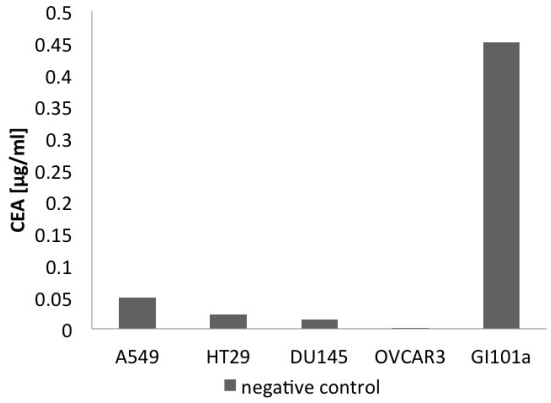

Figure 3.42: Intrinsic CEA levels found in untreated and uninfected human cancer cell lines. The assay was performed using a commercially available CEA ELISA kit from Abcam. The samples were uninfected cells from the following human cell lines: A549 (lung carcinoma), HT29 (colorectal adenocarcinoma), DU145 (prostate cancer), GI-101A (breast cancer) and OVCAR3 (ovarian epithelial carcinoma).

figures generally show, that compared to the GLV-1h68 group, all CEA viruses show a greater cell killing capacity. However, this trend in concurrent with the viral titre shown to be present in the samples (Fig. 3.44b), as the CEA viruses shown a generally higher replication than GLV-1h68. GLV-1h181 is the only virus shown to be less efficient in GI-101A cells compared to GLV-1h68, with its viral titre also being the lowest amongst all viruses tested. The same experiment was repeated using CV-1 cells and the result shown in Fig. 3.44a. Again, a similar trend could be seen when compared to the same experiment done in GI-101A cells, mentioned before. GLV-1h181 has a slightly greater cell killing effect when compared to GLV-1h68, whereas all CEA viruses are have a greater cell killing capacity than the control virus.

Two further tests had to be completed prior to commencement of an animal study, the MTT and viral replication assays. An MTT assay was required to test the virus' possible toxicity by infected cells *ex vivo*. The details of this assay are mentioned in chapter 2.1.5. The data in Fig. 3.43a and 3.44a shows the result of two MTTs performed using GI-101A and CV-1 cells respectively. The first figure shows that when compared to the parental virus GLV-1h68, all CEA viruses exhibited an increased cytotoxic effect in GI-101A cells, with the CEA viruses resulting in 30 to 50% cell survival after an infection of 96 hours post infection. GLV-1h68 showed that just under 60% of the cells had survived the infection. It was thought that this increased cytotoxic effect could be explained by an increased viral replication due to the modifications performed on the CEA viruses.

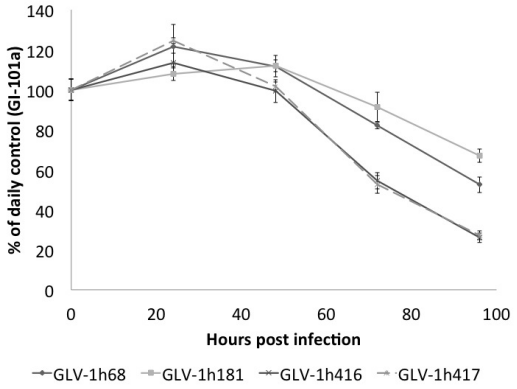

(a) MTT Assay for cytotoxicity

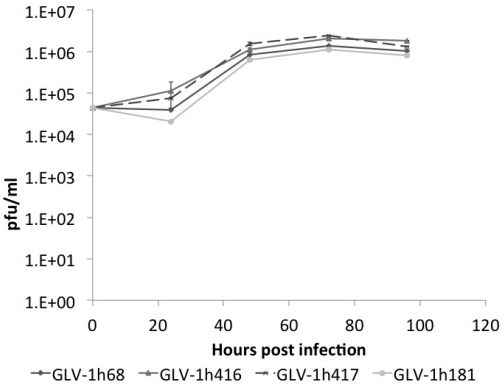

(b) Viral titration (quantification) data pertaining to samples co-infected during the MTT shown in Fig. 3.43a

Figure 3.43: MTT cytotoxicity assay of new viral constructs *in vitro*. Shown here is virus-mediated cell death. MTT is taken up and metabolised by living cells, thus resulting in a colorimetric reaction. The more living cells in a cell culture dish, the greater the absorbance at 570 nm. This experiment was performed using GI-101A cells, infected with an MOI of 0.1.

However, the replication assay of duplicated infected samples in Fig. 3.44b showed that the replication of all viruses in that study was comparable, implicating the CEA viruses in having a construct specific, cytotoxic effect. When tested in CV-1, the cell line used as a amplification cell line because VACV had shown to have the highest replication in that cell line, it was shown that the cytotoxic trend previously depicted was slightly different. In this instance, all viruses had eradicated around 80% of living cells after an infection of 96 hours post infection. The replication assay done on this cell line shows a higher viral titre reached by the end of the experiment (around $1x10^7$ pfu/ml) compared to the replication in GI-101A, which ended in a viral titre of $1x10^6$ pfu/ml. Since there was no discernible difference between viruses within the CV-1 experiment, it was surmised that the susceptibility of the tumour cell line to a viral infection and consequent lysis augmented the cytotoxic effect seen in GI-101A. This also indicates that while VACV is able to replicate and lyse in many different neoplastic cell lines, it does show preference in replication for certain types.

Analysis of CEA in early cell culture time points

The analysis of infected cells at early time points was done to elucidate the reason for the difference in replication and cytotoxicity seen in cell culture samples, but more obviously

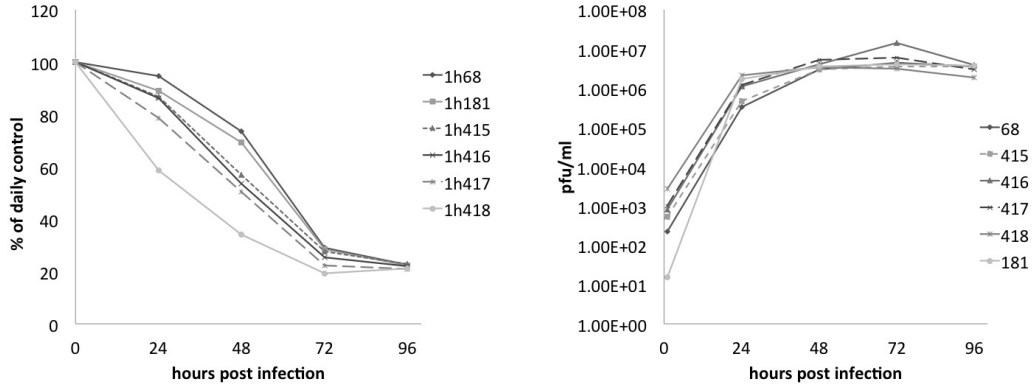

(a) MTT assay data **(b)** Viral titration data

Figure 3.44: MTT cytotoxicity assay of CEA viruses in CV-1. The cell killing activity of new viral constructs is tested *in vitro* using an MTT assay,from infected CV-1 cells with an MOI of 0.1. Fig. 3.44b shows the replication assay data corresponding to the MTT samples shown in Fig. 3.44a.

later on in animal samples. Fig. 3.45a shows the viral titration data for CV-1 cells infected with either GLV-1h416 or 1h417 at an MOI of 0.1. It shows that the while the titration data showed a more rapid increase in viral titre for GLV-1h416, the CEA concentrations measured showed the opposite trend, that in spite of being slower in replication, GLV-1h417 expressed more CEA in the same time frame than GLV-1h416.

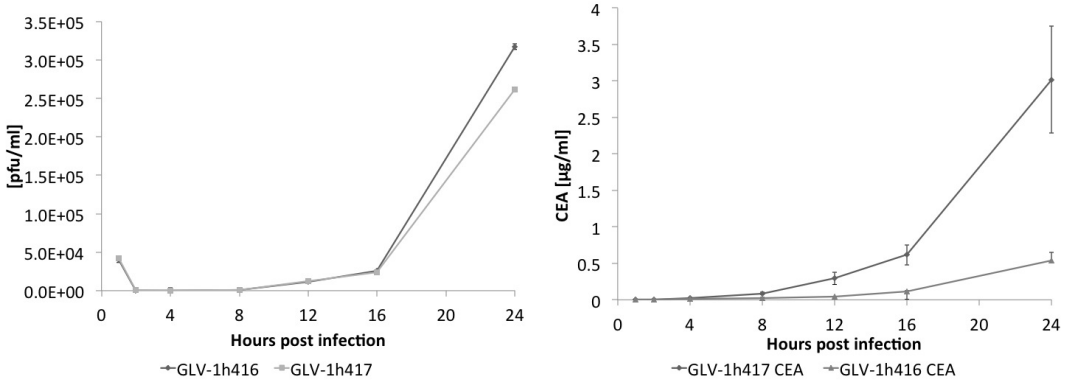

(a) viral titres **(b)** CEA concentration

Figure 3.45: Comparison of CEA and viral titre in GLV-1h416 and 1h417 at early time points. Infected cell culture samples were taken at early time points after viral infection, titrated and analysed for CEA and viral replication. Data pertaining to the concomitant gusA expression is found in Fig. 3.25a.

3.6.4 CEA in athymic nude mice

In order to test the efficacy and the hypothesis of this thesis, of the previously acquired viruses, GLV-1h416 and GLV-1h417 were selected for use in an animal study involving athymic nude mice, a common xenograft model for human cancer. These mice were injected with $5x10^6$ cells/mouse GI-101A cells into the right flank, subcutaneously in the lower thigh muscle. After reaching an average volume of 200-300 mm^3, each mouse was injected r.o. with $5x10^6$ pfu of the respective virus. Blood was taken from each mouse directly from the saphenous vein of the left thigh, using sterile insulin needles, and was collected in reaction tubes without the addition of anti-coagulants. The time-line shown here depicts the planned bleeds and mice sacrifices in a chronological order. Mouse weight and tumour volume were measured each week. GFP fluorescent images were taken every week as well. The groups were sized as followed: GLV-1h416 & 1h417 treatment groups (CPG2 & CEA): 20 mice per group; control (PBS) & GLV-1h68 group: 10 mice per group.

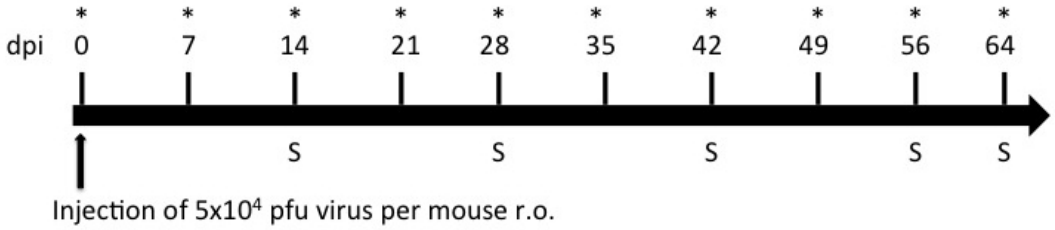

Figure 3.46: Outline of the animal study GL12-29a. This study was required to elucidate the relationship between the expression of biomarkers (CEA and β-glucuronidase) and the viral titre present in the mouse. S - Sacrifice of a minimum of four mice from each group. Blood (*) was taken from the saphenous vein once a week from study being till end, with some mice being bled at either 3, 5 or 7 dpi, leaving at least four days between bleeds, for the mouse to recover from the previous bleed.

Toxicity

The following, Fig. 3.47 shows the average group body weight of the mice in the PBS and GLV-1h68 control virus group, as well as the GEA virus treatment groups GLV-1h416 and GLV-1h417. All mice in the groups that had been weighed once a week for the duration of the above mentioned study. The total fractional net body weights stayed relatively stable, while the tumour size increases (Fig. 3.49), increasing the fractional tumour volume of the whole mouse. A stable body weight is generally considered to be indicative of good

health. However, all mice in the PBS group had to be sacrificed before the end of the study due to tumour burden. Compared to the other groups, the GLV-1h417-treated mice

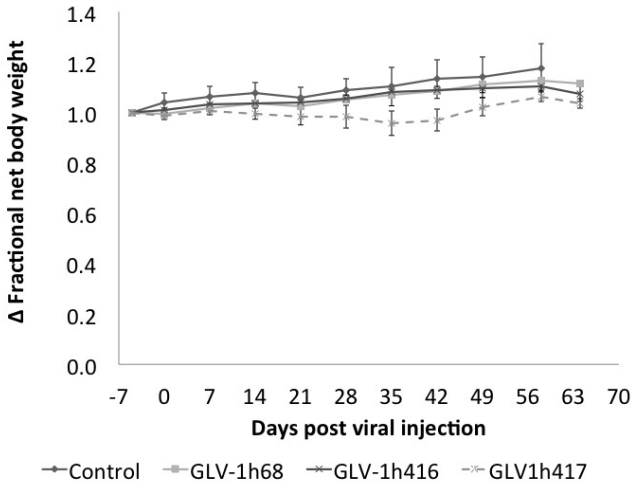

Figure 3.47: Fractional net body weight change for GLV-1h416 and 1h417-treatment groups. Also shown are mice treated with GLV-1h417 but without tumours, as well as GLV-1h68 treated and PBS control groups. The fractional body weight is the body weight without the tumour and was plotted as a change in weight compared to day 0 of virus treatment. Each mouse was injected with $5x10^6$ cells (excluding 1h417 no tumour group) and was treated with $5x10^6$ pfu of virus via r.o. injection, with PBS injected in lieu of virus in the control group.

seem to show a slight toxicity, with 2 mice having been removed prior to the end of the study. Having said that, the mice removed showed that they did not expire from excessive viral load (see titration data in fig. 3.50), as the virus was not found to have colonized other placed aside from the tumour. It stands to reason that these mice most likely died from reasons other than viral burden.

Survival

All groups in the animal study were always compared to the untreated control mice, as well as to the virus control group GLV-1h68. The survival of the groups on average was done using a Kaplan-Meier plot, depicting the deaths as percentages of all the subjects in that group that were present at the end of the study (Fig. 3.48). The average virus burden for each group over time is shown in Fig. 3.50. Additionally, log rank testing was undertaken to see if the survival of each group was significantly different compared to the GLV-1h68 group, which resulted in none of the groups being statistically different from the virus control group. Of this 120 subject study, none of the mice died from virus

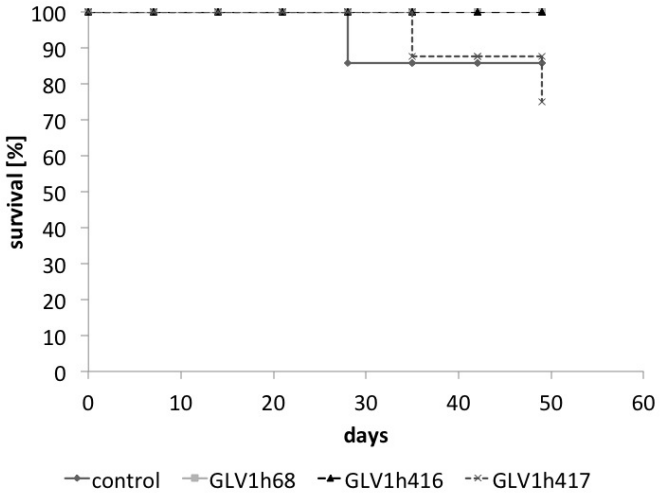

Figure 3.48: Kaplan-Meier survival diagram for GLV-1h416 and 1h417 treated mice, as well as the GLV-1h68 and untreated control groups. The number of mice analysed per group is shown as the samples size (n) at below the graph.

related causes.

Tumour regression and viral titre

Tumour regression and the viral titre in the subject go hand in hand, as the viral titre is dependent on the amount of tumour tissue available for replication. The following figures show the relationship between the two variables in this study. Fig. 3.49 shows the evolution of the tumour size in all groups treated in the animal study, as well as the control PBS mice. The significance depicted on the graph shows the difference between tumour volume at that time point to the PBS control group. These mice had to be sacrificed at day 49 of the study, as the tumour burden would have otherwise exceeded the volume permitted by Explora vivarium guidelines.

As such, mice were sacrificed at certain time points and their organs removed, along with the tumours. These tumours were then titred to establish the concentration of virus, presented as pfu per total tumour, taking tumour volume/weight into account. The data, shown in Fig. 3.50 shows an relatively unchanging trend in viral titres for all treatment groups present in the study.

CEA tumour level and release into the blood stream

As mentioned before in Fig. 3.29, it is very important to determine how much biomarker is produced in the tumour, and how much of that amount is actually circulated in serum after

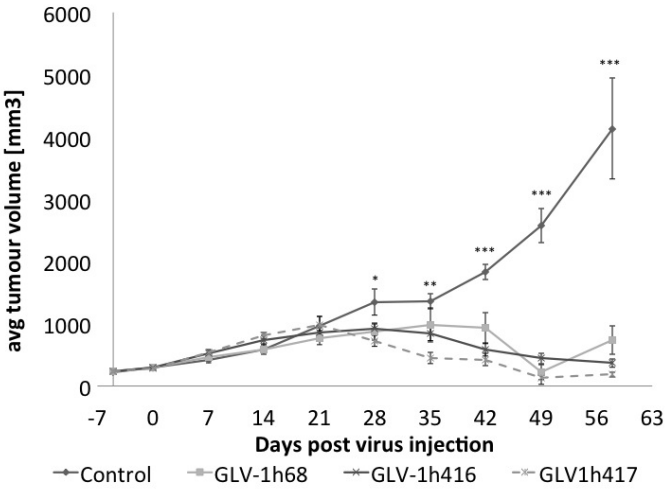

Figure 3.49: Tumour regression in nude mice. Shown here is the change in tumour volume for the CEA virus treatment groups, as wells as GLV-1h181, 1h68 and control groups for the course of the whole animal study. The notation represented on the graph shows the significance of the difference between tumour volume at that time point and the PBS control group.

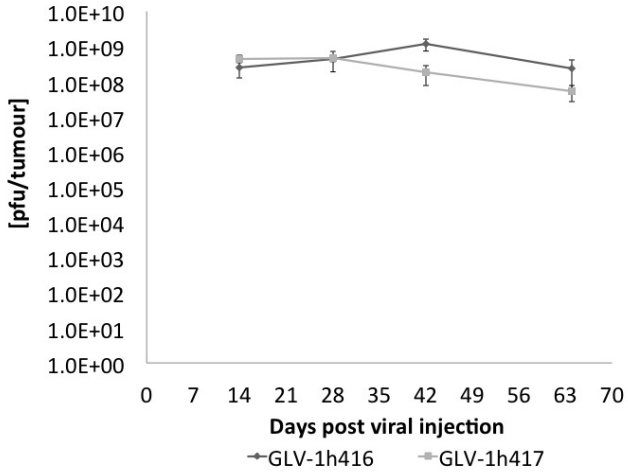

Figure 3.50: Change of viral titre present in tumour lysates over the course of the animal study. GLV-1h416 and 1h417 treatment groups are shown, with the titres were normalised to pfu per total tumour, taking the tumour volume into account. Mice were sacrificed at each time point and the tumour homogenates acquired.

release into the blood stream.The concentrations were determined in tumour homogenates and serum of the same mouse using an ELISA-specific for human CEA expressed by the virus. The data was then calculated to reflect the total amount present in the whole organ. The total amount of serum in a mouse was estimated to be 1.5 ml. Fig. 3.51

shows the data for this experiment. The overall secretion into blood, based on the data, was calculated to be 0.02% for GLV-1h416 and 0.007% for GLV-1h417. Mice treated with GLV-1h416 show that the amount of CEA in the tumour increases till 42 days, the drops to an extremely small level at 63 days post viral injection. The concentration in the serum has its peck at 28 days post viral injection, declining thereafter till the end of the study. As for the GLV-1h417-treated mice, over time, both CEA levels in tumour and in serum decline, albeit at different rates. The maximum level for both, however, was reached at day 14 post viral injection.

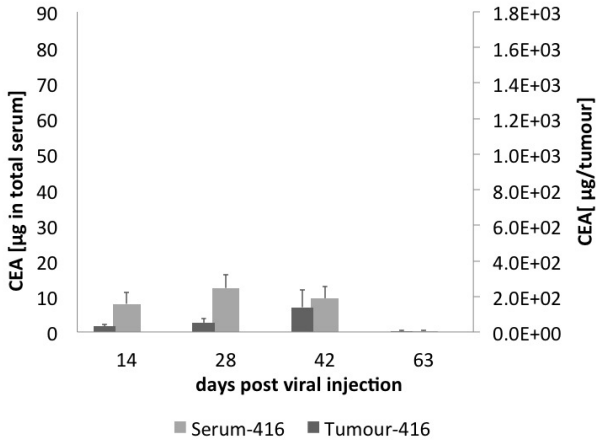

(a) GLV-1h416-treated mice

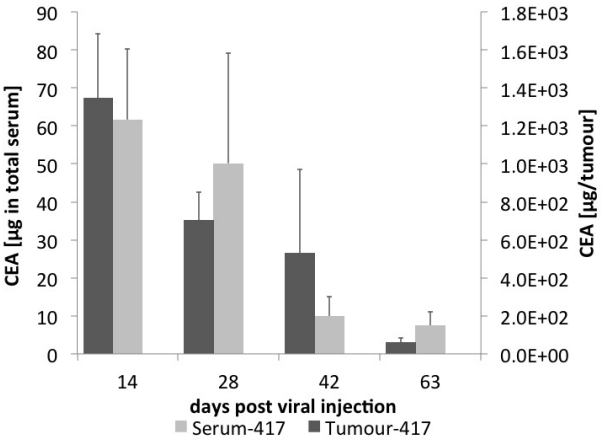

(b) GLV-1h417-treated mice

Figure 3.51: CEA levels in tumour and serum for mice treated with either GLV-1h416 or 1h417. Each time point comprises of data acquired from three mice. The concentration of CEA is presented as μg per whole organ, with the whole organ for serum samples being defined as 1.5 ml of serum per mouse. The tumour size was determined at time of excision.

3.6.5 Presence of CEA in the PBS control & GLV-1h68 treatment group

Assaying samples from the PBS and GLV-1h68 control groups was done in order to show that what the baseline CEA levels in the serum of tumour-bearing mice would be, as those levels were high in cell culture. Fig. 3.52 shows that this is the case, as the serum levels are comparable with those determined to be the tumour intrinsic baseline of CEA in GI-101A. These graphs, depicting the level of CEA present in the serum of mice over the period of the study, show a stable level of CEA on average of 0.12 μg/ml of serum. These samples were taken from the whole group, of which all mice were bled repeatedly. The line showing the CEA level present in the serum of the GLV-1h68 group dips slightly towards the end of the study, whereas the CEA levels of the control (uninfected) group increases towards the end.

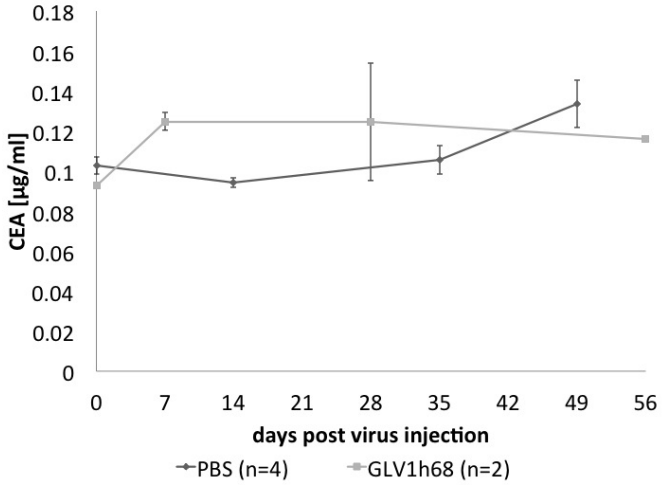

Figure 3.52: CEA for PBS and GLV-1h68 groups. The results of an ELISA assaying CEA in serum samples gathered from mice from the control group as well as the GLV-1h68-infected group. The graphs show that both groups display similar levels of CEA resulting from tumour intrinsic production.

3.7 Presence of VACV as determined by histological sectioning of tumours from the nude mice

It is possible, using histological staining methods, to detect for the presence of vaccinia virus in paraffin-embedded, histological tumour slices. Whole tumours from human cells were isolated from nude mice in the study that had received virus treatment and embedded according to the method mentioned in section 2.5. Adjacent slides were stained with either H & E or for VACV using a custom α-A27L antibody and then compared under a stereo microscope, as well as a normal microscope, under various magnifications. The H & E staining results in a pinkish stain for cytoplasm, muscle fibres and collagen (eosin), and a blue-purple stain for cell nuclei and other acidic cell compartments (hematoxylin). Fig. 3.53 shows adjacent tumour slices, one having been stained with H & E (a), and the other slice stained for the presence of VACV (b). These images show that the areas of viral replication (brown staining) overlap with the areas of necrotic tissue formation, which has cytoplasm stained pink by the eosin counterstain, but lack the blue/purple colouring associated with the hematoxylin staining for cell nuclei. The H& E staining also shows the morphology of tumour cells in the surrounding tissue area, as tumour cells are generally larger than their surrounding counterparts and have distinctly large nuclei.

An overview of most of the tumour was done with a stereo microscope. This was done on VACV, with the positive stain resulting in a darker area than the surrounding tissue, as can be seen in Fig. 3.54. Image (a) shows a tumour at 14 days post viral injection. The virus is not spread throughout the tumour, but is localised in focal points. Image (b) is of a different tumour at 64 days post viral injection, showing a more widespread viral infiltration. Both tumours were the result of the mouse inoculation with GI-101A cells and the subsequent treatment with virus, in this case GLV-1h417. The spread of virus throughout the tumour can be seen when both images are compared, with image (b) showing a larger area of positive VACV staining than image (a). Both tumours were estimated to have a similar size.

Also seen during the histological analysis were manifold levels of differentiation displayed by the H & E stained cells. Fig. 3.55 shows an stained slide from a GLV-1h417-treated mouse. The image shows that within the tumour area pictured, various different cell structures can be seen. Some tissue, stained only pink by the eosin counterstain, represents necrotic tissue; other cells with enlarged nuclei are tumour cells. Some cells form secondary

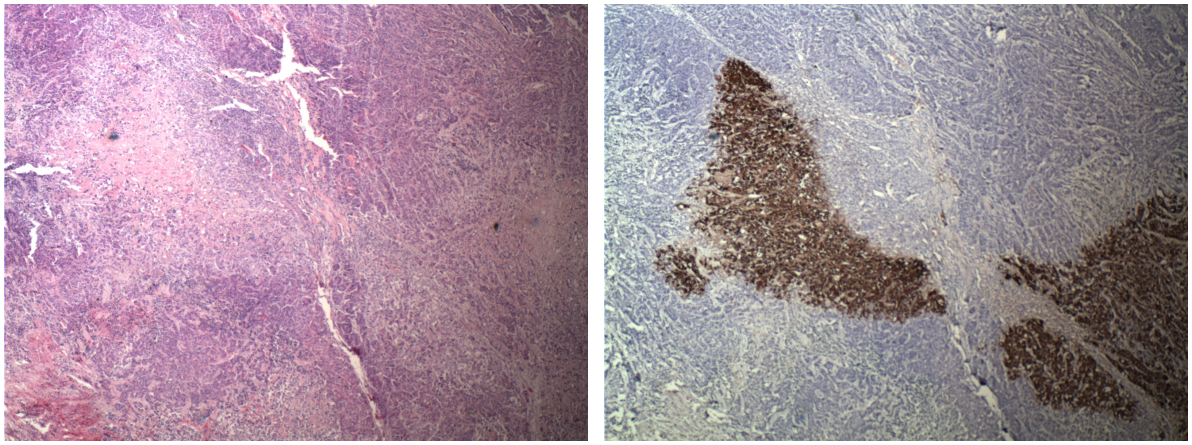

(a) H & E staining of a GLV-1h417-treated GI-101A tumour

(b) VACV staining of a GLV-1h417-treated GI-101A tumour

Figure 3.53: H & E and VACV histological staining of adjacent GI-101A tumour slices. These were isolated from nude mice 14 days post viral injection. Fig. 3.53a shows the H & E staining, with cytoplasm and other basic structures being stained pink/orange, and cell nuclei and other acidic structures being stained purple/blue. Fig. 3.53b shows a neighbouring tumour slice, stained for the presence of VACV. Both images were taken of the same area with a microscope at 4x magnification.

structures, that at first glance seem to resemble ductal structures, with interspersed fibrous regions.

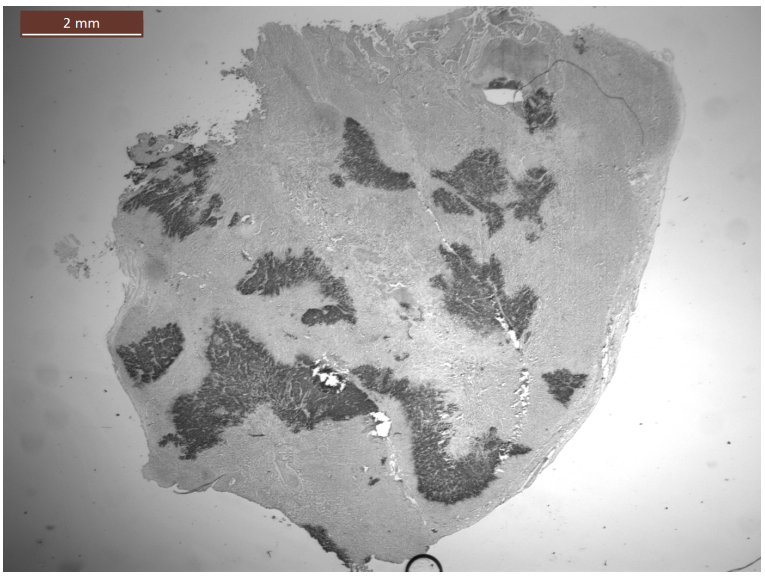

(a) VACV staining of a virus-treated GI-101A tumour, 14 dpi

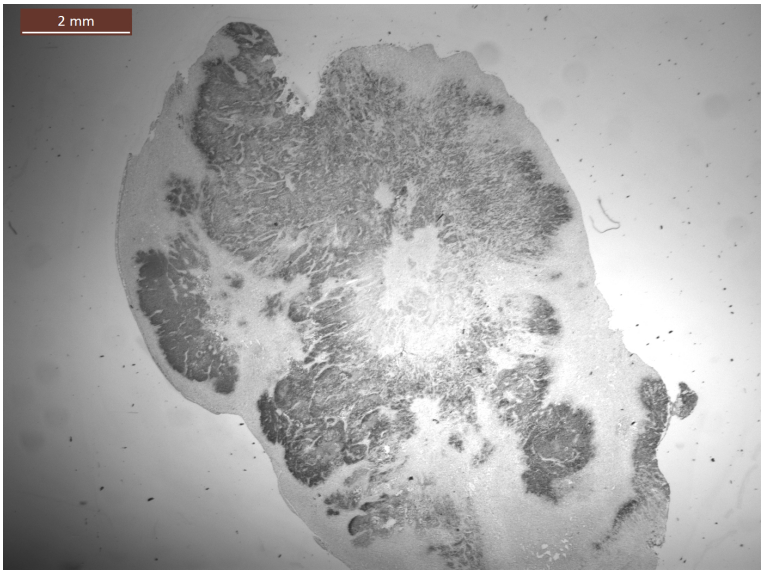

(b) VACV staining of a virus-treated GI-101A tumour, 64 dpi

Figure 3.54: Overview of two infected GI-101A tumours at (a) 14 and (b) 64 days post viral injection of GLV-1h417. The dark areas show areas positive for VACV staining, with the colour density representing the concentration of VACV in that particular location. Lighter areas surrounding show either necrotic tissue or tissue unaffected by virus. A scale bar in the top right hand corner indicates the magnification.

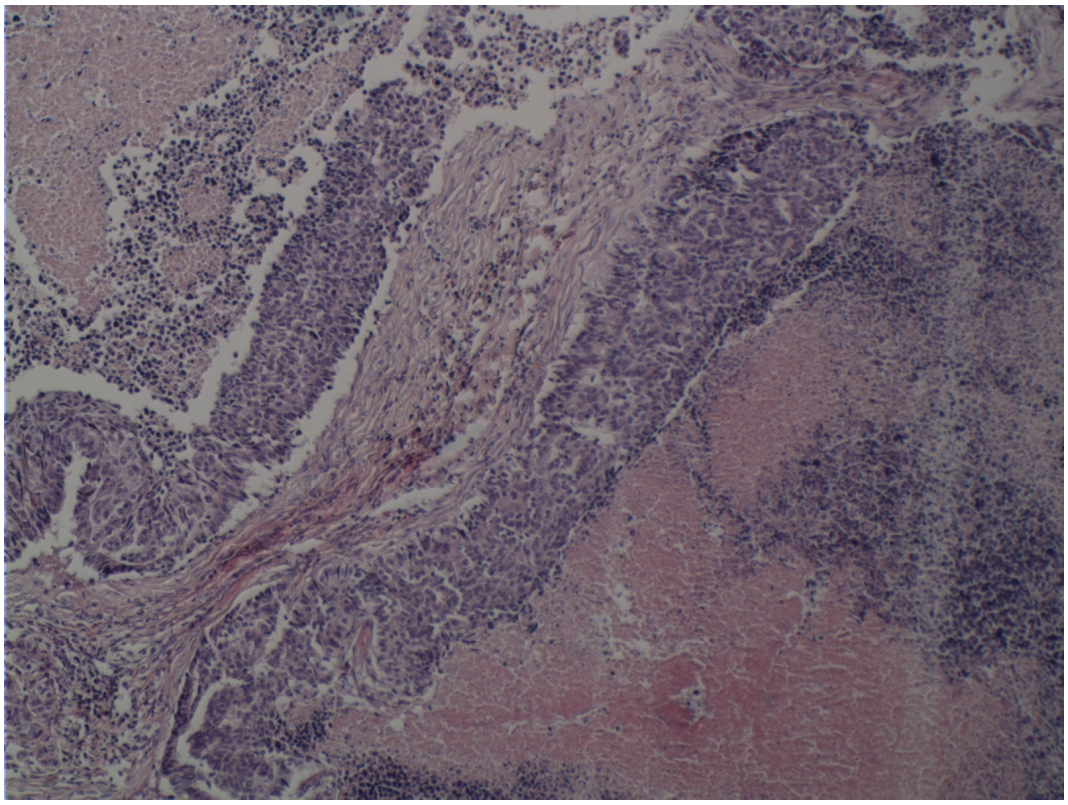

Figure 3.55: Micrograph of a H & E stained tumour slide. Staining shows various differentiated cells types within one tumour, ranging from fibrous to tumourous, with some larger areas resembling ductal structures. The tumour was grown in athymic nude mice from GI-101A cells injected into the right flank s.c. These mice were then treated with one dose of the CEA-expressing oncolytic GLV-1h417 virus. This image was taken from the middle to peripheral area of a tumour slice done 14 days after virus injection. The slide underwent histological H & E staining for cell nuclei and cytoplasm. Image was taken at 10x magnification

3.8 Relationships between CEA, β-glucuronidase and the viral titre *in vivo*

3.8.1 Correlation between CEA and the viral titre in tumour-bearing mice

Having determined the correlations between the biomarkers and viral-replication-dependent parameters, e.g. viral titre, in a idealised environment, such as in cell culture, it was attempted to make the same correlations in the athymic nude mouse model. Fig. 3.56 shows the results of the correlation between the CEA levels present in murine serum samples and the viral titre found in the tumour homogenates from the CEA-treated group (GLV-1h416 and 1h417). These data points were take from all samples that had titres present along with their representative CEA serum concentration. As the figure shows, the most mathematically accurate fit was a logarithmic one, as determined by regression analysis. The R^2 values of 0.25 and 0.724 for GLV-1h416 and 1h417 respectively shows that, in this case, GLV-1h417 displays a better correlation between CEA and the viral titre than GLV-1h416.

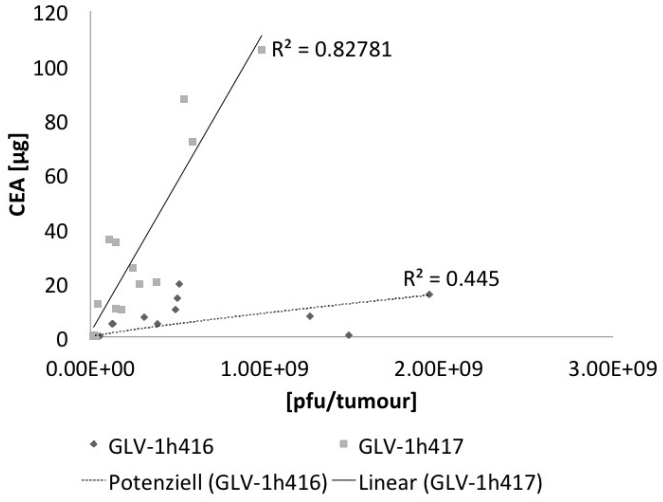

Figure 3.56: Scatter plots of CEA concentrations in murine serum samples and their respective tumour titres. The regression analysis performed yielded that an logarithmic fit was mathematically the most accurate fit for the data points present. R^2 shows a fit of 0.25 and 0.724 for GLV-1h416 and 1h417 respectively.

Carcinoembryonic antigen over time

It is imperative to also elucidate the time-dependent character of CEA and its secretion into the murine blood circulation. In order to monitor the levels of CEA over time, serum samples taken from the same mice over the course of the study were analysed in regards to the CEA concentration using the commercial ELISA. The results of this experiment can be seen in Fig. 3.57. The CEA levels of the GLV-1h416 and 1h417 increase in the beginning, reaching a maximum at 14 days post viral injection, declining from there on till the end of the study. The steepness of the decline depicted by the curve shows the promoter and time-dependent decrease of CEA in the serum. The dotted line in the graph represents the data shown from the GLV-1h417 group without tumours. CEA concentrations in this group decline rapidly to baseline levels, as expected since this group of mice had not been inoculated with tumour cells.

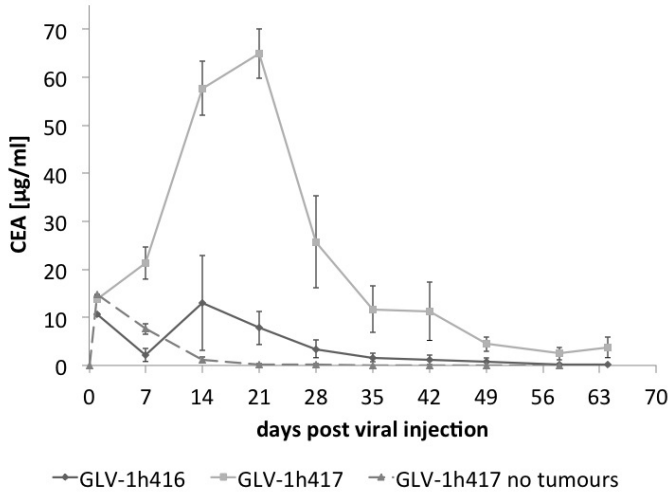

Figure 3.57: Time point-dependent measurements of CEA in the serum of tumour bearing and infected mice. Measurements began at 7 days post virus injection and continued until 63 days. The same mice were bled repeatedly for this period. The CEA levels peak at day 14 and start to decline either immediately (GLV-1h416) or with a 7 day delay at day 14. The CEA concentration in the GLV-1h417 group without tumour (dotted line) only decreases rapidly, being cleared to baseline level by day 28.

3.8.2 Correlation between CEA and β-glucuronidase in blood serum

This next data set shows the correlation between the concentration of CEA and β-glucuronidase in serum levels. CEA is under the synthetic $p^{sE/EL}$ promoter, and β-glucuronidase is under the native p^{11K} promoter. CEA was quantified using a commercial ELISA and β-glucuronidase was quantified using the activity assay mentioned in the methods section. The data presented in Fig. 3.58 shows line graphs with data comprising of CEA concentrations and the level of β-glucuronidase present within the same sample at the given time points. This was generated for each of the viruses. It shows that in the case of GLV-1h416, CEA and β-glucuronidase follow each other less closely as when compared to the GLV-1h417 virus, in which the overlap of the two markers correlated much better to each other. While CEA shows a premature decline in the 1h416 virus, the behaviours of β-glucuronidase and CEA in the 1h417 virus correlate well, showing no lag time in reaction and declining at the same time. Since the p^{11K} promoter is slightly weaker than the p^{sEL} promoter, it is not surprising to see that β-glucuronidase and CEA correlated well in GLV-1h417 treated mice.

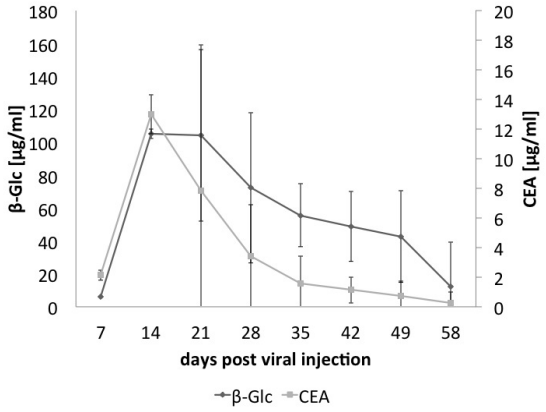

(a) Comparison of trends of CEA and β-glucuronidase for GLV-1h416

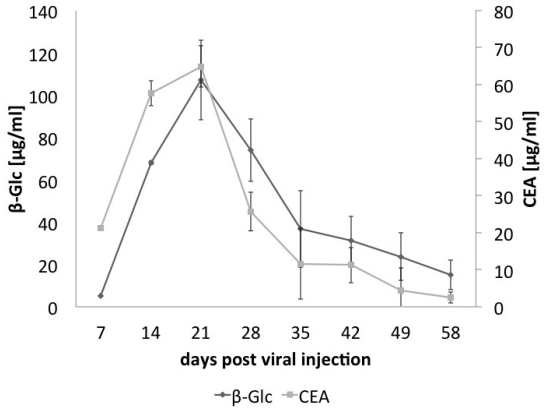

(b) Comparison of trends of CEA and β-glucuronidase for GLV-1h417

Figure 3.58: Comparison of CEA and β-glucuronidase between GLV-1h416 and 1h417 treatment groups. Line graphs show the correlation present between CEA and β-glucuronidase both viruses, with n=4 for each group). CEA is under the $p^{sE/EL}$ promoter respectively, whilst β-glucuronidase is controlled by the native p^{11K} promoter.

3.8.3 CEA in non-tumour bearing nude mice

This graph shows the data from the group of mice which had not been treated to exhibit tumours, but had been dosed with GLV-1h417. Blood serum for these mice had also been collected and the CEA level measured for four individuals over the whole study. The result of this is shown in Fig. 3.59. Initially, solely with the injected dose of viral agent, the CEA level in blood is high, declining rapidly within two weeks, and reaching baseline level at day 35 post viral injection. As these mice had not been inoculated with tumour

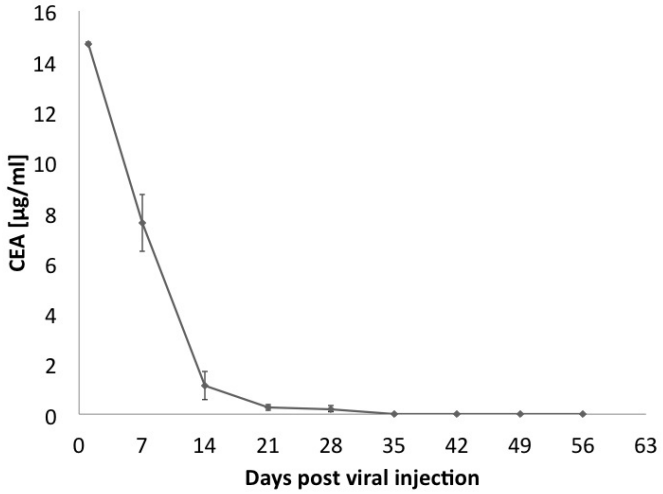

Figure 3.59: Development of CEA in the serum of tumourless, GLV-1h417 treated nude mice. CEA was measured in the serum using an ELISA and plotted over time.

cells, they did not display any viral replication, since our virus replicated exclusively in tumour tissue. Thus, the levels shown here must be the result of the sporadic and abortive infection of blood cells, e.g. PBMCs, or other cell types.

3.9 Lactate dehydrogenase as an indicator of on-going cell lysis

Lactate dehydrogenase (LDH) is an enzyme known to facilitate the conversion of pyruvate to lactate. Clinically, this enzyme is measured in blood work panels as a surrogate for tissue disruption, as it is released stream through that mechanism. LDH is also indicative of many diseases, e.g. cancer, meningitis, pancreatitis and HIV.[89] [90] This experiment was to test for the relationship between LDH and the lysis of tumour cells, which is measured via tumour regression. It was decided that serum from the GLV-1h68 group was to be used for analysis. LDH was measured using an ELISA-specific for human LDH B, as mouse LDH would be released during haemolysis and other metabolistic functions. Fig. 3.60 shows the concentration of LDH in the serum at the time of analysis, as well as the corresponding tumour volume. The trend indicated by graphs is not as expected.

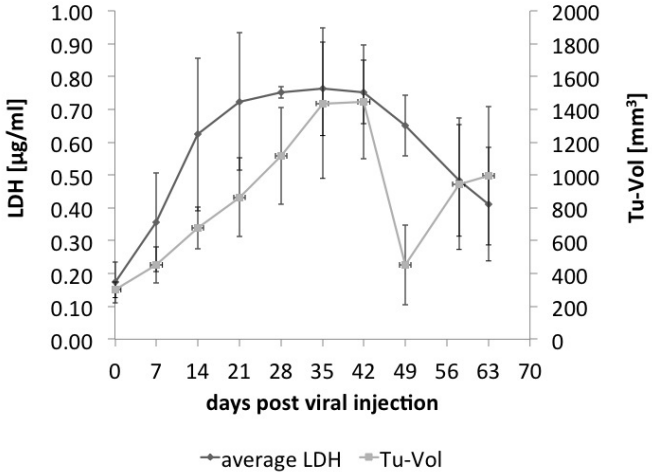

Figure 3.60: Fluctuations of LDH levels in serum of GLV-1h68-treated mice. The tumour volume was also plotted on this graph, as a direct representation of tumour cell lysis. LDH is released into the blood stream upon tissue disruption. The same three mice were analysed over the 63 day period after receiving a viral injection of $5x10^6$ pfu.

With the increase in tumour cell lysis, and the concurrent decrease in tumour volume, the LDH level was expected to increase. That is not the case here, as human LDH levels seem to increase with tumour volume, instead of against. The resurgence of tumour toward the end of the study does not translate to a change in LDH levels.

4 Discussion

This discussion aims to debate the reliability of all the biomarker detection methods mentioned before by comparing them to established standards currently being applied. For that reason, if applicable, the biomarker data will be compared to viral titres and/or β-glucuronidase data.

4.1 Indigenous Vaccinia virus proteins as replication-dependent markers in VACV colonised mice

The simplest place to start looking for viral replication-dependent proteins was to start with the virus itself. Viral proteins would make a logical and simple biomarker, as they would be virus-specific and differentiated from host proteins, lending themselves to be detectable with little or no cross-reactions. They are distinctly viral replication-dependent and would only be present when the virus had replicated enough to release these proteins from the cell into the blood stream. No replication would mean a lack of detectable biomarker concentration, with the background possibly being negligible as this would have been a foreign protein.

The two viral proteins chosen originated from the A27L and B5R genes. These targets are the ones most frequently used in literature for the analysis and detection of vaccinia virus, i.e. the B5R protein is the target of most neutralising antibodies used by medical physicians to determine the level of vaccination present in a patient. The A27L protein is the antigen that is used, for the most part, in fluorescent microscopy and for the histological detection of vaccinia virus. Western blot analysis of both proteins in spiked plasma, using antibodies directed against custom-made antigens from both proteins, showed that both proteins were only detectable in samples containing high titres of heat-inactivated GLV-1h68 virus, e.g. upwards of $2x10^6$ pfu. Other samples containing mouse serum from GLV-1h68-infected mice, spiked human plasma samples and cell lysates from *ex vivo* infected CV-1 cells showed no indication of a A27L or B5R detection. The double-bands shown in all Western blots suggest the decay of protein or the presence of possible protein modifications resulting in that difference of mass. Fig. 3.2 shows that diluting heat-inactivated virus down from $1x10^7$pfu/ml, a faint signal can still be detected

at 1.25x10^{6}pfu/ml, a more reliable signal can be found at 2.5x10^{6}pfu/ml. However, the detectability of a protein in a Western blot does not mean that this protein lends itself to being a good target for an ELISA. This was tested with both proteins. In the case of B5R, it was not possible to establish a reliable standard using GLV-1h68 as a basis for comparison. As shown in Fig. 3.3, it was possible to correlate optical density readings (OD) with the peptide or virus concentration in analyte only solutions. However, the correlation of viral pfu and B5R concentration in those samples did not result in any positive linear correlation, showing that this method was either not sensitive enough to detect B5R, or that B5R was not readily "accessible" to the detection antibody. The difference in concentrations of A27L and B5R in the same viral samples reflects the biological difference between the two proteins. A27L is predominantly present in IMV particles, which make up more than 99% of virus particles in the purified product, and is also predominantly located on the outer membrane of the virus. B5R, on the other hand, is found only in EEV particles, which are scarce in the purified product, as only the infected cells were harvested, and not the supernatant, where EEV particles are mostly found. Also, the particular strain of vaccinia virus used in this lab is not known to produce large amounts of EEV. Thus, the data presented here correlates well with known information on GLV-1h68. Taking all this into consideration, it seems that A27L would become the most logical choice for monitoring viral replication and it was decided to establish an ELISA based on the capture and detection of this protein. Yet when the experiments moved into plasma sample studies, it was shown that components of the blood inhibited readings in an unpredictable manner, rendering this mode of observation obsolete. Data for this assessment is shown in Fig. 3.5, where the standard shows no mathematical correlation whatsoever between the OD readings and the A27L concentration present. The possibility exists that the data presented here may be a direct result of the low concentration present in the samples. However, increasing protein concentrations in these samples would not be feasible, as the low threshold for detection would lower even further when this detection system is brought to mouse xenograft models, or even human patients. Development of a more sensitive sandwich ELISA was also not feasible because a sandwich ELISA would require a minimum of two different, non-overlapping epitopes to be available, and the size of the protein was not conducive to this requirement. As such, this method was not deemed viable for our requirements. However, this does not exclude other viral proteins that may become targets, should a more systematic analysis be undertaken.

4.2 GFP as a quantifiable biomarker in a human xenograft mouse model

4.2.1 GFP as a visual biomarker is not representative of viral titre in the tumour

The usage of GFP as a visual biomarker has its merits. As mentioned before in the introduction (chapter 1.3.1), extensive use of this protein as a visual indicator of replication has made it a common place appearance in developmental biology, cloning and molecular biology.

Here, we attempt to correlate the visual GFP readings taken from tumours in human xenograft models performed in athymic nude mice. The GFP inserted into the virus genome is only expressed upon viral replication within tumour tissue, for which GLV-1h68 and similarly attenuated viruses have a particular tropism. These GFP readings were gained using a multitude of methods. The main method used was applying GFP as an imaging modality and correlating this with tumour regression and viral titre determination. The pictures in image (a) clearly show an increase in GFP signal from day 7 to day 21. The tumour volume increases from day 7 to day 21, reaching its greatest measured volume at day 28 and steadily decreases from then on till day 49. This correlated visually with available GFP images, showing an increase in trans-dermal GFP signal at the tumour site, peaking at day 21 and 28, with the signal distribution on day 21 being more focal than the distribution visual on day 28. After that, the GFP signal decreases along with the tumour volume regression. This is a known occurrence and can be explained by the lytic activity of the GLV-1h68 virus in tumour cells, which has been previously published.[29] As the virus replicates in the tumour, it lyses the cells it uses for replication and concomitantly produces GFP. As GFP is release during cell lysis, it is spread within the cell, possibly explaining the diffusion of a previously focal GFP signal within the growth. The tumour itself shrinks during the duration of the treatment, as cells are lysed faster than the new formation of neoplastic cells can occur. Less cells give the virus less replication opportunities, as such, any GFP signal decreases along with the lack of replication and protein decay within the body.

In order to make a more quantitative statement on the relationship between a visible GFP signal and the viral titre present in the tumour, GFP images of all titred tumours were

analysed and assigned a number between zero (0) to five (5), with half (0.5) increments used for a more accurate estimation of the GFP signal. Both attributes were plotted against each other on a graph, shown in fig. 3.7.

A linear regression trend line was applied in this case resulted in$R^2 = 0.072$. As this value here is close to zero, it indicated that this graph would only be accurate in 7.2% of all cases, proving that the visual GFP signal is not an adequate measurement of a viral titre present. Having said that, the downside/inapplicability of this mode of measurement stems from multiple issues. Firstly, the assignment of a GFP score is a strictly subjective attribute, and as thus is neither objective nor reproducible between experimenters. Secondly, an image captured as shown above only a two-dimensional representation of a three-dimensional structure. However, three-dimensional imaging of a tumour could help alleviate this issue. If replication occurs near the skin surface, then the GFP signal would be more readily visible than replication that is far within the tumour growth, resulting in the first signal being perceived as stronger than the second. As such, the deeper the GFP signal originates from, the less likely it is to be seen, as tissue and blood (haemoglobin) readily absorb the GFP emission at 507 nm. Diffusion and distribution of the protein within the tumour is also a factor to be considered. It is easier to discern a discrete, focal site of replication which may result from a heterogeneous viral distribution, compared to a more diffuse replication indicative of a more homogeneous spreading of the virus. For factors influencing the distribution of a treatment agent within the tumour, please refer to chapter 1.1. Even using our imager, the detection threshold would not have allowed for a quantification at early time points, but would have allowed for a more accurate quantification.
Taking all the above mentioned points into consideration, the usage of a visual GFP signal as a basis for correlation with the viral titre, from which the signal originates is not an accurate quantification method. In this context, GFP can be used solely as a qualitative guideline, from which no statistically viable or exact quantitation can be achieved.

4.2.2 Blood plasma/serum impedes GFP quantification via fluorescence

There are other, more sensitive methods of GFP quantification available. One of those, which was chosen for closer analysis, was using a commercial kit to assay GFP via fluorescence in serum collected from tumour-bearing mice infected with GFP-producing viruses.

As a proof of concept, the kit was first tested for reliability. This analysis resulted in an R^2 of 0.998, confirming the validity of the assay (Fig. 3.10). Human blood plasma with spiked the control peptide provided in the kit yielded an R^2 of 0.751, which is a substantial drop in predictability when compared to the R^2 for an unspiked kit standard run on the same day (Fig 3.11). This lead to the hypothesis that a component present in the blood influenced the reading, in spite of compensation with a suitable blank, that was later subtracted from all readings. It is possible that residual haemoglobin, or any other coloured component in the plasma or serum, could interfere, as it is known that any colour present within the samples, e.g. phenol red in cell culture, influences the sample measurement in an optical assay method.

Further attempts to assay GFP in plasma/serum samples using the fluorescence method were performed, but a high baseline and background reading prevented the samples form being reliably quantified. Another hindrance was that the sample amount required by the kit was not feasible for analysis of GFP in serum samples derived from animal models, as it is not permitted to remove more than 2% of the mouses body weight during repeated interval bleeding. The samples would not lend themselves to be diluted, detection waned markedly with dilution, in spite of the standard for this kit ranging from 1000 pg/ml to 15.6 pg/ml. Even though these levels were stated in the kit, empirically, a concentration of 60 pg/ml was the lowest concentration reliably detectable within the given samples. This level was determined using the standards in the kit, as cell culture samples, regardless of dilution or handling, did not yield a reproducible quantification.

Figure 3.12 shows a graph (a) with the calculated GFP levels, as determined from the fluorescent readings of infected cell culture samples. With exception of the data representing supernatant without phenol red, none of the other samples show a time-dependent difference in GFP levels, which are usually associated with tumour cell-dependent viral replication. Graph (b) shows the viral titre for the respective cell culture samples without phenol red. This graph is the same for samples with phenol red, as the lack of phenol red in no way impedes cell growth. When comparing both graphs with each other, the time-dependent trend of change in viral titre is not reflected in a concomitant change in concentration of GFP, thus showing an incompatibility in the comparison of both methods with each other.

4.2.3 Detection of GFP from serum using antibody-mediated assays results in less serum interference

ELISA, enzyme-linked immunosorbant assays, are considered to have very little cross-reaction or contamination issues, based on the property that antibodies are uniquely specific to their antigens, with the likelihood of cross-reactions depending on antigen sequence specificity. These assays are also known for being able to detect minute concentrations of target protein, mostly within the nano- to picogram range, again depending on the specificity of the antibody used. As it is imperative to have a sensitive assay when quantifying biomakers in blood, a commercially available ELISA targeted against GFP was acquired and tested.

The time-dependent, concomitant increase in GFP concentration is directly reflected by the increase in viral replication. As more virus produces more GFP, upon lysis of the cells, this GFP is released into the supernatant. In an *in vivo* system, this would theoretically translate in GFP (or any other viral replication-dependent marker) being released into the cardiovascular system. Under these confined circumstances, the GFP level is expected to plateau at a maximum, just after the lysis of all remaining cells in the dish has been completed. In an *in vivo* system, this would only occur when the tumour has been completely infected. The GFP signal is then expected to decrease, along with tumour volume regression and tumour titre reduction, whereas in cell culture, the signal would simply decay according to the protein's half-life or stability.

The next step was to test this method with plasma samples spiked with the standard peptide provided with the kit, in order to test its validity in that situation and to see if any cross-reactions, primarily with blood serum, would occur. It is generally known, that any antibody used could cross-react with samples, if both are from similar species, or if the antigen has a strong homology to another protein.

However, a factor that must be taken into consideration is that of the influence of blood plasma on the ELISA reading of blood samples. In Fig. 3.17, the difference between samples with blood plasma and samples without blood plasma can be seen, with the samples containing blood plasma resulting in measurements that were two to four fold higher than the reading of the same sample amount without blood plasma. This is not an expected outcome, as the amount of GFP in the cell culture samples is the same as in the plasma samples. The expected graph would have shown the GFP levels to be

comparable. Also, the time-dependent concentration change of GFP is not visible in this graph, indicating that some component present in the blood plasma is interfering with GFP concentration determination. The trend being discussed here is the same when taking supernatant samples from these cells into consideration, showing the same trend (data not shown). This might not seem to influence the outcome of readings markedly in cell culture, but, when taking into consideration the applicability of this method in *in vivo* experiments, or even as a way of monitoring human patients undergoing oncolytic virotherapy, it could mean that this method would not be befitting a method for clinical monitoring.

4.3 β-Galactosidase as a correlation basis for viral replication

Another biomarker in the pool of assay-able, artificially inserted biomarkers in the vaccinia virus genome is β-galactosidase, the protein resulting from the expression of the *lacZ* gene. This biomarker has been used prior as a basis for correlation between viruses as had been inserted as a reporter gene. As this biomarker is a cytoplasmic enzyme, and only released into the surrounding blood and tissue upon cell lysis, it was considered for analysis because the quantification of such an enzyme would enable a sensitive and accurate measurement of a sample for replication-dependent and released biomarkers. Activity mediated quantification is highly specific and unique to the enzyme being assayed, due to the high affinity most enzymes have for their substrate.

4.3.1 Using chemiluminescence to quantify β-galactosidase

Since β-galactosidase is usually used as a reporter gene, it was thought that using a chemiluminescence-dependent kit to assay this enzyme would lead to more exact quantification possibility, as the visual correlation method between biomarker and viral titre had already been shown to be inaccurate in the case of GFP. A commercially available kit was acquired and used to test cell culture and blood plasma samples, later progressing to *in vivo* samples from a study conducted in an athymic nude mouse model. Looking at Fig. 3.18, it can be seen that the high coefficient of determination lends itself to interpreting any prediction made based on this data to be 99.97% accurate, as opposed to

previously mentioned, lower values for R^2, showing the reliability of this kit. The cell culture samples used in these experiments were the same that were used in the GFP and any other quantification experiment. This was done in order to keep with the interest of being able to correlate with biomarkers, same and different but all on the same virus, "across the board", so to speak. In doing so, a basis for comparison was created. More information on the cell culture samples used is given here in at the beginning of chapter 3. When analysing the quantification of β-galactosidase in these cell culture samples, it was not surprising to see that the levels of said marker mimicked the chronological development of the corresponding viral titres, as shown in Fig. 3.19. The dip seen at the end of this time course most likely indicates a change in β-galactosidase concentration due to decay of the protein over time and from the lack of production needed to sustain that concentration level. The viral titres corresponding to this sample can be found in Fig. 3.12b. The marker concentration in cells is shown to mimic the increase in viral titre well, with the correlation in supernatant lagging behind by 12 hours and never reaching the same levels as that of the cells within the same time frame. This correlates well with the hypothesis that β-galactosidase is released into the supernatant upon lysis, whereby some loss of protein is to be expected. This loss of enzyme would be reflected in a biological system as well, but likely on a larger, more obvious scale. The recovery of 100% of a secreted/released marker is unlikely, due to degradation, sequestration into other locations and protein misfolding rendering the enzyme inactive.

The next step was to test if human plasma caused an interference in the sample readings. So, as before, the peptides used for quantification were spike with human blood plasma and assayed. The data from this assay, shown in Fig. 3.20, shows that plasma somehow obscures the β-galactosidase quantification, as the levels measured in the samples not containing plasma are certainly higher than those of the same cell lysate sample set. Since this kit is based on chemiluminescence, it is reasonable to assume that any endogenous colour in the plasma could alter the readings, making quantification of β-galactosidase from patient serum an uncorrelatable process, since biological variability dictates that not all serums are the same. Red blood cell lysis that may occur during blood sampling can cause serum to turn redder than the usual yellow colour, ultimately influencing the luminescent reading.

4.3.2 β-galactosidase antibody-mediated detection reduces background

Having shown that blood plasma itself could interfere significantly in a chemiluminescence based method, it was decided to use an ELISA to quantify β-galactosidase, as it seemed to be the modality combining both the ability to detect minute amounts of target protein, and to be impervious to physiological differences resulting in serum sample variance. As it turned out, the ELISA method was not necessarily the better method, due to the fact that even this antibody-specific method was susceptible to interference caused by the presence of blood serum/plasma. In the end, lacZ was removed from the viral genome in order to make way for the insertion of CEA into its loci. The decision was made, due to the fact that the genome already carried an enzymatic reporter, β-glucuronidase, which is also cytoplasmic, and more importantly, lent itself to an elegant and sensitive quantification method based on its reaction with a fluorigenic compound. Because of this, β-galactosidase can only be measured in the GLV-1h68 group as this group still contains lacZ in the *J2R* locus.

4.4 β-Glucuronidase is a well-correlated marker

β-Glucuronidase and its use as a biomarker, and possible pro-drug catalyst, had been previously discussed by Hess *et al.*[84], but had not been previously correlated with any titres relating to the viral concentration present in the tumour. Thus, establishing a correlation, and with that a quantitative basis for β-glucuronidase, was important. This biomarker, as mentioned before, is considered in our terms to be a cytoplasmic protein, that would be released into the blood stream upon cell lysis. Additionally, it is an enzyme, making the quantification of this individual protein at low concentrations accurate when calculating from its activity over time.

β-Glucuronidase had been chosen for the simplicity of its assay method, which requires an incubation of the enzyme with its substrate for 1 hour at 37°C and a subsequent measurement using a photometer, making it the least time-consuming assay so far. The number of handling steps required is greatly reduced compared to other standard procedures and meant that less inaccuracies could be attributed to the experimenter. Thus, after the preliminary cell culture experiments had proven to be promising, it was decided that β-

glucuronidase would become the correlation standard between all the newly constructed viruses, resulting in the lacZ gene being removed in order to facilitate the addition of CEA to the viral genomes. When regarded in conjunction with the titration data shown in Fig. 3.45a, it shows a very good correlation between the concentration of β-glucuronidase and the amount of virus present in the sample. The linear regression analysis shown for the viruses GLV-1h416 and GLV-1h417 resulted in high R^2 values, indicating a strong correlation and good predictability resulting from this data, which is a prerequisite for biomarker usability.

4.4.1 Blood serum does not effect the β-glucuronidase assay

The next step in biomarker analysis was to test the assay in serum samples. Until now, most biomarkers had not shown a successful recovery from blood serum, which is indicative of cross-reactions or similar disturbances. The method used for quantifying β-glucuronidase based on its enzyme activity was shown to be a sensitive detection method, as the standard range was shown to start at 1 pg/ml. This is much lower than some of the kits used in this thesis. Blood serum from infected athymic nude mice inoculated with GI-101A tumour cells was collected and measured using the β-glucuronidase assay. The data shown in Fig. 3.27 represents the time-dependent change in β-glucuronidase concentration in infected mice for the duration of the animal experiment. As shown for all groups with tumours, the concentration in β-glucuronidase in blood at first appears to be very low, only barely detectable at day 7. Group GLV-1h417 no tumour shows no significant increase in β-glucuronidase concentration for the duration of the animal study. This was to be expected as this group gave the virus no place to replicate, effectively preventing an expression of β-glucuronidase past baseline level. As for the other groups, the concentration of β-glucuronidase in the serum increases rapidly, reaching its maximum of about 100 μg per ml for GLV-1h417. Group GLV-1h416 shows a lag of seven days, reaching the same plateau as GLV-1h417, albeit at day 21. Both groups then start to regress in concentration until the end of the study. The tumour volume data (Fig. 3.49) shows a definite decrease in tumour volume over time. This indicates that once the virus has spread within the tumour, it seems to attain a certain maximum concentration which it keeps until the tumour shrinks. The size constraint of tumour shrinkage translates into less tumour tissue which is available to the virus for replication. Looking at the tumour regression and the concentration of β-glucuronidase in the serum, one can say that the development seen in the tumour size decrease is similar to the one seen in the decline

of β-glucuronidase in the serum over time, thus resulting in the conclusion that in this case, the concentration of β-glucuronidase in the blood mimics that of the actual tumour regression well.

4.5 CPG2 - the other enzyme

The other enzyme in our testing arsenal of biomarker proteins was CPG2. This enzyme, as mentioned before, had previously been defined in quantification assay by Sherwood *et al.* and McCollough *et al.*. Using the enzyme activity-dependent metabolism of the substrate methotrexate it is possible to determine the enzyme concentration in an unknown sample. But in order to do that, a standard had to be had against which the activity of the enzyme in that particular assay could be quantified against. As CPG2 is not a commercially available protein, steps were taken to overexpress it in *E. coli* and it was planned to used that as the standard.

4.5.1 CPG2 activity - eating away at the substrate

Samples from nude mice infected with GLV-1h181, the virus containing DNA encoding for CPG2, were taken. The attempt to quantify CPG2 in these sample showed precipitation of an unknown substance. As this substance precipitated during the assay reading over two hours, the change in optical density could not be measured as the reading was obscured. It is unknown at which part of the automated reading process that this precipitate occurs. At first it was thought that the substrate, MTX had somehow had an adverse reaction of the blood plasma, but MTX is usually administered as a chemotherapeutic via i.v. injection. As such, if MTX were to have an adverse reaction in relation to blood or blood clotting, it would have been reported in literature, of which no evidence was found. It was then hypothesised, that a serum component had reacting to the assay buffer, however, the volume of precipitate did not correlated with the volume of serum assayed, 20 μl. It was not possible to add EDTA or heparin to the samples, as this chelator would have reacted with the zinc ions in the buffer. The importance of divalent zinc ions as an enzyme co-factor was shown in Goda's article.[87] The conclusion was reached that the adverse reaction must stem from either a reaction of MTX to a blood serum component other than CPG2, or that the serum was reacting to being heated to 37 °C in order to be read under assay conditions. Also, one of the reasons for choosing CPG2 was that the levels of

proteins expressed in the tumour was shown to be extremely high, making it a very likely candidate to exhibit a high concentration in serum. Since β-glucuronidase also showed the same large amounts found in the tumours and is also a cytoplasmic protein released upon lysis, the decision was made to focus on β-glucuronidase instead and no further experiments on CPG2 were undertaken. However, further research into and fine-tuning of the quantification of CPG2 could make the method viable in the future.

4.6 CEA-dependent monitoring of viral replication *ex vivo*

CEA, carcinoembryonic antigen, is a glycoprotein with as yet undefined function. It is known to be expressed during the early stages of human fetal development, but shows markedly decreased expression at birth, reducing even further later in life.CEA has long been used as a prognostic indicator for colorectal cancer and is generally considered to be indicative for many other cancer types, i.e. adenocarinomas of the pancreas and lung.[91] Since it is already used to indicate tumour status after surgical resection or to analyse body fluids for the presence of tumour cells, validated kits are already on the market to facilitate the quantification of this marker. It was decided to use this previously established cancer marker and integrate it into one of the viruses, resulting in VACV constructs that express CEA under the control of different viral promoter strengths. Literature states that a normal healthy human has a CEA level of $\leq$ 2.5 ng/ml, where as smokers have a level of $\leq$ 5 ng/ml. The idea was to insert CEA into the virus, knowing that it is already detectable in the serum, and have the virus express it in a replication-dependent manner, making it a model of an exemplary marker. This would theoretically lead to a direct correlation between viral titre and CEA concentration, as the production of one is dependent on the other. CEA underwent modifications to increase secretion into the blood, thus augmenting the window for measurement. Taking baseline readings and subtracting these readings from readings on serum after treatment would remove any CEA concentration present prior to the treatment. Only the change in CEA level would be reflected, indicating if there was indeed any correlation between the two variables. This correlation would then be compared to β-glucuronidase measurements, providing some comparability between different viruses across the board.

Before going into *in vivo* studies involving nude mice, preliminary experiments had to be performed in cell culture using human tumour cell lines and the virus amplification cell line CV-1. Infections experiments of diverse tumour cell lines *ex vivo* were performed to give insight into the intrinsic expression of CEA. It was important to chose a tumour cell line that did not express in excessive amounts as these cells line would have obscured differences in CEA measurements at low concentrations. Having said that, that does not imply that this virus would not be applicable for tumours over-expressing CEA. On the contrary, in the end, the CEA virus would be applicable to all tumour types and the change in CEA levels visible, as long as baseline measurements before treatment had been performed, taking intrinsic and prior CEA expression into account.

Since the virus containing the p^{sL} promoter showed similarities to the early/late promoter samples *in vitro* and the up-scaling of the full-length CEA virus GLV-1h415 did not yield the minimum amount required in order to initiate an animal study, the decision was made to go forward with two viruses, GLV-1h416 (p^{sE} promoter) and GLV-1h417 (p^{sEL} promoter).

4.6.1 In the early stages of infection - CEA and the virus

Analysis of infected cell culture samples taken at early time points revealed that while the levels of β-glucuronidase produced by GLV-1h416 and GLV-1h417 were comparable, as was the viral titre, the concentration of CEA produced was obviously different. This effect is due to the difference in promoter strength, which governs the strength of CEA expression within each insert as there are no other genomic or otherwise known to influence viral expression at this point. GLV-1h417 expression of CEA was shown to be 10 fold higher than CEA levels in GLV-1h416-infected samples. It was decided to analyse the CEA viruses separately, as the difference in promoter strength of the CEA insert could effect the expression and thus the kinetics of the biomarker in serum.

4.6.2 CEA detectable in virus treatments groups in a tumour xenograft model

As outlined in Fig. 3.46, an animal study was conceived in order to examine, if the hypothesis relating to the detectability of secreted human CEA in blood circulation was

valid and if the viruses constructed had differing effects compared to GLV-1h68. Since CEA had long been established as a prognostic tool in the clinic and known to be stable in blood, a positive correlation between the level of CEA in serum and the viral titre present in the study subject was anticipated. All mice of the study had been inoculated with the tumour cell line GI-101A, which had been derived from a patient with solid breast tumour. The study comprised of five groups. First was the control group, a group of mice that had tumours, but were not treated with virus. This group is generally used to compare the overall efficacy of the treatment. The second group was a group of mice which had a single treatment of GLV-1h68, representing the "standard of care" in virotherapy treatment. The third and fourth group both involved the CEA viruses, one group with the GLV-1h416 and the other with the GLV-1h417 virus. The logic behind having two CEA viruses with similar inserts was to see if and how the promoter strength, which controlled the expression of CEA, would effect the detection of that same protein in blood. It is known, that while the early/late promoter has a longer replication duration, the early promoter might exhibit a higher viral replication *in vivo*, since the burden of expression a payload would have been restricted to only the early phase of viral replication, and not the complete replication cycle. The fifth group in this study was a group of subjects that had not received any tumour cells. They had only been infected with one dose of GLV-1h417. This group was expected to show the behaviour of GLV-1h417 in a tumour-free environment and to see if the virus would infect other tissue types, thus changing the CEA concentration present in the subject before and after treatment.

4.6.3 Toxicity, survival & therapeutic effect of GLV-1h68, GLV-1h416 & GLV-1h417

The analysis of a subject's body weight during treatment provides indications on whether the administered treatment has an adverse effect on its overall well-being. All the members of the GLV-1h68 group did not show any substantial deviations in their body weight, other than slight fluctuations that were to be expected in a living organism. The individuals in the GLV-1h416 group also showed no signs of toxicity based on body weight changes. However, the GLV-1h417 group showed two individuals with loss in body weight that had to be removed from the study earlier than initially planned (Fig. 3.48). Viral titration analysis of both these mice post-mortem showed no higher viral load to be present in the body than when compared with subjects removed at similar time points. Since this untimely demise only effected two mice in this group,and since CEA is not known to be

toxic, the cause of death was deemed not related to viral load or toxicity. The tumour regression shown does not differ much from that of the GLV-1h68 group, the virus to which all comparisons are made. Since CEA is not know to have any therapeutic effect and the viral backbone is identical to GLV-1h68, with exception of the *J2R* locus, the therapeutic activity seen must come from the viral infection and lysis of the tumour cells present.

4.6.4 Released CEA is measurable in serum samples of treated nude mice

Using a commercial ELISA kit, the serum samples collected from athymic nude mice treated with either GLV-1h416 or GLV-1h417 were assayed. A dilution factor of 1:100-1:500 was shown to be helpful, especially when measuring samples at later time points, as the CEA present in the sample could be outside the standard range of the kit if not diluted. This is a positive attribute, as it adds to the sensitivity of the kit, while also reducing the volume of sample required. As shown in Fig. 3.57, the level of CEA secreted by the tumour into the circulatory system differs according to the promoter under which the gene was inserted. GLV-1h416 has sCEA under the p^{sE} promoter, whereas GLV-1h417 has the insert under control of the p^{sEL} promoter. The difference in promoter is not only temporal, e.g. when within the replication cycle the promoter is active (early vs. early and late transcription), but also in the promoter strength, whereby the synthetic early/late promoter is about 50 times stronger that the synthetic early promoter alone. Ultimately, the promoter strength is then reflected in the concentration of CEA measurable in samples, for both cell culture (Fig. 3.45b), as well as in serum samples over a period of 56 days post viral injection (Fig. 3.57). The concentration of CEA in serum generally was found to be in the microgram range and the baseline readings were found mostly to be in the nanogram range.

The fact that the *in vivo* data shows that the baseline readings are so low in the study subjects goes against the expected outcome when taking the the intrinsic CEA concentration of different tumour cell lines *ex vivo* into account. Having said that, it is important to consider that the readings shown in Fig. 3.42 are from $2x10^5$ cells in cell culture, which were later lysed prior to being assayed. Not only would this reflect a very large amount of CEA in the culture dish itself, but also, when looking at the biological system, i.e. the human body or the mouse model, this amount would be diluted by the blood found in the

circulatory system. This also includes the assumption that 100% of all produced protein ends up in the blood stream, which is not the case (Fig. 3.51 & 3.29). In serum samples, the baseline readings for serum taken from mice prior to virus injection were shown to be on average around 0.11 μg/ml (Fig. 3.52). In summary, the high baseline readings seen in cell culture did not translate into the athymic nude mice model, showing that the intrinsic expression of CEA by the cell line was not interfering with the detection of CEA expressed by the virus in any way.

4.6.5 CEA levels decline after injection into nude mice without tumours

In the animal study mentioned previously, a group of mice was present, which had received a dose of virus, but not an injection of tumour cells. This group was used to determine if an injection of the virus, in this case GLV-1h417, might caused any unexpected replication during the course of the study. As shown in Fig. 3.59, the amount of CEA declines rapidly over a period of 14 days, after which the concentration declines until baseline levels are reached, at approximately 35 days post viral injection. The CEA concentration present one hour post viral injection should be CEA that is introduced into the animal body via the viral injection. However, a CEA assay of pure, heat-inactivated GLV-1h417 virus showed levels that were much lower that that of the 1 hour time point depicted in the graph and could not account for the level of CEA found in the serum. Abortive replication of the virus in the blood cells, or certain other cell types, could explain this phenomena, as VACV is known to infect certain sub-populations of blood cells. This means that the virus would enter the blood stream and infect cells, but stop before the replication cycle is completed. However, this time frame would be sufficient to express genes under control of early promoters, such as CEA in GLV-1h417. The cells present would not be lysed, due to the VACV not being able to unfold its full lytic potential. Thus CEA would be secreted into the blood stream, but without the requisite viral replication, as any attempt to quantify virus based on its activity would not yield viable results. As the virus itself is rapidly cleared from the system, it is know that CEA has a half-life of around five to seven days, making the concentration decline of CEA in the first part of the graph most likely the decay of the protein in the blood stream. This is, however, an idealised thought, as it assumes that there is no residual replication of the VACV in any other part of the mouse. The viral titration data gathered from these tumour-less mice show that most mice do not have any active virus present in homogenates from different organs, with

the exception of two mice which displayed minimal viral replication, the highest level of which was seen in the lung (around 60 to 100 pfu/organ). Minimal replication aside, hypothetically speaking, if one were to do a regression analysis, one would find that an exponential regression curve would fit with an R^2 of 0.95 (Fig. 4.1. This represents a very good curve to data point fit and would indicated that any prediction made from this mathematical model would be 95% accurate. As the type of regression curve in this case is an exponential one, this shows that this protein might follow the general law of decay, from which one could mathematically calculate the half-life $\tau/_2$. The equation, the exponential rate of change, is usually used to calculate an exponential decay of any kind. By looking at the graph, it is possible to estimate the half-life of CEA to be around seven days post viral injection, which is in accordance to what is generally known within the clinic to be the half-life of CEA. Supporting this idea of abortive replication, the

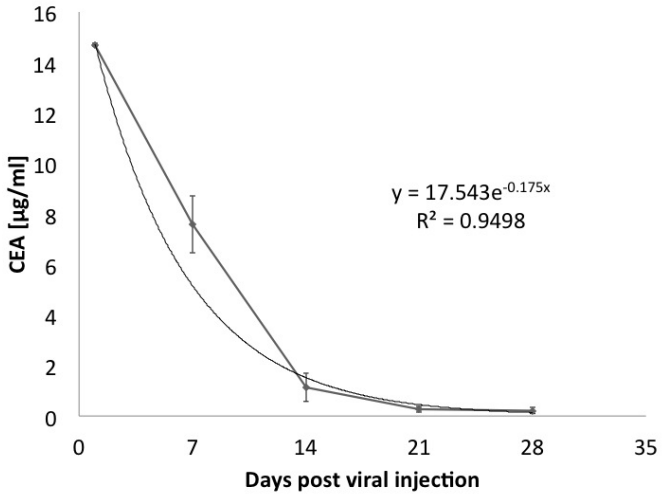

Figure 4.1: Development of CEA over time in tumourless mice.The exponential trendline was superimposed over the graph data. This regression trendline shows an R^2 of 0.95, dictating a good predictability of calculated estimates based on this data here.

β-glucuronidase measurements in the serum of these non-tumourous mice did not show any increase after initial viral injection. As lacZ is under the control of the $p^{11K\ L}$ late promoter, it would not be expressed in an abortive replication.

4.6.6 Virus-specific staining shows viral spread within histological slides

Fig. 3.53 and 3.54 illustrate the immuno-histological staining done on slides containing paraffin-embedded microtome slices of extracted tumours from GLV-1h417-treated mice. Fig. 3.53 shows the same area of a 14 day post viral injection extracted tumour, on the left stained with hematoxylin & eosin counterstain, and on the right using an α-VACV-specific brown staining. The cross-section showing vein-like structures was used as a location reference. Fig. 3.54 shows two tumour specimens at 14 days and 64 days post viral treatment. This overview shows the viral infiltration of the tissue starting out at day 14 from discrete foci within the tumour, having almost completely engulfed the tumour slide by day 64 post viral injection. The lightening of the VACV staining in the middle of the tumour pictured on the right-hand image indicated that the infected tissue is being cleared away by immunological components, possibly macrophages, at the same time lessening the viral load of that particular area. The area of VACV presence increases between 14 and 64 days, indicating viral spread and the synchronous viral replication required to facilitate the spreading.

4.7 Correlation analysis

The individual analysis of each (bio)marker by itself so far yielded interesting information. However, the more important aspect of this analysis is the relationship between the all the markers, most importantly, any marker and their respective correlation to the titre present in the tumour.

Some may say that the tumour volume, having seen the mathematically strong correlation present between various markers and the tumour size/regression displayed during this study (Fig. 4.3 & 4.2). However, as strong as this correlation may seem, the tumour regression is very tumour cell line-dependent variable. This tumour model, GI-101A, is a good responder to our virotherapeutic treatment, thus tumour size and regression. A less responsive tumour model might not respond well to a treatment or might actually respond to treatment, but not display tumour regression. Instead, the stroma/matrix within the tumour tissue might still sustain long after the actual tumour cells had been lysed and cleaned up by the immune system. Using LDH, lactate dehydrogenase, a known indicator

of tissue disruption, as an indicator of cell lysis and tumour regression did not result in entirely conclusive data. Fig. 3.60 shows the average levels of LDH measured from three mice bearing GI-101A tumours, treated with GLV-1h68. The average tumour volume of the three mice is overlaid on a secondary axis. It is shown that the regression in tumour volume, effectively the lysis of tumour cells, and the concurrent release of LDH into the blood stream, does not seem to be followed closely by the measurement of LDH in the serum of these mice. While showing the same trend, the LDH measurements in blood seem to gloss over any changes in tumour volume, e.g. at the end of the study where the tumour volume dips but the LDH measurements decline unchanged. This could be due to a number of causes, of which interference due to murine LDH is not one of them, as this was counteracted by using an ELISA specific to human LDH produced and released by the tumour. Factors that play a role are possibly the half life of the protein in circulation, but also the fact that cell lysis and release of LDH into the blood stream is not a perfect occurrence. Immunological interactions with the released protein, protein decay and the resulting detectability via ELISA are all aspects that contribute to the resulting effect seen in the graph shown. Viewing the data in relation to the amount of virus present in the tumour is a more effective and accurate way of correlating the biomarker data, as the biomarkers are expressed in a viral-replication-dependent manner, thus allowing for a direct relationship between any marker and its respective viral titre. Interestingly enough, this also creates a comparison basis between viruses, as it also makes it possible to compare them on the basis of viral expression. As such, the basis for comparison had been created and confirmed in Fig. 3.50, where the tumour titre is presented in chronologically as pfu per total organ, taking tumour size into consideration. This shows that the titre is comparable between the two different CEA viruses (GLV-1h416 and 1h417) and that any difference in marker level is resultant of the promoter strength with which the gene is being expressed, and not due to differences in viral replication between the two viruses. Tumour regression in all viruses is comparable, thus showing that the therapeutic effect exhibited by GLV-1h68, the parental virus from which all of the other viruses were derived, was not lost due to the genetic modifications undertaken whilst replacing TFR with β-galactosidase or CEA (Fig. 3.49).

When looking at the tumour titre and size in tandem, it can be seen that toward the end of the study, the virus density within the tumour increases. This is visualised in Fig. 3.54, where the viral infiltration begins in focal points in image (a), then progressing towards large areas positive for the presence of VACV (b). What can also be seen in image (b) is that the outer borders of the viral infiltration are of darker intensity than

the areas in middle of the tumour, indicating that once the virus has lysed the cells, it moves on to further infect cells, pushing the front forward towards uninfected cells, whilst leaving small amounts of virus in its wake. The dark borders are thus a representation of high concentrations of actively replicating virus, compared to lighter areas of indicating a weaker presence of virus. However, in total, the tumour titre reaches a maximum at 14 days post viral injection, and does not change during the course of the study, only reducing slightly at the end of the study, when tumour regression forces the viral titre to reduce. Fig. 4.5 shows this among other trends. The viral titre is dependent on the amount of tumour cells available for replication. The dynamics of the infection show that it begins as infections in focal points, spreading outward from there to further infect the tumour. As a result, it was expected that the tumour titre was to increase rapidly until the whole tumour was infiltrated, and then decrease when the system begins to clear the tumour of virus. This, however, is not what the data shows, since the level virus plateaus, but the levels of biomarkers measured resulting from tumour infection and viral replication show a peak and a subsequent, gradual decrease in expression on the whole. This can be explained by a hypothesis suggesting a ring of actively replicating virus that pushes outward from the focal point of infection. The areas left behind show the presence of virus that is not replicating actively in the tumour. The tumour titre is established by using the viral plaque assay. This assay quantifies the amount of virus in any samples that is actively able to infect CV-1 cells. If the virus however, is present but not replicating (inactive/dormant), it would also be quantified using this method, as the plaques counted are a direct result of lysed CV-1 cells. Within the tumour, after lysis, "replication substrate", i.e. the tumour cells, would be limited, regulating the amount of actively replicating virus. In cell culture, whilst performing the viral plaque assay, the "substrate", i.e. the cells used, are in abundance as not to become a limiting factor. All virus in the sample then begins replicating, with no rate limiting step interfering with the replication. Thus the titre being determined via viral plaque assay is higher than the actual replicating virus titre. This is also compounded by the biomarker analysis.

Generally, CEA and β-glucuronidase both increased in serum concentration until 21 days post viral injection, then declined steadily till the end of the study. And this is in spite of the indication that the viral titre plateaus. As both are directly related, the biomarker quantification was expected to mimic the trend dictated by the replicating virus present in the tumour. However, as stated previously, the viral plaque assay used to quantify the viral titre accounts for all virus, replicating as well as dormant, meaning the change in biomarker levels indicate a change in active viral replication, as opposed to the change in

total viral titre. As such, this data shows a possible flaw in the viral plaque assay used to quantify virus, since the virus present in the sample is quantified under ideal conditions, prompting dormant virus to "become active". The data presented in Fig. 3.58 shows a further relationship between CEA and β-glucuronidase. The graphs plotted there show the change of CEA and β-glucuronidase in the serum of four mice, which had been dosed with either GLV-1h416 or 1h417. It was these same mice that were monitored by measuring serum samples over the course of the study. In relation to each other, CEA seems to follow β-glucuronidase more closely in GLV-1h417, albeit in what seems to be a steeper fashion than the decline of β-glucuronidase. The proximity of the data points is most likely due to the fact that the p^{sEL} and p^{11K} promoters are comparable in expression strengths. As such, similar amounts of marker would be produced and detectable. This cannot be said for the GLV-1h416 group, in which the CEA promoter is a weaker early promoter. Consequently, the concentration of CEA in serum starts declining almost immediately after reaching a peak at 14 days post viral injection, whereas β-glucuronidase only begins its decent one week later. Since the early promoter is 50 times weaker than the early/late promoter, it produces less CEA. A change in concentration, due to protein decay and other clearing factors within a biological system, is likely to be more obviously when the overall amount is less, making the change in concentration level in the case of GLV-1h416 more striking. The promoter strength comprises of two components, a temporal aspect and the replication efficiency. Not only is p^{sEL} active for a longer part of the viral replication cycle, the amount of copies made through this activity is higher than the weaker p^{sE} promoter. This data is shown in summary in conjunction with the tumour regression in Fig. 4.3 and 4.2.

This difference in promoter strength and its effect on the expression of CEA is most distinct when the CEA concentration is visualised as it is in Fig. 3.57. There the absolute levels of expressed CEA are plotted as a time course. Again, this set of data was acquired by monitoring one set of four mice for each treatment group over a period of 63 days. The maximum concentration reached by the GLV-1h417-treated group is six times higher than the peak reached by GLV-1h416. Also, there is a temporal difference, as in when the maximum is reached. GLV-1h416 reached its peak already at day 14, whereas GLV-1h417 reaches its peak a week later at 21 days post viral injection.

Another point of consideration here is not only the expression of the biomarker in the tumour, but also that of its secretion or lytic release into the blood stream. CEA was engineered to be released into the blood stream, as opposed to its normally membrane-bound

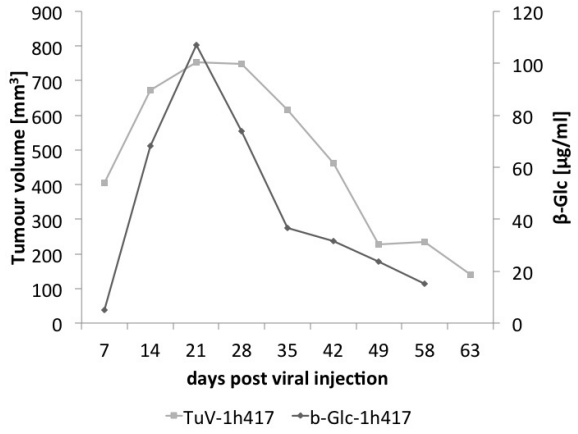

(a) β-Glc and tumour volume

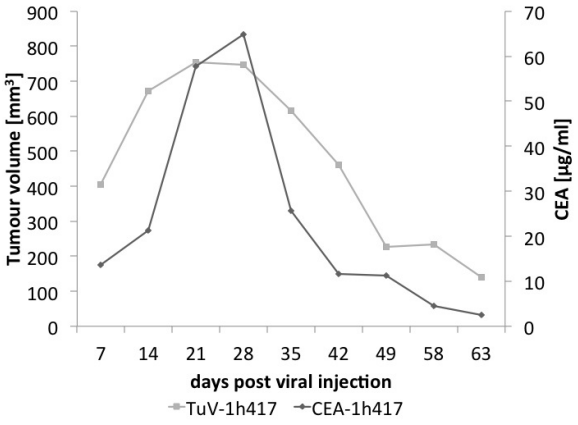

(b) CEA (p^{sEL}) and tumour volume

Figure 4.2: β-Glucuronidase and CEA with tumour volume over the course of the study for the GLV-1h417-treated group. These measurements were taken from the same mice at each time point. The levels of marker were determined via ELISA and activity-assay based serum analysis. The scale used to the tumour volume in the primary axis on the left, the markers are plotted on the right scale in the respective magnitude.

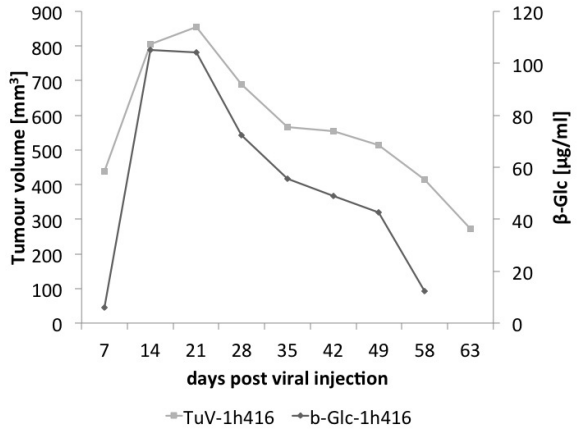

(a) β-Glc and tumour volume

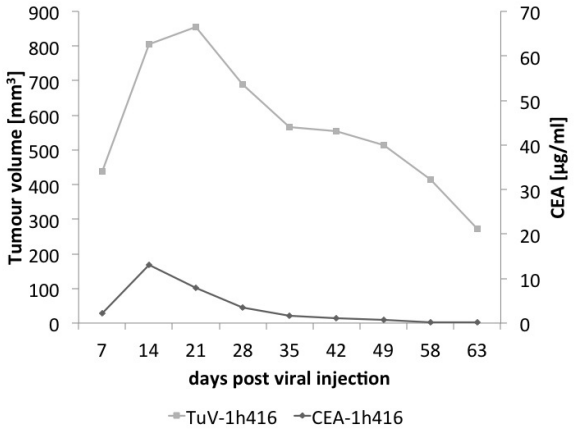

(b) CEA (p^{sE}) and tumour volume

Figure 4.3: β-Glucuronidase and CEA with tumour volume over the course of the study for the GLV-1h416-treated group. These measurements were taken from the same mice at each time point. The levels of marker were determined via ELISA and activity-assay based serum analysis. The scale used to the tumour volume in the primary axis on the left, the markers are plotted on the right scale in the respective magnitude.

state. β-Glucuronidase is an enzyme that is produced within the cytoplasm and released upon lysis of the cell. However, in both cases, differing amounts of marker eventually reach the blood stream, with 7% of CEA produced in the tumour actually detectable in

serum. With β-glucuronidase, the secretion rate into the serum was at 0.3%, despite the high concentration of marker in the tumour (Fig. 3.29). A previous study showed that the detection of α-VEGF in serum and in tumour fluid showed a fifteen-fold difference between the two, making it comparable to the CEA levels presented in this study.[92] The factors that influence this uptake of marker into the blood stream are so diverse, it is difficult to actually pinpoint them. The dynamics of cell lysis, tumour micro-environment, interstitial pressure, the innate immune system and macrophage clean-up are all involved in this complex mechanism of biomarker release.[37] [35] Data indicates that the size of the marker plays an important role, possibly accounting for the discrepancy between β-glucuronidase and CEA. As far as size is concerned, a single subunit of β-glucuronidase is similar to CEA. However, this plays a secondary role since CEA is a secreted protein, relying on different transport mechanisms compared β-glucuronidase, which is a cytoplasmic protein and is only release upon cell lysis. This makes for a compelling argument to choose CEA over β-glucuronidase, as this would reflect the viral replication in a more timely fashion. Some factors are based on hypothesis and observation, only few factors are known, and even fewer are quantifiable, making it difficult to ascertain how large an effect these variables have on the markers' bio-availability.

When regarding the entirety of the markers chosen analysed side-by-side, the differences between the two viral constructs becomes quite obvious. Theses trends are shown in the graph showing a panel of markers for each virus, Fig. 4.4 and 4.5. In these panels, all the data points were normalised to the average reading for that particular marker over the whole time course. Each individual time point has a sample size of minimum 3 and the standard error in ratio was calculated from the individual standard errors for each reading, also normalised to the average reading over all time points.

GLV-1h417 follows the overall, and most expected trend, which is that of all markers reaching their peak at 14 days post viral injection, then decreasing in concentration until the end of the study. This correlates well along all markers in each time grouping, even though the rate of change differs slightly for each marker. Setting the tumour titre as a guideline, all other markers follow the trend dictated by this characteristic. The relative rate of change within each marker is also similar to that of the titre. GLV-1h416 on the other hand, shows quite the opposite trend, with all markers still increasing within the time frame viewed, as opposed to the peak and decline of all markers in the 1h417 panel. But, this trend also correlates well with the trend set by the titre present in the tumour, our defined reference. With the increase in tumour titre, the markers all increase as well.

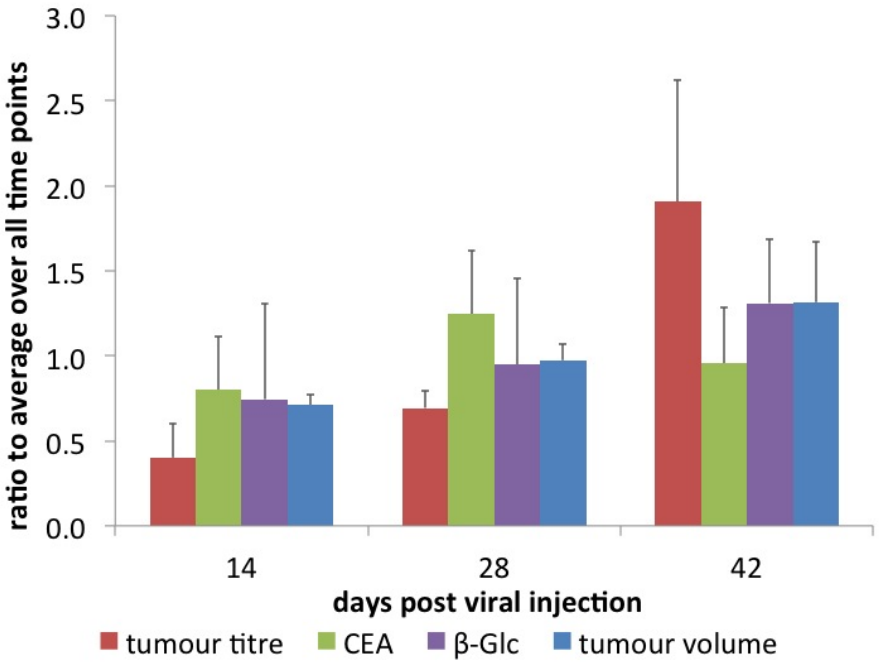

Figure 4.4: Marker panel for GLV-1h416. Tumour volume, tumour titre, CEA and β-glucuronidase serum levels presented as ratios. The overall average of each biomarker over the whole time period was set as reference and the respective time point data calculated as a ratio of the reference. Time points shown are days 14, 28 and 42 days post viral injection.

However, when comparing and interpreting any data to the tumour titre, one should keep in mind that the method of quantifying the titre from homogenised tissue is one that could result in a large variance. Homogenising tumours is not a simple task, as slight variations within the sample handling could result in differences in released virus, hence result in different titres for samples that in actuality have the same titre. Biological variance and tumour formation also play an influential role, with cystic tumour formation being more difficult to break than semi-solid growths. The method of homogenisation also effects the total titre determined. Mechanical disruption of the cells using bead mills and sonication is extremely effective, but also destroys virus in the sample. For that reason, a more gentle homogenisation was achieved using a mortar & pestle, as well as freeze/thaw cycles and vortexing the samples. It is assumed that the release of virus from the disrupted cells is the same for all cases.

The mini correlation graphs presented here (Fig. 4.6 & 4.7) help to illustrate the correlation analysis performed. The graphs presented here are first presented separately for each virus, then divided into the respective time points. The first column shows the correlation between CEA (y-axis) and the total tumour titre (x-axis), the second column the

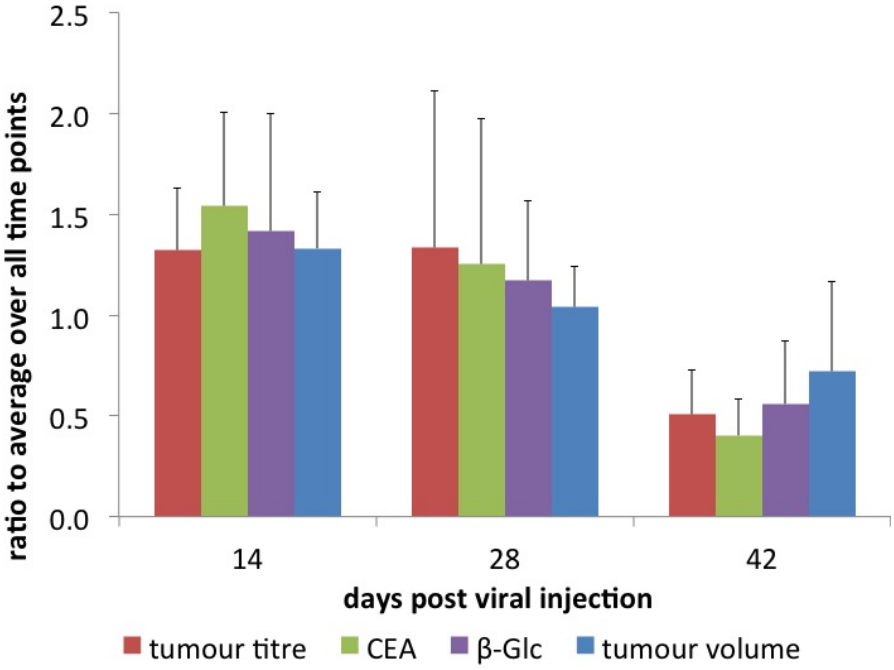

Figure 4.5: Marker panel for GLV-1h417. Tumour volume, tumour titre, CEA and β-glucuronidase serum levels presented as ratios. The average of all data points for each biomarker over the whole time period was set as reference (total average) and the respective time point data calculated as a ratio of average per time point divided by total average.

correlation between β-glucuronidase and the tumour titre and thirdly, CEA in relation to β-glucuronidase. The lines show the correlation for each time point. These time points were restricted to the time points of viral titre determination, since it was necessary to sacrifice the mouse in order to obtain this information. As of yet, it is not possible to quantify virus using a non-lethal, non-invasive method.

Generally speaking, the trends here are all reflect a positive relationship between CEA, β-glucuronidase and the tumour titre. For both viruses, it is shown, that CEA and β-glucuronidase each increase with the titre, thus the two markers also increase in relation to each other. Looking at each graph more closely, the coefficients of determination for each graph range between 0.34 to 0.99 for GLV-1h416, and 0.51 to 0.99 for GLV-1h416. This would indicate anything from a bad to a very good predictability for the time point in question. However, statistically speaking, the distribution of the data points along the regression line is what decides how reliable a correlation is.

Another important factor that has to be taken into consideration is the fact that the sample size for each time point is small. With only three, at best four, individuals for

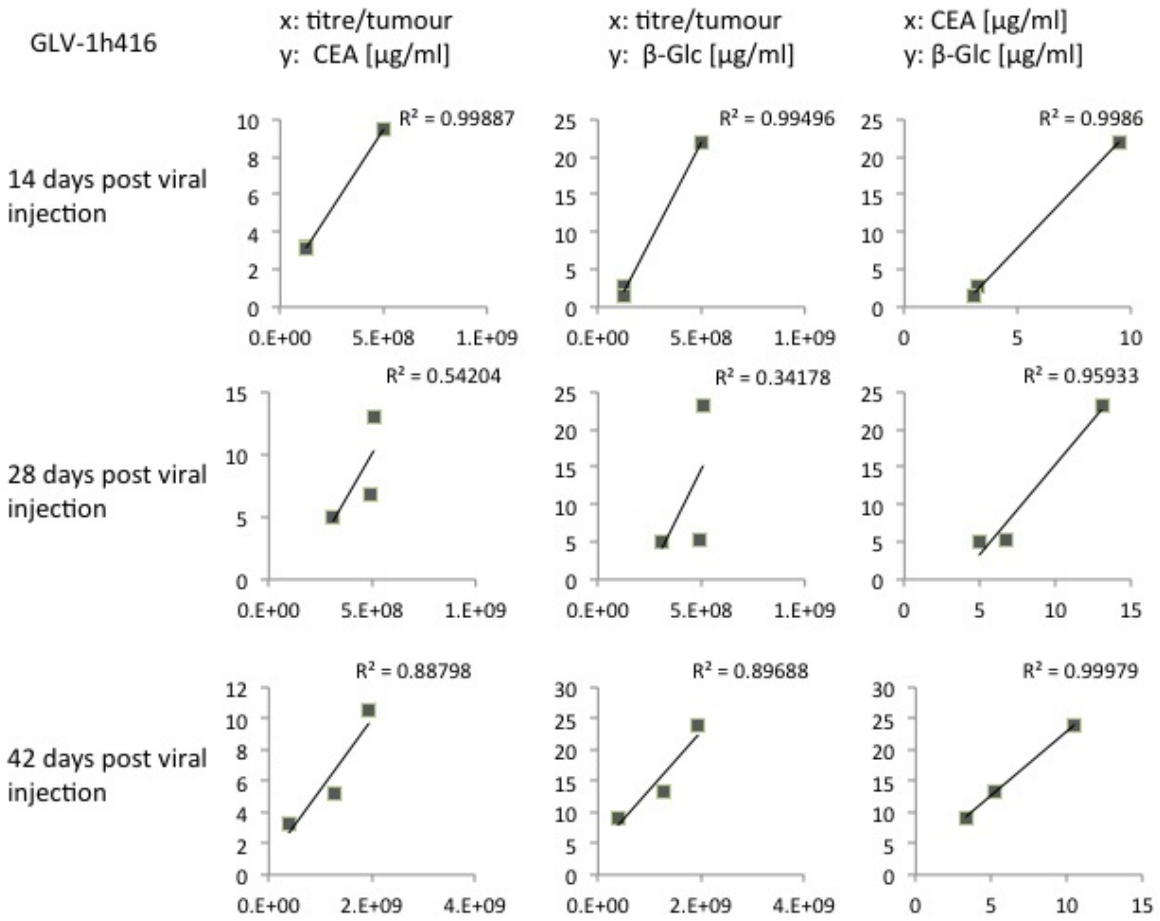

Figure 4.6: Mini correlation graphs for all correlations for each time point between CEA, β-glucuronidase and the viral titre for GLV-1h416 in the tumour. Each time point and each marker is mapped individually. The first column represents the correlation between CEA (y-axis) and the viral titre (x-axis); the second column β-glucuronidase (y-axis) and the viral titre (x-axis), and lastly, the third column showing CEA (x-axis) vs β-glucuronidase (y-axis). Each line represents the time point of the measurement. The sample size for each time point is 3. R^2 is shown in the top right hand corner of each graph.

each time point in most of the analysis, the variance would be very high, having an effect of the standard deviation, and thus the error, for all analysis done. The same goes for the limited range that is seen *in vitro*, as the range for titres in cell culture is between $1x10^4$ to $2x10^6$ pfu/ml. *In vivo*, the tumour titres are found in a narrower range of $1x10^8$ to $1x10^9$ pfu/tumour. This effects any correlation analysis performed based on this data set. An example of sample size influencing the overall correlation can be seen in Fig. 4.8. The population is made up of points corresponding to two variables,

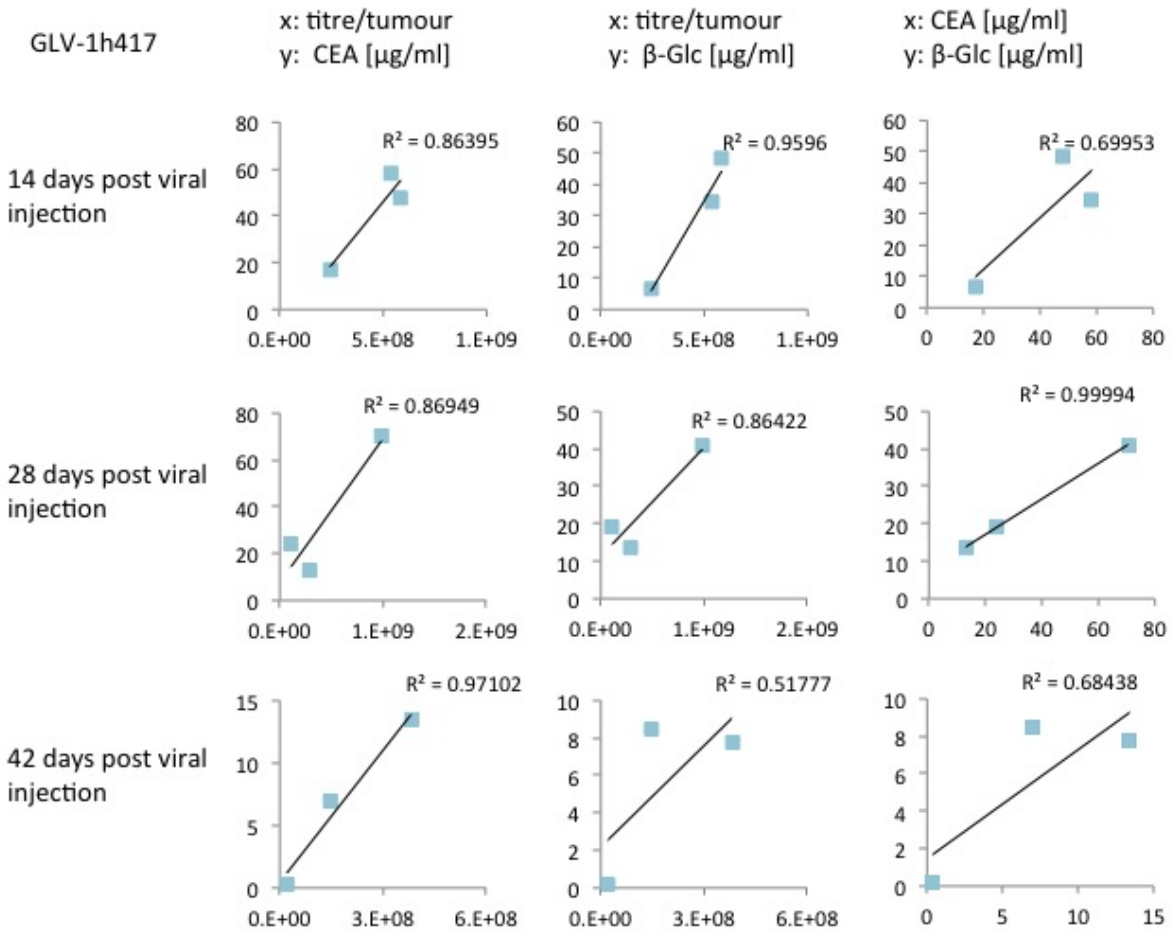

Figure 4.7: Mini correlation graphs for all correlations for each time point between CEA, β-glucuronidase and the viral titre in the tumour, in this case for GLV-1h417. Each time point and each marker is mapped individually. The first column represents the correlation between CEA (y-axis) and the viral titre (x-axis); the second column β-glucuronidase (y-axis) and the viral titre (x-axis), and lastly, the third column showing CEA (x-axis) vs β-glucuronidase (y-axis). Each line represents the time point of the measurement.The sample size for each time point is 3. R^2 is shown in the top right hand corner of each graph.

x and y. The Pearson/Spearman correlation shown for the sample size (yellow points) for a restricted range is not as significant compared to the correlation for the whole (unrestricted) population.

This statistical complication could be rectified by repeating the experiments with more mice, substantiating the information gathered. This problem is one that is most often faced in science, as it is sometimes not logistically possible to gather enough data for

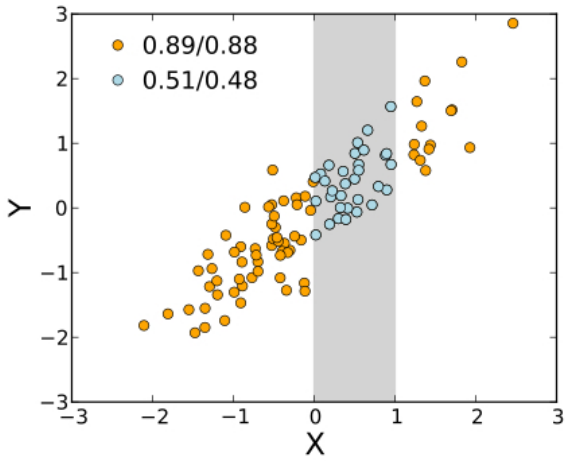

Figure 4.8: Correlation analysis of a restricted (blue) and unrestricted (total) data population change the Pearson/Spearman correlation coefficient. What seems to be an average correlation in a restricted population becomes a strong one, when more data points are acquired (unrestricted population).

the same variables to counteract the statistical effect mentioned prior. Most commonly, as much data is gathered as possible, and the correlations are done based on those data points, which could change if the population size changes. Considering that the correlation could change for the better when analysing a larger population, it is interesting to see that the correlation between the titre and biomarker concentration in cell culture is generally very good, than compared with the correlations for both markers *in vivo*. In cell culture, the markers are released upon cell lysis into the supernatant. This direct release in the reason why the correlation in culture is so good. There are no other biological/kinetic factors further associated with the displacement of marker from cytoplasm to supernatant. In the biological system however, this is not the case as the lytic release of markers into the blood stream is not a locationally direct process. The markers are first released into the tumour microenvironment and then proceed to be taken up by the circulation. Immunological and inflammatory factors influence not only the transport of marker into circulation, but also the amount of marker ending up in blood. As that may be, the most important factor pertaining to marker up-take in blood is the degree of vascularisation in the tumour, as a less perfused tumour would result in a lower/delayed up-take compared to a well perfused tumour. In conclusion, the data shown in this thesis proves that virally encoded, replication-dependent markers are detectable in serum and correlated well with the viral titre present in the tumour, more precisely, with the fraction of virus that is actively replicating, making it a good representation for viral replication (Fig. 4.9). The expression of these proteins is also high in tumours, effectively ameliorating any

Biomarker	Type	Detection methods	Expression in tumour	Detection in serum	Correlation to viral titre	Comments
sCEA psE (1h416) psEL (1h417)	All secreted, recombinant	ELISA	+++ +++	++ ++	+++ ++++	Efficient transfer into serum
β-Glucuronidase	Cytoplasmic, recombinant	Enzymatic	++++	++	+++	Sensitive detection method
β-Galactosidase	Cytoplasmic, recombinant	Luminescence/ ELISA	n.a. / +	– / (+) [1]	n.a. / –	Serum interference
GFP	Cytoplasmic, recombinant	Optical/ ELISA	(+)[1] / ++	– / –	– [2] / n.a.	Serum interference
CPG2	Cytoplasmic, recombinant	Western Blot/ Enzymatic	++++ / n.d.	n.d. / –	n.a. / n.a.	Serum interference
A27L Protein (IMV)	Intrinsic viral protein	ELISA	n.d.	–	n.a.	Serum interference
B5R Protein (EEV)	Intrinsic viral protein	ELISA	n.d.	–	n.a.	Below detection limit

Figure 4.9: Summary of biomarkers tested in murine system. This table summarises all the biomarkers tested in xenograft mouse model and the most important results gained and discussed in this thesis. N.a. - not applicable; n.d. - not determinable; "-" - no reliable quantification possible; "+" - amount quantified; [1]detectable, but not quantifiable; [2]correlation to tumour signal.

issues caused by detection limits. The production of viral encoded proteins is dependent on the promoter strength and the availability of cellular substrates, i.e. tumour cells. The promoters which control marker expression also in turn influence the concentration of biomarker found in serum, giving rise to the possibility of using different promoter strengths to modulate any gene product in serum and also to minimise any toxicity that could arise from using a virus as a therapeutic substance delivery system. The release of the analysed biomarker into serum seems to be restricted, as the concentration measured in the tumour is much higher that of that measured in the blood. The limitations seen in the athymic nude mouse animal model are not representative of the human, immune competent system. This influences the impact of viral replication and and subsequent clearing of the virus, which would also effect marker measurements in serum.

5 Outlook

A tumour is, as a whole, a very complex and intricate system, in which a myriad of physiological and biological factors influence the treatment outcome. More often than not, these factors are known, but not quantifiable with the current technology. With the measurement of various viral-replication-specific biomarkers in blood, it is hoped that a prognosis modality would emerge, enabling us to monitor viral replication and patient progress in a non-invasive manner. However, deeper and more detailed analysis of the different influencing factors is required. As mentioned by Rustum *et al.*, structural heterogeneity in tumours is key to intratumoural drug distribution.[93] Vascularisation, interstital fluid pressure and other factors influence any drug distribution to the point of being central to the success, or failure, of any neoplastic treatment. As it is known that the athymic nude mouse models, with which most cancer research is performed on, are imperfect as to the applicability and transfer of information gathered from said models to immune competent humans. Lutz *et al.* have published a linear one-compartment mathematical model with which they attempt to estimate the minimal detectable size of tumours on the basis of serum biomarkers.[94] But since this is a purely mathematical model, the assumptions made in order to even establish a basis for calculations take the model further away from reality, even though it is based on published experimental data. Having said that, further research has to be done pertaining to the secretion of any biomarker into the blood stream and the subsequent effect of the above mentioned biological factors. Repetition of said experiments would help lower the amount of statistical variance seen in this thesis, which decreases with increasing sample size. The data and information provided by this thesis point to CEA being the marker of choice, as the secretion rate from tumour into serum is at a level that would enable more direct quantification method than β-glucuronidase, as the latter shows a less than optimal excretion rate. This, coupled with a direct method of measurement (ELISA), makes for a more timely manner with which a viral replication-dependent quantification in patient serum would be possible, as shown in the mouse model. This systematic analysis of viral genome-borne markers shows that it is possible to indirectly quantify viral replication by monitoring marker levels in blood and tumour regression as a primary indicator of the treatment's therapeutic effect.

A Abbreviations

°C	Degrees Celsius
μg	Microgram
μl	Microlitre
4-MUG	4-Methylumbelliferyl-β-D-glucuronide
Å	Ångström
aa	amino acid
bp	Base pairs
c	Concentration
CEA	Carcinoembryonic antigen
CO_2	carbon dioxide
CPG2	Carboxypeptidase G2
DHFR	Dihydrofolate reductase
DMEM	Dubelcco's Modified Eagles Medium
DNA	Deoxyribonucleic Acid
dpi	days post viral injection/infection
ECL	Enhanced Chemical Luminescence Detection System
EDTA	Ethylenediamine Tetra Acetate
EtOH	Ethanol
FBS	Fetal Bovine Serum
g	Grams
GFP	Green Fluorescent Protein
gpt	guanidine phosphoribosyltransferase
gusA	gene resulting in expression of β-Glucuronidase
h	Hour
hpi	Hours post infection
HRP	Horse Radish Peroxidase
IPTG	Isopropyl β-D-1-thiogalactopyranoside
Kb	Kilo bases
kDa	Kilo Dalton
lacZ	gene for β-galactosidase expression
LB	Luria Bertani
LHD	Lactate dehydrogenase
M	Moles per litre

mA	Milliampere
MeOH	Methanol
mg	Milligram
min	Minute
ml	Millilitre
mm	Millimetre
mM	Millimolar
mmol	Millimol
MOPS	3-(N-morpholino)propanesulfonic acid
MTT	Dimethyl thiazolyl diphenyl tetrazolium salt
MTX	Methotrexate
ng	Nanogram
nm	Nanometre
OD	Optical density
PAGE	Polyacrylamide gel electrophoresis
PCR	Polymerase chain reaction
pmol	Picomol
p^{sE}	Synthetic early promoter
p^{sEL}	Synthetic early/late promoter
p^{sL}	Synthetic late promoter
SDS	Sodium Dodecylsulfate
SOC medium	Super optimal broth with catabolite repression medium
TBS	Tris-buffered Saline
TEM	Transfer electron microscope
Tris	Tris(hydroxymethyl)amino Methane
U	Units
v/v	volume / volume
VACV	Vaccinia Virus
VEGF	Vascular endothelial growth factor
w/v	weight / volume
WHO	World Health Organisation

B Antibodies

α-A27L antibody (rabbit, lot 45887-4)	Genscript
α-B5R antibody (rabbit, lot 45887-2)	Genscript
FLEX α-CEA antibody clone II-7 (mouse, IR622)	Dako
α-CPG2 antibody (rabbit)	Genscript
α-β actin antibody	Jackson Immunoresearch
Goat α-mouse IgG (A8924)	Sigma Aldrich
Goat α-rabbit IgG (BA-1000) for histology	Vector Laboratories
Goat α-rabbit (IgM)-HRP Conjugate	Biorad
Donkey α-rabbit (IgM)-HRP Conjugate (NBP1-73718)	Novus Biotech

Sequences used for antibody generation

A27L

CAKKIDVQTGRRPYE (Lot: 45887-4) Genscript also provided the resulting antibody using their "Complete affinity-purified polyclonal antibody package" (rabbit polyclonal). 7 ml antibody (0.938 mg/ml) was delivered and stored in PBS (pH 7.4) with 0.02% sodium azide.

B5R

RTNEKFDPVDDGPDC (Lot: 45887-2) The corresponding rabbit polyclonal antibody was delivered as a lyophylised powder and reconstituted to a 0.327 mg.ml solution in PBS (pH 7.4) with 0.02% sodium azide.

C Cell lines

Human

A549	Human lung carcinoma cell line (ATCC)
CV-1	Green monkey kidney fibroblast cell line (ATCC)
DU145	Human prostate cancer cell line (ATCC)
GI-101A	Human metastatic breast cancer cell line (ATCC)
HT-29	Human colorectal adenocarcinoma cell line(ATCC)
OVCAR3	Human ovarian epithelial adenocarcinoma cell line (NIH/ATCC)

Bacterial

BL21(DE3) Competent cells (69405-4)	Novagen
One Shot TOP10 chemically competent cells (C4040-06)	Invitrogen

D Cloning

Synthetic oligonucleotides (Primers)

Target	**Sequence (5′ to 3′)**
sCEA-SalI for	GTC GAC CAC CAT G GAG TCT CCC TCG GCC C 3
sCEA-PacI rev	CCA TAG TCA AGA GCA TCA CAG TCT CTG CA TA GTT AAT TAA
fCEA-PacI rev	AGT GCT GGT TGG GGT TGC TCT GAT ATA GTT AAT TAA
CEA-mid for	AGT GCC AGG CGC AGT GAT TC
CEA domain 1	CCA GAA TGA CAC AGG ATT CTA CAC CCT A
CEA domain 2	CAT AAC TCA GAC ACT GGC CTC AAT AGG A
CPG2 BamHI for	TGG GTC GGC GGA TCC ATG CAG AAG CGC GAC AAC GTG
CPG2 HindIII rev	AAGCTT TCA CTT GCC GGC GCC

Vectors

Overexpression vector pET-28a (+) (69864-3)	Novagen
Viral TK transfer vector	

Ladders

DNA

1 kbp DNA ladder	BioRad
Hyperladder I (10k - 200 bp)	Bioline
Hyperladder IV	Bioline

E Consumables

β-Galactosidase	Sigma Aldrich
β-Glucuronidase	Sigma Aldrich
β-Mercaptoethanol	Sigma Aldrich
12% Bis-Tris Acrylamide Gels	Life Technologies
Acetic acid	J.T. Baker
Agarose, low melting low EEO	Fischer
Ammonium persulfate	AppliChem
Ampicillin	Applichem
Antibiotic/Antimycotic solution for cell culture	Cellgro
Bovine serum albumine (BSA)	Sigma
Bromphenol blue	Serva
cDNA mix for CEA isolation	Clontech
Calcium chloride	Merck
Carboxymethylcellulose (CMC)	MP
Chloramphenicol	Sigma
Complete proteinase inhibitor cocktail tablets	Roche
Coomassie brilliant blue G-250	Sigma
Crystal violet	Sigma
Dehydration alcohol	VWR
Dulbecco's modified Eagles media (DMEM)	Cellgro
Dulbecco's phosphate buffered saline (PBS) 1x	Cellgro
Dried skim milk powder	Dibco
Ethylendiaminetetraacetic acid (EDTA)	Sigma Aldrich
EDTA-Trypsin solution	Cellgro
Eagles minimum essential media (EMEM)	Cellgro
Eosin	Richard Allen Scientific
Ethanol	Sigma Aldrich
Ethidium bromide	Sigma Aldrich
Fetal bovine serum (FBS)	Cellgro
Formaldehyde	Fischer
Formalin	Fischer
Glycerol	Fischer
Glycerine	Sigma Aldrich

Hematoxylin QS (Gill's formula)	Vector
HEPES buffer	Cellgro
Hydrochloric acid (HCl)	Sigma
Hydrogen Peroxide (H_2O_2)	Sigma
H_2O HPLC grade	Life Technologies
Indicator paper, pH = 2–5	Merck
Isoflurane	Explora
Isopropanol	Sigma Aldrich
Kanamycin	Sigma
Laemmli sample buffer 4x	Invitrogen
LB-Broth	Dibco
Methanol	J.T.Baker
Methotrexate (USP grade)	Sigma Aldrich
MOPS running buffer	Life Technologies
Nitrocellulose Membrane	Life Technologies
OneShot TOP10 *E. coli* chemically competent cells	Invitrogen
Paraplast tissue embedding medium	McCormick Scientific
Parafilm laboratory film	Pechiney Plastic Packaging
Phosphate buffered saline sachets	Sigma
Roswell Memorial Institute media, phenol free (RPMI)	Cellgro
SDS sample loading buffer	Life Technologies
Sodium chloride (NaCl)	Sigma Aldrich
Sodium hydroxide (NaOH)	Merck
Sodium hydroxide 2N solution	Fischer
Tricine	Applichem
Tris	Sigma
Tris-HCl	Sigma
Transfer Buffer for Western blotting	Life Technologies
Tris Base	Sigma Aldrich
Tris-HCl	JT Baker
Trypan blue solution	Cellgro
Tween 20	Sigma Aldrich
Xylene substitute	Sigma
Zinc chloride ($ZnCl_2$)	Sigma
Zinc sulfate ($ZnSO_4$)	Merck

F Kits

β-Galactosidase ELISA kit (11 539 426 001)	Roche
AccuPrime Pfu Supermix (123444-040)	Invitrogen
Coomassie (Bradford) Protein Assay kit (23200)	Pierce Thermo Scientific
DNA Clean & Concentrator (D4003)	Zymo Research
ECL Plus Western Blotting Kit (PRPN2132)	Amersham
FailSafe PCR PreMix selection kit (FS99060)	Epicenter
Galacto-Light Plus System for detection of β-Galactosidase (T1011)	Applied Biosystems
GFP Quantification kit (K815-100)	Biovision
GFP ELISA Quantitation Kit (AKR-121)	Cell Biolabs
Human CEA ELISA (ab99992)	Abcam
MagneHis Protein Purification System (V8550)	Promega
Mammalian β-Galactosidase Assay kit (75707)	Pierce Thermo Scientific
Opti-4CN Substrate kit (170-8235)	Biorad
Purelink Quick Plasmid Miniprep kit (K2100-11)	Invitrogen
Quick Ligation Kit (M2200S)	New England Biolabs
VectaStain ELITE ABC Kit (Goat IgG; PK-6105)	Vector Laboratories
Vector ImmPact DAB Peroxidase substrate (SK-4105)	Vector Laboratories
ZeroBlunt TOPO PCR Cloning kit (K2800-20)	Invitrogen
Zymoclean Gel DNA Recovery Kit (D4002)	Zymo Research

G Laboratory equipment

Amicon Ultra-15 centrifugal filter unit 10 kDA cut-off	Millipore
Alcohol prep pad, sterile	PDI
Balance PL 1501-S	Mettler Toledo
BSL 2 safety bench	The Baker Company
Cell culture plates (6-, 24- & 96-well)	Corning
Cell culture flasks	Corning
Cell scrapers	Corning
Cell culture incubator HERA Cell 150	Thermo Electron
Centrifuge for reaction caps	Eppendorf
Cup sonifer 450	Branson
Digital caliper	VWR
Embedding Mould TISSUE-TEK	IMEB Inc
Falcon (50 ml, 15 ml)	Greiner
Fastblot Semi-dry Blotting system	Invitrogen
Film Developer	Kodak X-OMAT M35
Firewire DFC/IC monochrome CCD camera	Leica
Forceps and surgical scissors	Braintree Scientific
Hotplate stirrer 375	VWR
IX71 inverted fluorescence microscope	Olympus
Laboratory scale LC 4800P	Sartorius
Legende RT, centrifuge for falcons (15 & 50 ml)	Sorvall
Microcentrifuge tubes easy open cap	Sarstedt
Microscope glass coverslips	Fischer
Microslides Premium Superfrost Plus	VWR
Microtome Leica RM 2125	IMEB Inc
Microwave	Sharp
Multichannel pipettor, 8 & 12 channel	Eppendorf
MZ 16 FA stereo fluorescence microscope	Leica
Nikon Eclipse 6600 microscope	Nikon
PCR Machine	Applied Biosystems
pH Meter Accumet AR15	Fischer Scientific
Photometer Biomet3	Thermo Scientific
Pipettor	Drummond

Pipettes 10, 20, 200 & 1000 μl	Gilson
Pipettes 5, 10 & 25 ml	Corning
Pipette tips	Biohit
Power pack (PCR, gels)	Biorad
RC 6 Plus, centrifuge	Sorvall
Repeater stream pipette	Eppendorf
Rocking platform	VWR
SDS -PAGE system	Life Technologies
Shaker for ELISA plates	Thermo Scientific
Scalpel, sterile disposable	Sklar Instruments
Stereo fluorescence macro imaging system	Lighttools Research
Syringes with attached needle (29G)	BD
Syringe Driven Filter Unit Millex-VV PVDF 0.2 μm	Millipore
Tissue embedding bench	Reichert Jung
Tissue processing and embedding cassettes with lid	Simport
UV/visible Microplate reader SpectraMax M5	Molecular Devices
Vortexer	Scientific Industries
Water bath Isotemp 202	Fischer Scientific
X-ray film SuperXR	FujiFilm

H Markers

For DNA ladders, refer to D

Protein

Precision Plus Protein standards (250 - 10 kDa)	BioRad
Spectral Prestained broad range protein marker	Thermo Scientific
Ultra Low Range Marker (1 - 26.6 kDa)	Sigma-Aldrich

I Solutions

Citrate buffer for histology	0.1 M citric acid 0.1 M sodium citrate pH 6
CMC Overlay	1.5% carboxymethylcellulose 2% FBS 1% A/A DMEM
β-Glucuronidase assay buffer	69.8 μl 2% FBS in PBS 0.2 μl of 4-MUGlc per well of a 384-well plate
β-Glucuronidase assay dilution buffer	PBS 2% FBS for pre-dilution of samples
CPG2 assay buffer	0.1M Tris-HCl (pH 7.3) 0.2mM $ZnCl_2$
CPG2 Tris lysis buffer	20 mM Tris-HCl 137 mM NaCl 1 mM EDTA pH 7.6 Add lysozyme (0.25 μg) just before use
CPG2 dialysis buffer	100 mM Tris-HCl 0.2 mM $ZnSO_4$ pH 7.3

CPG2 refolding buffer	100 mM Tris-HCl 0.1 mM EDTA 0.5 M arginine pH 8.5
Crystal violet staining solution	1.3 g crystal violet 5% ethanol 30% formaldehyde (37%) ad 1 l ddH_2O
DMEM 2%	2% FBS 1.2% A/A solution ad 1 l DMEM
DMEM 10%	10% FBS 1.2% A/A solution ad 1 l DMEM
LB-Medium (Luria)	1% (w/v) Tryptone 0.5% (w/v) yeast extract 0.5% (w/v) NaCl
MTT solution	2.5 mg/ml dimethyl thiazolyl diphenyl tetrazolium salt (MTT) in RPMI 1649 without phenol red
MTX stock solution	25 mg/ml MTX in 0.1 M sodium hydroxide Aliquot and store at -20 °C
PBS-T Buffer	PBS-Buffer (1x) 0.05% Tween

RBM tissue homogenisation buffer	50 mM Tris-HCl 2 mM EDTA PBS (pH 7.4) add one Complete Mini proteinase inhibitor cocktail tablet for every 25 ml
SDS Sample Buffer (3x)	200 mM Tris-Base (pH 6.7) 6% SDS 30% glycerine 10% β-mercaptoethanol 10 mg bromphenol blue
Tris/Borate/EDTA (TBE) 5x buffer	54 g Tris-Base 27.5 g boric acid 20 ml 0.5M EDTA (pH 8.0) Ad H_2O 1 l
Western Blot Transfer Buffer (10x)	25 mM Tris base 192 mM glycine 10% methanol pH 10 Ad H_2O 1 l

Bibliography

[1] S. Mukherjee, *The Emperor of All Maladies: A Biography of Cancer*, Scribner, reprint edition, **2012**.

[2] United States Cancer Statistics (USCS).

[3] A. Jemal, R. Siegel, E. Ward, Y. Hao, J. Xu, T. Murray, and M.J. Thun, Cancer statistics, 2008., *CA Cancer J. Clin.*, **2008**, *58*, 71–96.

[4] J.M. Bishop and R.A. Weinberg, *Molecular Oncology, 1e (Scientific American Introduction to Molecular Medicine)*, Scientific American, Inc., New York, NY, **1996**.

[5] D. Hanahan and R.A. Weinberg, Hallmarks of Cancer: The Next Generation, *Cell*, **2011**, *144*, 646–674.

[6] C.C. Harris, p53 tumor suppressor gene: from the basic research laboratory to the clinic–an abridged historical perspective., *Carcinogenesis*, **1996**, *17*, 1187–1198.

[7] T.J. McDonnell and S.J. Korsmeyer, Progression from lymphoid hyperplasia to high-grade malignant lymphoma in mice transgenic for the t(14; 18)., *Nature*, **1991**, *349*, 254–256.

[8] V.T. DeVita, Cancer, Principles & Practice of Oncology, Lippincott-Raven, 1, 7th edition, **2004**.

[9] C.M. Southam and A.E. Moore, Clinical studies of viruses as antineoplastic agents with particular reference to Egypt 101 virus., *Cancer*, **1952**, *5*, 1025–1034.

[10] M.J.V. Vähä-Koskela, J.E. Heikkilä, and A.E. Hinkkanen, Oncolytic viruses in cancer therapy, *Cancer Lett.*, **2007**, *254*, 178–216.

[11] T. Etoh, Y. Himeno, T. Matsumoto, and M. Aramaki, Oncolytic viral therapy for human pancreatic cancer cells by reovirus, *Clin. Cancer Res.*, **2003**, *9*, 1218–1223.

[12] R. Alemany, C. Balague, and D. Curiel, Replicative adenoviruses for cancer therapy, *Nat. Biotechnol.*, **2000**, *18*, 723–727.

[13] R.L. Chu, Use of Replicating Oncolytic Adenoviruses in Combination Therapy for Cancer, *Clin. Cancer Res.*, **2004**, *10*, 5299–5312.

[14] D. Kuruppu and K.K. Tanabe, Virla Oncolysis by Herpes Simplex Virus and Other Viruses, *Cancer Biol. Ther.*, **2005**, *4*, 524–531.

[15] T. Nakamura and S.J. Russell, Oncolytic measles viruses for cancer therapy, *Exp. Opin. Biol. Ther.*, **2004**, *4*, 1685–1692.

[16] T. Asada, Treatment of human cancer with mumps virus, *Cancer*, **1974**, *34*, 1907–1928.

[17] W.A. Cassel and R.E. Garrett, Newcastle Disease Virus as an Antineoplastic Agent, *Cancer*, **1965**, *18*, 863–868.

[18] A.D. Flanagan, R. Love, and W. Tesarr, Propagation of Newcastle disease virus in Ehrlich ascites cells in vitro and in vivo., *Proc. Soc. Exp. Biol. Med.*, **1955**, *90*, 82–86.

[19] L.K. Csatary, G. Gosztonyi, J. Szeberenyi, Z. Fabian, V. Liszka, B. Bodey, and C.M. Csatary, MTH-68/H oncolytic viral treatment in human high-grade gliomas., *J. Neurooncol.*, **2004**, *67*, 83–93.

[20] J. Altomonte, S. Marozin, R.M. Schmid, and O. Ebert, Engineered newcastle disease virus as an improved oncolytic agent against hepatocellular carcinoma., *Mol. Ther.*, **2010**, *18*, 275–284.

[21] S. Modrow, D. Falke, U. Truyen, and H. Schatzl, *Molekulare Virologie*, Spektrum Akademischer Verlag, **2010**.

[22] G.L. Smith, Vaccinia virus vectors for gene expression., *Curr. Opin. Biotechnol.*, **1991**, *2*, 713–717.

[23] P.H. Verardi, A. Titong, and C.J. Hagen, A vaccinia virus renaissance: New vaccine and immunotherapeutic uses after smallpox eradication, *Hum. Vac. Immuno.*, **2012**, *8*, 961–970.

[24] D.H. Kirn and S.H. Thorne, Targeted and armed oncolytic poxviruses: a novel multi-mechanistic therapeutic class for cancer, *Nat. Rev. Cancer*, **2009**, *9*, 64–71.

[25] N.G. Chen and A.A. Szalay, Oncolytic vaccinia virus: a theranostic agent for cancer, *Future Virol.*, **2010**, *5*, 763–784.

[26] R.M. Buller and G.J. Palumbo, Poxvirus pathogenesis, *Microbiol. Rev.*, **1991**, *55*, 80–122.

[27] C. Goldsmith, Vaccinia Virus EM Image, ID# 2143, *CDC. PHIL.*, **2002**, 1–3.

[28] Q. Zhang, C. Liang, Y.A. Yu, N. Chen, T. Dandekar, and A.A. Szalay, The highly attenuated oncolytic recombinant vaccinia virus GLV-1h68: comparative genomic features and the contribution of F14.5L inactivation, *Mol. Genet. Genom.*, **2009**, *282*, 417–435.

[29] Q. Zhang, Y.A. Yu, E. Wang, N. Chen, R.L. Danner, P.J. Munson, F.M. Marincola, and A.A. Szalay, Eradication of solid human breast tumors in nude mice with an intravenously injected light-emitting oncolytic vaccinia virus, *Cancer Res.*, **2007**, *67*, 10038–10046.

[30] S. Chakrabarti, J.R. Sisler, and B. Moss, Compact, synthetic, vaccinia virus early/late promoter for protein expression., Technical report, National Institute of Allergy and Infectious Diseases, National Institutes of Health, Bethesda, MD 20892-0445, USA., **1999**.

[31] N.G. Chen, Y.A. Yu, Q. Zhang, and A.A. Szalay, Replication efficiency of oncolytic vaccinia virus in cell cultures prognosticates the virulence and antitumor efficacy in mice, *J. Trans. Med.*, **2011**, *9*, 164–174.

[32] X.Q. Lun, J.H. Jang, N. Tang, H. Deng, R. Head, J.C. Bell, D.F. Stojdl, C.L. Nutt, D.L. Senger, P.A. Forsyth, and J.A. McCart, Efficacy of systemically administered oncolytic vaccinia virotherapy for malignant gliomas is enhanced by combination therapy with rapamycin or cyclophosphamide, *Clin. Cancer Res.*, **2009**, *15*, 2777–2788.

[33] K.W. Peng, R. Myers, A. Greenslade, E. Mader, S. Greiner, M.J. Federspiel, A. Dispenzieri, and S.J. Russell, Using clinically approved cyclophosphamide regimens to control the humoral immune response to oncolytic viruses., *Gene Ther.*, **2012**, 1476–1478.

[34] S.J. Russell and K.W. Peng, Viruses as anticancer drugs., *Trends Pharmacol. Sci.*, **2007**, *28*, 326–333.

[35] R. Bilbao, M. Bustos, P. Alzuguren, M.J. Pajares, M. Drozdzik, C. Qian, and J. Prieto, A blood-tumor barrier limits gene transfer to experimental liver cancer: the effect of vasoactive compounds., *Gene Ther.*, **2000**, *7*, 1824–1832.

[36] Z.Y. Li, S. Ni, X. Yang, N. Kiviat, and A. Lieber, Xenograft models for liver metastasis: Relationship between tumor morphology and adenovirus vector transduction., *Mol. Ther.*, **2004**, *9*, 650–657.

[37] R.K. Jain, Delivery of molecular medicine to solid tumors: lessons from in vivo imaging of gene expression and function., *J. Control. Rel.*, **2001**, *74*, 7–25.

[38] A. Marusyk, V. Almendro, and K. Polyak, Intra-tumour heterogeneity: a looking glass for cancer?, *Nat. Rev. Cancer*, **2012**, *12*, 323–334.

[39] R. Fisher, L. Pusztai, and C. Swanton, Cancer heterogeneity: implications for targeted therapeutics, *Br. J. Cancer*, **2013**, *108*, 479–485.

[40] S.J. Advani, L. Buckel, N.G. Chen, D.J. Scanderbeg, U. Geissinger, Q. Zhang, Y.A. Yu, R.J. Aguilar, A.J. Mundt, and A.A. Szalay, Preferential replication of systemically delivered oncolytic vaccinia virus in focally irradiated glioma xenografts., *Clin. Cancer Res.*, **2012**, *18*, 2579–2590.

[41] T. Kottke, J. Chester, E. Ilett, J. Thompson, R. Diaz, M. Coffey, P. Selby, G. Nuovo, J. Pulido, D. Mukhopadhyay, H. Pandha, K. Harrington, A. Melcher, and R. Vile, Precise scheduling of chemotherapy primes VEGF-producing tumors for successful systemic oncolytic virotherapy., *Mol. Ther.*, **2011**, *19*, 1802–1812.

[42] L.R. Kelland, Of mice and men: values and liabilities of the athymic nude mouse model in anticancer drug development., *Eur. J. Can.*, **2004**, *40*, 827–836.

[43] J. Schneider-Schaulies, V.t. Meulen, and S. Schneider-Schaulies, Measles infection of the central nervous system., *J. Neurovirol.*, **2003**, *9*, 247–252.

[44] G. Halldén, R. Hill, Y. Wang, A. Anand, T.C. Liu, N.R. Lemoine, J. Francis, L. Hawkins, and D. Kirn, Novel immunocompetent murine tumor models for the assessment of replication-competent oncolytic adenovirus efficacy., *Mol. Ther.*, **2003**, *8*, 412–424.

[45] Biomarkers Consortium.

[46] N. Saijo, Critical comments for roles of biomarkers in the diagnosis and treatment of cancer., *Cancer Treat. Rev.*, **2012**, *38*, 63–67.

[47] M. Chalfie, Y. Tu, G. Euskirchen, W.W. Ward, and D.C. Prasher, Green fluorescent protein as a marker for gene expression., *Science*, **1994**, *263*, 802–805.

[48] R.Y. Tsien, The green fluorescent protein, *Annu. Rev. Biochem.*, **1998**, *67*, 509–544.

[49] F. Yang, L.G. Moss, and G.N. Phillips, The molecular structure of green fluorescent protein., *Nat. Biotechnol.*, **1996**, *14*, 1246–1251.

[50] J.D. McCarter and S.G. Withers, Mechanisms of enzymatic glycoside hydrolysis., *Curr. Opin. Struct. Biol.*, **1994**, *4*, 885–892.

[51] R.A. Jefferson, S.M. Burgess, and D. Hirsh, beta-Glucuronidase from Escherichia coli as a gene-fusion marker., *Proc. Natl. Acad. Sci.*, **1986**, *83*, 8447–8451.

[52] R.A. Jefferson, T.A. Kavanagh, and M.W. Bevan, GUS fusions: beta-glucuronidase as a sensitive and versatile gene fusion marker in higher plants., *EMBO J.*, **1987**, *6*, 3901–3907.

[53] S. Jain, W.B. Drendel, Z.W. Chen, F.S. Mathews, W.S. Sly, and J.H. Grubb, Structure of human beta-glucuronidase reveals candidate lysosomal targeting and active-site motifs., *Nat. Struct. Biol.*, **1996**, *3*, 375–381.

[54] P. Goldman and C.C. Levy, Carboxypeptidase G: purification and properties., *Proc. Natl. Acad. Sci.*, **1967**, *58*, 1299–1306.

[55] J.M. Berg, J.L. Tymoczko, and L. Stryer, *Biochemistry*, W. H. Freeman, New York, 5th edition, **2002**.

[56] C.C. Levy and P. Goldman, The enzymatic hydrolysis of methotrexate and folic acid., *J. Biol. Chem.*, **1967**, *242*, 2933–2938.

[57] K.T. Barnhart, G. Gosman, R. Ashby, and M. Sammel, The medical management of ectopic pregnancy: a meta-analysis comparing "single dose" and "multidose" regimens., *Obstet. Gynecol.*, **2003**, *101*, 778–784.

[58] B.I. Korelitz and D.H. Present, Methotrexate for Crohn's disease., *N. Engl. J. Med.*, **1995**, *333*, 600–601.

[59] P.T.R. Rajagopalan, Z. Zhang, L. McCourt, M. Dwyer, S.J. Benkovic, and G.G. Hammes, Interaction of dihydrofolate reductase with methotrexate: ensemble and single-molecule kinetics., *Proc. Natl. Acad. Sci.*, **2002**, *99*, 13481–13486.

[60] F.M. Huennekens, The methotrexate story: a paradigm for development of cancer chemotherapeutic agents., *Adv. Enzyme Regul.*, **1994**, *34*, 397–419.

[61] S. Schwartz, K. Borner, K. Müller, P. Martus, L. Fischer, A. Korfel, T. Auton, and E. Thiel, Glucarpidase (carboxypeptidase g2) intervention in adult and elderly cancer patients with renal dysfunction and delayed methotrexate elimination after high-dose methotrexate therapy., *Oncologist*, **2007**, *12*, 1299–1308.

[62] P. Gold and S.O. Freedman, Specific carcinoembryonic antigens of the human digestive system., *J. Exp. Med.*, **1965**, *122*, 467–481.

[63] K. Murphy, P. Travers, and M. Walport, *Janeway's Immunobiology*, Garland Science, 7th edition, **2008**.

[64] N. Beauchemin, S. Benchimol, D. Cournoyer, A. Fuks, and C.P. Stanners, Isolation and characterization of full-length functional cDNA clones for human carcinoembryonic antigen., *Mol. Cell. Biol.*, **1987**, *7*, 3221–3230.

[65] S. Hammarström, The carcinoembryonic antigen (CEA) family: structures, suggested functions and expression in normal and malignant tissues., *Semin. Cancer Biol.*, **1999**, *9*, 67–81.

[66] S. Watanabe and J.Y. Chou, Human pregnancy-specific beta 1-glycoprotein: a new member of the carcinoembryonic antigen gene family., *Biochem. Biophys. Res. Commun.*, **1988**, *152*, 762–768.

[67] K.W. Peng, S. Facteau, T. Wegman, D. O'Kane, and S.J. Russell, Non-invasive in vivo monitoring of trackable viruses expressing soluble marker peptides., *Nat. Med.*, **2002**, *8*, 527–531.

[68] D.M. Thomson, J. Krupey, S.O. Freedman, and P. Gold, The radioimmunoassay of circulating carcinoembryonic antigen of the human digestive system., *Proc. Natl. Acad. Sci.*, **1969**, *64*, 161–167.

[69] J.E. Shively and J.D. Beatty, CEA-related antigens: molecular biology and clinical significance., *Crit. Rev. Oncol. Hematol.*, **1985**, *2*, 355–399.

[70] R.A. Graham, S. Wang, P.J. Catalano, and D.G. Haller, Postsurgical surveillance of colon cancer: preliminary cost analysis of physician examination, carcinoembryonic antigen testing, chest x-ray, and colonoscopy., *Ann. Surg.*, **1998**, *228*, 59–63.

[71] A. Terskikh, J.P. Mach, and A. Pèlegrin, Marked increase in the secretion of a fully antigenic recombinant carcinoembryonic antigen obtained by deletion of its hydrophobic tail., *Mol. Immunol.*, **1993**, *30*, 921–927.

[72] B. Sodeik, S. Cudmore, M. Ericsson, M. Esteban, E.G. Niles, and G. Griffiths, Assembly of vaccinia virus: incorporation of p14 and p32 into the membrane of the intracellular mature virus., *J. Virol.*, **1995**, *69*, 3560–3574.

[73] M.I. Vázquez and M. Esteban, The vaccinia virus 14-kilodalton (A27L) fusion protein forms a triple coiled-coil structure and interacts with the 21-kilodalton (A17L) virus membrane protein through a C-terminal alpha-helix, *J. Virol.*, **1998**, *72*, 10126–10137.

[74] C.F. Lai, S.C. Gong, and M. Esteban, Structural and functional properties of the 14-kDa envelope protein of vaccinia virus synthesized in Escherichia coli., *J. Biol. Chem.*, **1990**, *265*, 22174–22180.

[75] C.S. Chung, J.C. Hsiao, Y.S. Chang, and W. Chang, A27L protein mediates vaccinia virus interaction with cell surface heparan sulfate, *J. Virol.*, **1998**, *72*, 1577–1585.

[76] J.F. Rodriguez and G.L. Smith, Inducible gene expression from vaccinia virus vectors., *Virology*, **1990**, *177*, 239–250.

[77] J.F. Rodriguez and G.L. Smith, IPTG-dependent vaccinia virus: identification of a virus protein enabling virion envelopment by Golgi membrane and egress., *Nucleic Acids Res.*, **1990**, *18*, 5347–5351.

[78] G.L. Smith, A. Vanderplasschen, and M. Law, The formation and function of extracellular enveloped vaccinia virus, *J. Gen. Virol.*, **2002**, *83*, 2915–2931.

[79] F. Takahashi-Nishimaki, S. Funahashi, K. Miki, S. Hashizume, and M. Sugimoto, Regulation of plaque size and host range by a vaccinia virus gene related to complement system proteins., *Virology*, **1991**, *181*, 158–164.

[80] T. Mosmann, Rapid colorimetric assay for cellular growth and survival: application to proliferation and cytotoxicity assays., *J. Immunol. Methods*, **1983**, *65*, 55–63.

[81] F.G. Falkner and B. Moss, Transient dominant selection of recombinant vaccinia viruses., *J. Virol.*, **1990**, *64*, 3108–3111.

[82] T. Pierce, *Assay Development Technical Handbook*, Thermo Scientific Pierce, Rockford, **2011**.

[83] W. Luttmann, K. Bratke, M. Kupper, and D. Myrtek, *Immunology*, The Experimentor, Spektrum Akademischer Verlag, Heidelberg, 3rd edition, **2009**.

[84] M. Hess, J. Stritzker, B. Härtl, J.B. Sturm, I. Gentschev, and A.A. Szalay, Bacterial glucuronidase as general marker for oncolytic virotherapy or other biological therapies, *J. Trans. Med.*, **2011**, *9*, 172–183.

[85] J.L. McCullough, B.A. Chabner, and J.R. Bertino, Purification and properties of carboxypeptidase G 1 ., *J. Biol. Chem.*, **1971**, *246*, 7207–7213.

[86] R.F. Sherwood, R.G. Melton, S.M. Alwan, and P. Hughes, Purification and properties of carboxypeptidase G2 from Pseudomonas sp. strain RS-16. Use of a novel triazine dye affinity method., *Eur. J. Biochem.*, **1985**, *148*, 447–453.

[87] S.K. Goda, F.A.B. Rashidi, A.A. Fakharo, and A. Al-obaidli, Functional Overexpression and Purification of a Codon Optimized Synthetic Glucarpidase (Carboxypeptidase G2) in Escherichia coli, *Prot. J.*, **2009**, *28*, 435–442.

[88] K. Hallermalm, S. Johansson, A. Bråve, M. Ek, G. Engström, A. Boberg, L. Gudmundsdotter, P. Blomberg, H. Mellstedt, R. Stout, M.A. Liu, and B. Wahren, Preclinical Evaluation of a CEA DNA Prime/protein Boost Vaccination Strategy Against Colorectal Cancer, *Scand. J. Immunol.*, **2007**, *66*, 43–51.

[89] A.A. Butt, S. Michaels, and P. Kissinger, The association of serum lactate dehydrogenase level with selected opportunistic infections and HIV progression., *Int. J. Infect. Dis.*, **2002**, *6*, 178–181.

[90] J.E. Heffner, L.K. Brown, and C.A. Barbieri, Diagnostic value of tests that discriminate between exudative and transudative pleural effusions. Primary Study Investigators., *Chest*, **1997**, *111*, 970–980.

[91] J.Y. Kim, N.K. Kim, S.K. Sohn, Y.W. Kim, K.J.S. Kim, H. Hur, B.S. Min, and C.H. Cho, Prognostic Value of Postoperative CEA Clearance in Rectal Cancer Patients with High Preoperative CEA Levels, *Ann. Surg. Oncol.*, **2009**, *16*, 2771–2778.

[92] A. Frentzen, Y.A. Yu, N. Chen, Q. Zhang, S. Weibel, V. Raab, and A.A. Szalay, Anti-VEGF single-chain antibody GLAF-1 encoded by oncolytic vaccinia virus significantly enhances antitumor therapy, *Proc. Natl. Acad. Sci.*, **2009**, *106*, 12915–12920.

[93] Y.M. Rustum, K. Tóth, M. Seshadri, A. Sen, F.A. Durrani, E. Stott, C.D. Morrison, S. Cao, and A. Bhattacharya, Architectural heterogeneity in tumors caused by differentiation alters intratumoral drug distribution and affects therapeutic synergy of antiangiogenic organoselenium compound., *J. Oncol.*, **2010**, *2010*, 1–13.

[94] A.M. Lutz, J.K. Willmann, F.V. Cochran, P. Ray, and S.S. Gambhir, Cancer screening: a mathematical model relating secreted blood biomarker levels to tumor sizes., *PLoS Med.*, **2008**, *5*, 1287–1297.

Erklärung gemäß § 4 Absatz 3 der Promotionsordnung der Fakultät für Biologie der Bayerischen Julius-Maximilians-Universität Würzburg

Hiermit erkläre ich, dass die vorgelegte Dissertation selbstständig verfasst wurde und keine anderen als die angegebenen Hilfsmittel und Quellen verwendet wurden.

Desweiteren erkläre ich, dass die vorliegende Arbeit weder in gleicher noch in ähnlicher Form bereits in einem anderen Prüfungsverfahren vorgelegt wurde.

Zuvor habe ich neben dem akademischen Grad "Diplom-Biologin Univ." keine weiteren akademischen Grade erworben.

Die vorliegende Arbeit wurde von Prof. Dr. A. A. Szalay betreut

Jacqueline Sui Lin Nube
Würzburg, April 2013

Acknowledgements

First and foremost, I would like to thank Prof. Dr. Szalay for giving me the opportunity to work on this exciting topic here at Genelux. Also I would like to thank him for his unerring support, continuous help and am also very grateful for the stipend provided by the Genelux Corporation and for giving me the once in a lifetime opportunity to live and work in San Diego.

My gratitude goes out to Qian for her patience and all her support and advice during the years. Thank you for giving me advice in all things cloning and shedding light on the oddities in the lab. I would also like to thank Jochen, Joe, Nanhai & Tony for their scientific guidance and support, be it helping with anything and everything virus and lab-related, literature questions or proof-reading my thesis. Furthermore, a big thank you to Terry Trevino and Jason Aguilar for their excellent technical support and their dedication to provide the graduate students and lab members with anything we need. I would also like to thank Camha for taking care of all the administrative aspects that came up during this time and more.

I would especially like to thank Prof. Grummt for his help in putting my thesis words on paper and his encouragement. And my gratitude also goes to Prof. Dandekar for agreeing to be my second examiner. A big thank you goes out to all my colleagues and fellow "Doktoranden", past and present. We made it! =) And to the group in Würzburg, thank you for all your help and support during my time at the university and afterwards; for the countless emails and phone calls, even a how-to video. Thank you all. Lorenz, thank you so much for lending me your legwork during submission. You're the best.

Thank you to my dear friends for their support and understanding during this time. For all the "care packages" that the USPS had the delight of heaving to my doorstep, the late night phone calls to Australia, Europe and Singapore (thank goodness for the time difference and yes, daylight savings is legal...), the coffee runs and the camping trips, in order to "get away from it all", only to end up sitting in ridiculous traffic for ages at the campsite. LOL.

Last, but in no way least, I would like to thank my family. I would be a much poorer person without all your love and support.